論文 / 著書情報
Article / Book Information

題目(和文)	
Title(English)	Fluid Motion in the Earth's Outer Core Derived from Geomagnetic Field Data and Its Implications for the Geodynamo
著者(和文)	松島政貴
Author(English)	MASAKI MATSUSHIMA
出典(和文)	学位:理学博士, 学位授与機関:東京工業大学, 報告番号:甲第2250号, 授与年月日:1991年3月26日, 学位の種別:課程博士, 審査員:
Citation(English)	Degree:Doctor of Science, Conferring organization: , Report number:甲第2250号, Conferred date:1991/3/26, Degree Type:Course doctor, Examiner:
学位種別(和文)	博士論文
Type(English)	Doctoral Thesis

Fluid Motion in the Earth's Outer Core Derived from Geomagnetic Field Data and Its Implications for the Geodynamo

by

Masaki Matsushima

A thesis submitted for the degree of
Doctor of Science

at

Department of Applied Physics
Tokyo Institute of Technology

January 1991

Acknowledgments

I express my sincere thanks to Associate Professor Y. Honkura for his encouragement, stimulative discussion and critical reading of the manuscript. I am grateful to Mr. T. Hamajima, Mr. S. Ino and Mr. T. Iijima for their support in completing basic programs for graphics. I would also like to thank the staffs and colleagues at Earth and Planetary Sciences Laboratories, Tokyo Institute of Technology for their kindness. The calculation was performed on NWS-3860 and NWS-1720 at Honkura Laboratory, Tokyo Institute of Technology, Sun-3 at Saito Laboratory, Tokyo Institute of Technology, and ETA^{10} at the Computer Center of Tokyo Institute of Technology.

Abstract

The Earth's magnetic field is generated and maintained by the dynamo action in the Earth's fluid outer core. In order to understand a realistic geodynamo mechanism, it is essential to clarify fluid motion in the electrically conducting outer core. The fluid motion in the core should be responsible for the characteristics of the Earth's magnetic field, which should be closely related to the geodynamo mechanism. In an opposite sense, information on fluid motion in the outer core would be provided by the characteristics of the Earth's magnetic field. Following such a presumption, fluid motion in the Earth's outer core is derived from geomagnetic field data by solving the induction and the Navier-Stokes equations. The basic standpoint is that the non-axisymmetric poloidal magnetic field is maintained by induction processes associated with a large-scale fluid motion within the outer core. The radial dependence of poloidal velocity field is unknown, but once a rather simple functional form is assumed, the magnitude is constrained by the magnetic field data. The toroidal velocity field can be derived by solving the Navier-Stokes equation. We examine several cases step by step.

In Cases 1 and 2, inducing magnetic fields for the generation of non-axisymmetric poloidal magnetic fields are assumed to be zonal toroidal magnetic fields which are expected to be generated by the interaction between the axial dipole magnetic field and a zonal toroidal motion (the ω-effect). It is then assumed that the non-axisymmetric poloidal magnetic fields are maintained by the interaction between poloidal velocity fields and the zonal toroidal magnetic fields. In Cases 3, 4 and 5, axisymmetric poloidal magnetic fields, in particular the dipole magnetic field, are also considered as inducing magnetic fields. Then the non-axisymmetric poloidal magnetic fields are assumed to be maintained by the interaction between poloidal velocity

fields and the axisymmetric poloidal and the zonal toroidal magnetic fields. In Cases 6 and 7, non-zonal toroidal velocity and non-zonal toroidal magnetic fields are further taken into consideration. The inducing magnetic fields for the non-axisymmetric poloidal magnetic fields are then assumed to be the toroidal and axisymmetric poloidal magnetic fields. In Cases 2, 5 and 7, an axisymmetric poloidal velocity field, which gives rise to zonal toroidal motions, is added with its magnitude varied variously.

In order to check the validity of solutions, time-dependent behavior of the magnetic field is examined with the velocity field fixed for respective cases. The time integration is performed using the fourth-order Runge-Kutta scheme. Unless the derived velocity field is realistic, the magnetic field would diverge or decay within a short time. This is because some other induction terms, which have not been taken into consideration in deriving fluid motion in the core, must also be important in maintaining a steady magnetic field. In this sense, it is found that the fluid motions derived for Cases 1 to 5 are not realistic. The most plausible fluid motion in the core is derived for Case 6; the magnetic energy increases only by 20 % for 500 years in the calculation of time-dependent behavior of the magnetic field. In addition, some of the marked features in the velocity field are similar to those derived on the frozen-flux approximation.

The fluid motion is characterized by two convection rolls; one is parallel to the Earth's rotation axis and the other inclined. The extension of convection roll axis goes through the core surface beneath Canada and Siberia in the Northern Hemisphere, where magnetic flux concentrations are also observed at the core-mantle boundary (CMB). This result is consistent with a geodynamo model in terms of convection rolls parallel to the Earth's rotation axis as proposed by Busse (1975). It is also consistent with the relation between the locations of convection roll axes and the

magnetic flux concentrations at the CMB as suggested by Gubbins and Bloxham (1987). The inclined convection roll seems to be related to the toroidal magnetic field in the core. The distribution of the toroidal magnetic field also seems to be consistent with the distribution of the radial component of the magnetic field at the CMB. The entire patterns of the derived fluid motion at the epochs of 1600, 1700, 1800, 1900 and 1980 AD vary little, whereas the magnitude of velocity field is different from one epoch to another. The locations of convection rolls may be controlled by the thermal interactions between the core and the mantle as pointed out by Bloxham and Gubbins (1987). All these results suggest that a large-scale zonal toroidal motion and a strong zonal toroidal magnetic field are not necessarily required by the geodynamo; that is, the geodynamo is more likely to be of α^2-type rather than of $\alpha\omega$-type.

Supporting Papers

1. Matsushima, M. and Y. Honkura, Fluctuation of the standing and the drifting parts of the Earth's magnetic field, *Geophys. J.*, **94**, 35–50, 1988.
2. Honkura, Y. and M. Matsushima, Lower bound for the electrical conductivity of the Earth's outer core, *Geophys. Res. Lett.*, **15**, 689–692, 1988.
3. Honkura, Y. and M. Matsushima, Fluctuation of the nondipole magnetic field and its implication for the process of geomagnetic polarity reversal in the Cox model, *J. Geophys. Res.*, **93**, 11,631–11,642, 1988.
4. Honkura, Y. and M. Matsushima, Time-dependent pattern of core motion inferred from fluctuations of standing and drifting non-dipole fields, *J. Geomag. Geoelectr.*, **40**, 1511–1522, 1988.
5. Matsushima, M. and Y. Honkura, Fluid motion in the outer core estimated from geomagnetic field, *Chikyu Extra*, **2**, 53–57, 1989 (in Japanese).
6. Matsushima, M. and Y. Honkura, Large-scale fluid motion in the Earth's outer core estimated from non-dipole magnetic field data, *J. Geomag. Geoelectr.*, **41**, 963–1000, 1989.

Table of Contents

1. Introduction

The Earth possesses its intrinsic magnetic field, which varies with various characteristic times; for example, polarity reversals of the axial dipole magnetic field and the westward drift of the non-dipole magnetic field are well known. The creation and maintenance of the Earth's magnetic field are generally believed to be due to the dynamo action in the Earth's fluid core. Fluid motion in the electrically conducting outer core should primarily be responsible for the characteristics of the Earth's magnetic field. In order to understand a realistic dynamo mechanism, which is operative in the core, it is essential to clarify the velocity field in the outer core, but this is an extremely difficult problem. In an opposite sense, the characteristics of the Earth's magnetic field should be related closely to the dynamo mechanism and they would provide information on fluid motion in the core. With such a presumption in mind, we attempt to derive fluid motion in the Earth's outer core from geomagnetic field data.

One conventional approach to derive fluid motion in the core is based on the frozen-flux approximation (Roberts and Scott, 1965); that is, the magnetic diffusion term in the induction equation is neglected for a time scale of some tens of years because of the high electrical conductivity of core fluid. Then the core behaves like a perfect conductor so that magnetic lines of force move with the fluid. According to Backus (1968), however, this approximation alone warrants no unique velocity field, and an additional constraint is required; for example, steady flow (Voorhies, 1986; Whaler and Clarke, 1988; Whaler, 1990), geostrophic flow (Le Mouël *et al.*, 1985; Gire and Le Mouël, 1990; Hulot *et al.*, 1990), or toroidal flow (Gubbins, 1982; Bloxham, 1989; Lloyd and Gubbins, 1990) has been considered as a constraint.

Meanwhile, Bloxham and Gubbins (1986) presented a line of evidence showing

that the frozen-flux approximation is invalid in the South Atlantic region where magnetic flux diffusion seems to be significant. Bloxham (1986) also pointed out that a strong toroidal magnetic field and upwelling motions existing near the core-mantle boundary (CMB) would invalidate the frozen-flux approximation. It should be noted, however, that the result of Bloxham and Gubbins (1986) depends on their error estimates and Bloxham (1988b) himself admits that their work does not necessarily mean that the frozen-flux approximation should be abandoned.

Another approach to fluid motion in the core is based on the presumption that a strong toroidal magnetic field must be generated by a differential rotation in the core (Rikitake, 1967; Honkura and Rikitake, 1972; Honkura and Matsushima, 1988c; Matsushima and Honkura, 1989a). The process is then simplified; non-axisymmetric poloidal magnetic fields observed at the Earth's surface are generated only by the interaction between poloidal velocity fields and such a strong zonal toroidal magnetic field. Then derivation of fluid motion in the core is rather straightforward.

Rikitake (1967), Honkura and Rikitake (1972), and Honkura and Matsushima (1988c) further assumed that a strong zonal toroidal magnetic field with degree two and order zero of spherical harmonics (hereafter we will express it as $\boldsymbol{B}[T_2^0]$) with an arbitrarily given magnitude exists only in a narrow shell within the core, and derived poloidal velocity fields near the CMB. Matsushima and Honkura (1989a) improved the method by estimating differential rotation, which is expected to generate a strong toroidal magnetic field, and derived the magnitude and the radial dependence of the toroidal magnetic field $\boldsymbol{B}[T_2^0]$ through the interaction between the axial dipole magnetic field $\boldsymbol{B}[S_1^0]$ and the differential rotation $\boldsymbol{V}[T_1^0]$; this is the so-called ω-effect. In order to obtain the zonal toroidal motion $\boldsymbol{V}[T_1^0]$, they divided the outer core into spherical shells of equal volume, following the method of Watanabe and Yukutake (1975). An underlying assumption is that each spherical shell is subject to rigid

steady rotation as a result of the balance between the electromagnetic torque due to the Lorentz force and the effective torque due to the angular momentum transfer expected from virtual displacement of fluid particles. Then we can calculate the zonal toroidal velocity field and derive a zonal toroidal magnetic field from the ω-effect. The magnitude of poloidal velocity fields estimated in this way does not necessarily coincide with the magnitude of the initially given velocity fields. However, self-consistent solutions may be derived by an iterative calculation of the whole process.

We can easily realize that it is insufficient to represent differential rotation in terms of the zonal toroidal motion $\boldsymbol{V}[T_1^0]$ only. More realistically, differential rotation should depend not only on the r-direction but also on the θ-direction, as is the case for the Sun's convection zone (e.g. Babcock, 1961). Matsushima and Honkura (1989b; unpublished work), therefore, divided the outer core in the r- and θ-directions and derived differential rotation, again on the basis of the concept of virtual displacement of fluid particles. In this case, they regarded zonal toroidal magnetic fields $\boldsymbol{B}[T_l^0]$ $(l \leq 6)$ as responsible for the generation of non-axisymmetric poloidal magnetic fields and derived fluid motion in the outer core.

It should be noted that plausible estimation of differential rotation is crucially important when we try to derive fluid motion in the core on the basis of strong zonal toroidal magnetic fields. The previous results have relied on a physically very simplified model; that is, virtual displacement of fluid particles in estimating differential rotation. Until this concept is justified, the method is by no means reliable and improvements in this respect are obviously required in order to derive more reliable fluid motion in the core. The best way to estimate toroidal velocity fields is to solve the Navier-Stokes equation.

The line along which we proceed is now clear; fluid motion in the Earth's outer core is to be derived from geomagnetic field data by solving both the induction and

the Navier-Stokes equations. It is too difficult, however, to take into consideration the energy source in the Navier-Stokes equation; we must also solve the energy equation. Furthermore, the energy source for the geodynamo is a problem under debate; which type of convection is more likely, a thermal or a compositional one (e.g. Gubbins and Roberts, 1987)? Nevertheless, once poloidal velocity fields in the core are somehow known, it is possible to derive toroidal velocity fields by solving the Navier-Stokes equation for the toroidal constituent, as will be described in Section 2.

In this sense, the present approach may be considered as an intermediate stage between kinematic dynamo and magnetohydrodynamic (MHD) dynamo. In the kinematic dynamo, the velocity field in the core is given and it is examined whether the magnetic field is sustained with the given velocity field. In the present method, we assume the radial dependence of poloidal velocity field as in kinematic dynamo, since we do not consider the energy source. The magnitude is an unknown quantity to be determined. The toroidal velocity field is derived by solving the Navier-Stokes equation which includes the Coriolis force and the Lorentz force. This point is essentially different from the kinematic dynamo approach.

Another essential point is that fluid motion in the core is to be derived from geomagnetic field data; that is, the magnitude of poloidal velocity field is constrained by the magnetic field observed at the Earth's surface. As in our previous approaches (Matsushima and Honkura, 1989a, b), we do not consider the mechanism by which the axial dipole magnetic field is generated. For consistency, however, it must also be shown that the derived velocity field can maintain the axial dipole magnetic field. Although this is beyond the scope of the present study, the information on the velocity field in the core is crucially important in a realistic geodynamo model.

In the actual computation, we consider a large-scale convective motion and express it in terms of toroidal and poloidal velocity fields, each of which is expanded

into a series of spherical surface harmonics of up to degree four. First, we reexamine the previous unpublished work based on the assumption that non-axisymmetric poloidal magnetic fields are generated simply by the interaction between poloidal velocity fields and zonal toroidal magnetic fields created by the ω-effect. The strongest poloidal magnetic field is obviously the axial dipole magnetic field $\boldsymbol{B}[S_1^0]$. It turned out that there is no reason to exclude the axial dipole constituent as an inducing magnetic field from which non-axisymmetric poloidal magnetic fields are created. Second then, we try to extend the method so as to include the dipole magnetic field as one of the inducing magnetic fields. We can also include axisymmetric non-dipole magnetic fields as inducing magnetic fields, and examine the validity of the assumption that non-dipole magnetic fields as inducing magnetic fields can be neglected. Third, we try to further improve the second method. As mentioned above, we can derive toroidal velocity fields by solving the Navier-Stokes equation on the condition that poloidal velocity fields are known. These non-zonal toroidal velocity fields may generate strong non-zonal toroidal magnetic fields $\boldsymbol{B}[T_l^m]$ $(m \neq 0)$. Our final standpoint is that steady non-axisymmetric poloidal magnetic fields are maintained primarily by the interaction between the poloidal convective motion and the toroidal magnetic fields.

Velocity fields in the core are thus derived for various cases. However, no solution is likely to be unique, since we deal with non-linear algebraic simultaneous equations. We must somehow check the validity of solutions and examine whether the derived velocity field can maintain the magnetic field even when all the induction terms are taken into account. One way would to be to examine time-dependent behavior of the magnetic field with the velocity field fixed. If an assumption made in the derivation of fluid motion in the core is inappropriate, the magnetic field would diverge or decay within a short time because of the lack of induction terms which

should have been taken into account in deriving fluid motion in the core; that is, some other induction terms must be important in maintaining a steady magnetic field.

We found after all that the most plausible fluid motion in the Earth's outer core is derived when non-zonal toroidal velocity fields are taken into account. It should also be pointed out that some of the features of the velocity field are in common with those derived on the frozen-flux approximation. All these results suggest that a large-scale zonal toroidal motion and a strong zonal toroidal magnetic field are not necessarily required by the geodynamo; that is, the geodynamo is more likely to be of α^2-type rather than of $\alpha\omega$-type.

2. Method

2.1. Fundamental equations and mathematical formulation

In order to derive fluid motion in the Earth's outer core from geomagnetic field data, we solve both the induction and the Navier-Stokes equations.

The induction equation is derived from Maxwell's equations, ignoring the displacement current, as

$$\frac{\partial \boldsymbol{B}}{\partial t} = \nabla \times (\boldsymbol{V} \times \boldsymbol{B}) + \nu_m \nabla^2 \boldsymbol{B}, \tag{2.1}$$

where $\boldsymbol{B}$ is the magnetic field, $\boldsymbol{V}$ the velocity field, and $\nu_m = (\mu\sigma)^{-1}$ the magnetic diffusivity. The magnetic permeability μ is taken as that of vacuum $\mu_0 = 4\pi \times 10^{-7}$ Hm^{-1}. Also for the sake of simplicity the electrical conductivity σ is assumed to be constant throughout the inner and outer cores.

In the Boussinesq approximation (e.g. Chandrasekhar, 1961) and in a frame of reference rotating with a constant angular velocity $\boldsymbol{\Omega}$, corresponding to the angular velocity of the mantle, the Navier-Stokes equation is written as

$$\begin{aligned} \frac{\partial \boldsymbol{V}}{\partial t} - \boldsymbol{V} \times (\nabla \times \boldsymbol{V}) = -\nabla\chi - 2\boldsymbol{\Omega} \times \boldsymbol{V} + \frac{1}{\rho\mu_0}(\nabla \times \boldsymbol{B}) \times \boldsymbol{B} \\ - C g(r)\hat{\boldsymbol{r}} + \nu \nabla^2 \boldsymbol{V}, \end{aligned} \tag{2.2}$$

where $\hat{\boldsymbol{r}}$ is the radial unit vector, and ν, ρ and C denote the kinematic viscosity, the mean density of the core, and the buoyancy parameter, respectively. For example, if we consider thermal convection, the buoyancy parameter is expressed as $C = -\alpha_t \Theta$, where α_t and Θ denote the coefficient of volume expansion and the deviation of the temperature field from the reference. The reduced pressure χ is given as

$$\chi = \frac{p}{\rho} + \frac{1}{2}|\boldsymbol{V}|^2 - \frac{1}{2}|\boldsymbol{\Omega} \times \boldsymbol{r}|^2,$$

where p is pressure and $\boldsymbol{r}$ is the position vector. Since we consider a spherical shell of fluid subject to a spherically symmetric radial gravitational field, $g(r)$ is given as

$$g(r) = \frac{4}{3}\pi\rho G r,$$

where G is the constant of gravitation.

When fluid in the core is assumed to be incompressible, the velocity field is solenoidal, as verified from the equation of continuity. The magnetic field is also solenoidal, as verified from one of the Maxwell equations. Solenoidal vectors can be expressed in terms of toroidal and poloidal vectors (Chandrasekhar, 1961; Backus, 1986) given as

$$\boldsymbol{T} = \nabla \times (T(\boldsymbol{r}, t)\hat{\boldsymbol{r}}), \quad \boldsymbol{S} = \nabla \times \nabla \times (S(\boldsymbol{r}, t)\hat{\boldsymbol{r}}), \tag{2.3}$$

where $\boldsymbol{T}$ is a toroidal vector, $\boldsymbol{S}$ a poloidal vector, $T(\boldsymbol{r}, t)$ a scalar function for the toroidal vector, $S(\boldsymbol{r}, t)$ a scalar function for the poloidal vector, and t time. We use the spherical coordinates (r, θ, ϕ) to express the velocity field $\boldsymbol{V}$ and the magnetic field $\boldsymbol{B}$, and expand their scalar functions into a series of spherical surface harmonics for θ- and ϕ-dependence, since we consider large-scale velocity and large-scale magnetic fields. $T(\boldsymbol{r}, t)$, for example, is expressed as

$$T(\boldsymbol{r}, t) = \sum_{l=1}^{L} \sum_{m=0}^{l} T_l^{mz}(r, t)\, Y_l^{mz}(\theta, \phi). \tag{2.4}$$

$Y_l^{mz}(\theta, \phi)$ represents $P_l^m(\cos\theta)\cos m\phi$ or $P_l^m(\cos\theta)\sin m\phi$ according to $z = c$ or $z = s$, where $P_l^m(\cos\theta)$ is an associated Legendre function with degree l and order m. L corresponds to the truncation level of degree of spherical harmonics.

The velocity and magnetic fields are now expressed in terms of toroidal and

poloidal vectors as

$$\begin{aligned}
\boldsymbol{V}_T(r,\theta,\phi,t) &= \nabla\times(\sum_{l=1}^{L}\sum_{m=0}^{l} V[T_l^{mz}](r,t)\,Y_l^{mz}(\theta,\phi)\hat{\boldsymbol{r}}),\\
\boldsymbol{V}_S(r,\theta,\phi,t) &= \nabla\times\nabla\times(\sum_{l=1}^{L}\sum_{m=0}^{l} V[S_l^{mz}](r,t)\,Y_l^{mz}(\theta,\phi)\hat{\boldsymbol{r}}),\\
\boldsymbol{B}_T(r,\theta,\phi,t) &= \nabla\times(\sum_{l=1}^{L}\sum_{m=0}^{l} B[T_l^{mz}](r,t)\,Y_l^{mz}(\theta,\phi)\hat{\boldsymbol{r}}),\\
\boldsymbol{B}_S(r,\theta,\phi,t) &= \nabla\times\nabla\times(\sum_{l=1}^{L}\sum_{m=0}^{l} B[S_l^{mz}](r,t)\,Y_l^{mz}(\theta,\phi)\hat{\boldsymbol{r}}).
\end{aligned} \tag{2.5}$$

The orthogonality of toroidal and poloidal vectors and also of spherical surface harmonics enables one to separate the induction equation and the Navier-Stokes equation into equations for toroidal or poloidal scalar functions with the set of $(l,\ m,\ z)$.

From the induction equation (2.1), as in Bullard and Gellman (1954), we obtain

$$\begin{aligned}
r^2\frac{\partial B[T_\gamma]}{\partial t} &= \nu_m\left\{r^2\frac{\partial^2 B[T_\gamma]}{\partial r^2} - \gamma(\gamma+1)B[T_\gamma]\right\}\\
&+\sum_\alpha\sum_\beta\{(V[S_\alpha]B[S_\beta]T_\gamma) + (V[T_\alpha]B[S_\beta]T_\gamma)\\
&\quad + (V[S_\alpha]B[T_\beta]T_\gamma) + (V[T_\alpha]B[T_\beta]T_\gamma)\},
\end{aligned} \tag{2.6}$$

$$\begin{aligned}
r^2\frac{\partial B[S_\gamma]}{\partial t} &= \nu_m\left\{r^2\frac{\partial^2 B[S_\gamma]}{\partial r^2} - \gamma(\gamma+1)B[S_\gamma]\right\}\\
&+\sum_\alpha\sum_\beta\{(V[S_\alpha]B[S_\beta]S_\gamma) + (V[T_\alpha]B[S_\beta]S_\gamma) + (V[S_\alpha]B[T_\beta]S_\gamma)\}.
\end{aligned} \tag{2.7}$$

From the Navier-Stokes equation (2.2), as in Frazer (1974),

$$
\begin{aligned}
r^2\frac{\partial V[T_\gamma]}{\partial t} &= \nu\left\{r^2\frac{\partial^2 V[T_\gamma]}{\partial r^2} - \gamma(\gamma+1)\,V[T_\gamma]\right\} \\
&\quad - 2\Omega\sum_\alpha\left\{(V[S_\alpha]S_1^\Omega S_\gamma) + (V[T_\alpha]S_1^\Omega S_\gamma)\right\} \\
&\quad + \frac{1}{\rho\mu_0}\sum_\alpha\sum_\beta\left\{[B[S_\alpha]B[S_\beta]S_\gamma] + [B[T_\alpha]B[S_\beta]S_\gamma] + [B[T_\alpha]B[T_\beta]S_\gamma]\right\} \\
&\quad - \sum_\alpha\sum_\beta\left\{[V[S_\alpha]\,V[S_\beta]S_\gamma] + [V[T_\alpha]\,V[S_\beta]S_\gamma] + [V[T_\alpha]\,V[T_\beta]S_\gamma]\right\}.
\end{aligned}
\tag{2.8}
$$

In these equations, Greek letters appearing as a suffix denote the set of (l, m, z) or otherwise the degree l of the spherical surface harmonics, as in Bullard and Gellman (1954). The interaction terms in parentheses are given by Bullard and Gellman (1954), and those in brackets by Frazer (1974). All the interaction terms are expressed in terms of Gaunt or Elsasser integrals, α, β, γ, scalar functions, and their partial derivatives with respect to r. The conditions imposed on α, β and γ are known as the selection rules and shown in Bullard and Gellman (1954).

The scalar function $S_1^\Omega(r)$, which is derived from the angular velocity $\mathbf{\Omega}$, is equal to $\frac{1}{2}r^2$, since $\mathbf{\Omega}$ can be expressed as

$$
\mathbf{\Omega} = \Omega\hat{z} = \Omega\nabla\times\nabla\times(S_1^\Omega(r)\,Y_1^{0c}(\theta,\phi)\hat{\boldsymbol{r}}), \tag{2.9}
$$

where $\hat{z}$ is the unit vector along the rotation axis.

In numerically solving (2.6), (2.7) and (2.8) to derive fluid motion in the core, the toroidal and poloidal scalar functions and their partial derivatives with respect to r must be expressed in terms of finite differences or series of orthogonal functions. In the present study, we rely on the latter, since derivatives can be accurately evaluated and a possible numerical instability arising from the finite difference scheme can be

avoided. We expand the scalar functions in Chebysev polynomials to describe their radial dependence, as discussed in Orszag (1980) and Glatzmaier(1984). For example, the scalar function for a toroidal velocity field with degree l and order m is expressed as

$$V[T_l^{mz}](r,\, t) = \sum_{n=0}^{N}{}' \, V[{}_nT_l^{mz}](t)\, T_n(x), \tag{2.10}$$

where $T_n(x)$ is a Chebyshev polynomial of order n defined as

$$T_n(x) = \cos(n\cos^{-1}x). \tag{2.11}$$

N is the truncation level of order of Chebyshev polynomials, and the summation $\sum'$ means that the $n = 0$ and $n = N$ terms are multiplied by $\frac{1}{2}$. The radial coordinate r in the outer core is transformed into coordinate x by

$$x = \frac{2r - r_{oc} - r_{ic}}{r_{oc} - r_{ic}}, \tag{2.12}$$

where r_{oc} and r_{ic} denote the radii of the outer and inner cores, respectively.

For simulation of global convection and magnetic field generation with a Chebyshev collocation method, Glatzmaier (1984) used the Chebyshev mesh-points defined as

$$x_k = \cos\left[\frac{k\pi}{N}\right] \qquad k = 0,\, 1,\, \cdots,\, N. \tag{2.13}$$

Then from (2.11)

$$T_n(x_k) = \cos\left[\frac{nk\pi}{N}\right], \tag{2.14}$$

and furthermore, from the orthogonality of Chebyshev polynomials and (2.10),

$$V[{}_nT_l^{mz}](t) = \frac{2}{N}\sum_{k=0}^{N}{}'\, V[T_l^{mz}](x_k,\, t)\, T_n(x_k). \tag{2.15}$$

Hence fast Fourier transform algorithms are applicable to Chebyshev transformations, and the calculation of transformation is extremely efficient (Glatzmaier, 1984).

However, we do not use the Chebyshev mesh-points for the reason as follows. From (2.11), the first-order derivative of a Chebyshev polynomial with order n is given as

$$\frac{dT_n(x)}{dx} = -\sin(n\cos^{-1}x)\, n \frac{\pm 1}{(1-x^2)^{1/2}}, \tag{2.16}$$

where the plus sign is taken if the value of $\cos^{-1}x$ is in the third or fourth quadrant and the minus sign otherwise. At a Chebyshev mesh-point x_k defined in (2.13),

$$\frac{dT_n(x_k)}{dx} = \sin\left[\frac{nk\pi}{N}\right]\frac{n}{\sin(k\pi/N)}. \tag{2.17}$$

Then for order $n = N$,

$$\frac{dT_N(x_k)}{dx} = \sin(k\pi)\frac{N}{\sin(k\pi/N)}, \tag{2.18}$$

that is, the value of the first-order derivative of the Chebyshev polynomial with maximum order N is always zero except for $k = 0$ and $k = N$.

In the present method of deriving fluid motion in the core, the terms associated with the first-order derivative of Chebyshev polynomials appear in the coefficient matrix of simultaneous equations to be solved (see Subsection 2.3). Because of (2.18), it would be inappropriate to use the Chebyshev mesh-points. Instead, we use the equi-interval mesh-points between the radii of the inner and outer cores; that is,

$$x_k = \frac{2k}{N} - 1. \tag{2.19}$$

Now, the equations (2.6), (2,7) and (2.8) are satisfied at the mesh-points for $k = 1$ to $k = N-1$. At the mesh-points for $k = 0$ and $k = N$, corresponding to the inner core – outer core boundary (ICB) and the CMB, boundary conditions are required to specify the problem and solve the second-order differential equations for each set of (l, m, z). We now have $N+1$ equations to determine $N+1$ unknowns for each set of (l, m, z). Boundary conditions for magnetic and velocity fields will be described in the next subsection.

2.2. Boundary conditions

Boundary conditions for magnetic fields are such that the normal component of $\boldsymbol{B}$ and the tangential components of $\boldsymbol{H} = \boldsymbol{B}/\mu$ must be continuous at boundaries.

The magnetic field outside the Earth is expressed, ignoring magnetic fields of external origin, in terms of the magnetic potential W given as

$$W = r_e \sum_{l=1}^{L} \left[\frac{r_e}{r}\right]^{l+1} \sum_{m=0}^{l} [g_l^m(t)\cos m\phi + h_l^m(t)\sin m\phi]\varepsilon_l^m P_l^m(\cos\theta), \qquad (2.20)$$

where g_l^m's and h_l^m's are the Gauss coefficients and r_e denotes the Earth's mean radius. The Schmidt spherical function has been used in spherical harmonic analysis of the Earth's magnetic field, but we here use associated Legendre functions and require, in (2.20), ε_l^m defined as

$$\varepsilon_l^m = \left\{\frac{(l-m)!}{(l+m)!}(2-\delta_{m0})\right\}^{1/2}, \qquad (2.21)$$

where δ_{ij} is the Kronecker's delta.

If we assume that the mantle is an insulator, the magnetic field above the core surface is obtained through downward continuation as

$$\boldsymbol{B}(r_{oc},\,\theta,\,\phi,\,t) = -\nabla W|_{r=r_{oc}}. \tag{2.22}$$

This assumption would be reasonable, since we deal with magnetic fluctuations of long time scale which are unlikely to be affected by the mantle conductivity. Also, downward continuation is unlikely to give rise to a severe problem as far as spherical harmonics of low degree are concerned. The boundary conditions for $\boldsymbol{B}[S_l^{mc}]$ at $r = r_{oc}$, for example, lead to

$$\frac{l(l+1)}{r_{oc}^2} B[S_l^{mc}](r_{oc},\,t) = (l+1)\left[\frac{r_e}{r_{oc}}\right]^{l+2} g_l^m(t)\varepsilon_l^m \tag{2.23}$$

and

$$\frac{1}{r_{oc}}\frac{\partial B[S_l^{mc}](r_{oc},\,t)}{\partial r} = -\left[\frac{r_e}{r_{oc}}\right]^{l+2} g_l^m(t)\varepsilon_l^m. \tag{2.24}$$

Eliminating $g_l^m\varepsilon_l^m$ in (2.23) and (2.24), we obtain

$$r_{oc}\frac{\partial B[S_l^{mc}](r_{oc},\,t)}{\partial r} + l\; B[S_l^{mc}](r_{oc},\,t) = 0. \tag{2.25}$$

For $B[S_l^{ms}](r,\,t)$, the same condition is derived at $r = r_{oc}$. On the other hand, toroidal magnetic fields vanish at the CMB because of the insulating mantle;

$$B[T_\gamma](r_{oc},\,t) = 0. \tag{2.26}$$

As we mentioned in the previous subsection, the electrical conductivity σ is assumed to be constant throughout the outer and inner cores. Boundary conditions for poloidal magnetic fields then yield

$$B[S_\gamma](r_{ic},\,t) = B^{(i)}[S_\gamma](r_{ic},\,t), \tag{2.27}$$

$$\frac{\partial B[S_\gamma](r_{ic},\,t)}{\partial r} = \frac{\partial B^{(i)}[S_\gamma](r_{ic},\,t)}{\partial r}, \tag{2.28}$$

where the superscript (i) denotes a scalar function for magnetic fields in the inner core. Boundary conditions for toroidal magnetic fields are given as

$$B[T_\gamma](r_{ic},\, t) = B^{(i)}[T_\gamma](r_{ic},\, t), \tag{2.29}$$

$$\frac{\partial B[T_\gamma](r_{ic},\, t)}{\partial r} = \frac{\partial B^{(i)}[T_\gamma](r_{ic},\, t)}{\partial r}, \tag{2.30}$$

where the latter condition is derived from the condition that the electric current density must also be continuous at the ICB.

When we consider the steady state, the induction equation which describes the magnetic field in the solid inner core is written as

$$\nabla^2 \boldsymbol{B}^{(i)} = 0. \tag{2.31}$$

The solution of (2.31) is obtained as

$$B^{(i)}[T_\gamma](r) = c_1 r^{\gamma+1} + c_2 r^{-\gamma}, \tag{2.32}$$

$$B^{(i)}[S_\gamma](r) = c_3 r^{\gamma+1} + c_4 r^{-\gamma}, \tag{2.33}$$

where c_1, c_2, c_3 and c_4 are constants. Since magnetic fields must be finite at $r = 0$, c_2 and c_4 vanish. From boundary conditions (2.27) to (2.30),

$$B^{(i)}[T_\gamma](r_{ic}) = c_1 r_{ic}^{\gamma+1} = B[T_\gamma](r_{ic}), \tag{2.34}$$

$$\frac{dB^{(i)}[T_\gamma](r_{ic})}{dr} = (\gamma+1) c_1 r_{ic}^{\gamma} = \frac{dB[T_\gamma](r_{ic})}{dr}, \tag{2.35}$$

$$B^{(i)}[S_\gamma](r_{ic}) = c_3 r_{ic}^{\gamma+1} = B[S_\gamma](r_{ic}), \tag{2.36}$$

$$\frac{dB^{(i)}[S_\gamma](r_{ic})}{dr} = (\gamma+1) c_3 r_{ic}^{\gamma} = \frac{dB[S_\gamma](r_{ic})}{dr}, \tag{2.37}$$

where partial derivatives are replaced with ordinary derivatives with respect to r

since we consider the steady state. From (2.34), (2.35), (2.36) and (2.37) we can express the boundary conditions for magnetic fields at the ICB in the steady state case as

$$r_{ic}\frac{dB[T_\gamma](r_{ic})}{dr} - (\gamma+1)B[T_\gamma](r_{ic}) = 0, \tag{2.38}$$

and

$$r_{ic}\frac{dB[S_\gamma](r_{ic})}{dr} - (\gamma+1)B[S_\gamma](r_{ic}) = 0. \tag{2.39}$$

One boundary condition for velocity fields is that the normal component of the velocity must vanish at boundary surfaces. Two further boundary conditions depend on the nature of the surface. On a rigid surface, no slip is allowed; that is, not only the radial but also the tangential components must vanish there. On a free surface, tangential viscous stresses must vanish (e.g. Chandrasekhar, 1961). Hence the boundary conditions for velocity fields are

$$V[S_\gamma] = \frac{\partial V[S_\gamma]}{\partial r} = V[T_\gamma] = 0 \qquad \text{for a rigid surface,} \tag{2.40}$$

$$V[S_\gamma] = \frac{\partial^2}{\partial r^2}\left[\frac{V[S_\gamma]}{r}\right] = \frac{\partial}{\partial r}\left[\frac{V[T_\gamma]}{r^2}\right] = 0 \qquad \text{for a free surface.} \tag{2.41}$$

2.3. Procedure of the derivation of fluid motion in the core

Basically we solve the non-linear simultaneous equations (2.6) for toroidal magnetic fields, (2.7) for poloidal magnetic fields, and (2.8) for toroidal velocity fields. If we take into account all the spherical harmonic modes up to order and degree L and Chebyshev polynomials up to order N, the total number of equations is $L(L+2)(N+1)$ for a toroidal or a poloidal field. In the present study, we assume the

quasi-steady state at various epochs in the sense that the steady state is realized at respective epochs, even if magnetic fields vary slowly from one epoch to another.

With regard to poloidal velocity fields, radial dependence of the scalar function is unknown unless the Navier-Stokes and the energy equations are fully solved. It is extremely difficult and beyond the scope of the resent study, however, to solve all the equations which describe the physical state in the Earth's core. In addition, the energy source for the geodynamo is still controversial (e.g. Gubbins and Roberts, 1987); that is, which mechanism is more probable, thermal convection or compositional convection? We are obliged to assume a scalar function with one of the simplest radial forms which satisfy boundary conditions given in (2.40) or (2.41). Now we express the scalar function for the poloidal velocity field as

$$\begin{aligned} V[S_l^{mz}](r,\, t) &= U[S_l^{mz}](t)\xi_l^{mz}(r) \\ &= U[S_l^{mz}](t) {\sum_{n=0}^{N}}' V[{}_nS_l^{mz}]\, T_n(x), \end{aligned} \tag{2.42}$$

where $V[{}_nS_l^{mz}]$'s are constants corresponding to the radial dependence $\xi_l^{mz}(r)$.

For the rigid CMB and the rigid ICB, we adopt the function as used by Matsushima and Honkura (1989a) or model 3 of Watanabe and Yukutake (1975) defined as

$$\xi_l^{mz}(r) = \xi(r) = r^2y^3(1-y^2)^2, \tag{2.43}$$

where $y = (r-r_{ic})/(r_{oc}-r_{ic})$. For the free CMB and the rigid ICB, we adopt the function defined as

$$\xi_l^{mz}(r) = \xi(r) = r^4(x+1)^2(x-1)\{(5-3\eta)x-7+3\eta\}, \tag{2.44}$$

where $\eta = r_{ic}/r_{oc}$ is the ratio of the inner to outer core radii and x is defined in (2.12). Here the radial dependence of poloidal velocity field is assumed to be

independent of degree l and order m of spherical harmonics. The radial dependence for these functions is shown in Fig. 2.1. For simplicity, we further assume that the inner core rotates identically with the mantle. In the present study, we do not consider the case of free CMB and free ICB. As will be mentioned in Subsection 3.2, a problem arises in the case; that is, nearly free body rotation of the outer core is allowed. If this is the case, strong shear arises at the ICB and generates a strong toroidal magnetic field, which will in turn work against the shear. This implies that in practice we may consider the rigid case only.

In the case of poloidal velocity field, the problem is now reduced to the calculation of magnitude $U[S_\gamma](t)$ for a certain epoch. We need more equations so that the number of equations is equal to the number of unknowns. We introduce the boundary condition (2.23) into the simultaneous equation to be solved, since it provides information on the strength of poloidal magnetic fields at the CMB and specifies the radial dependence there if combined with (2.25). Then the magnitude of poloidal velocity field is constrained by the magnetic field. For the Gauss coefficients in the right-hand side of (2.23), we use a geomagnetic secular variation model (Matsushima and Honkura, 1988) which will be described in the next subsection.

Now unknowns are $U[S_l^{mz}]$, $V[{}_nT_l^{mz}]$, $B[{}_nS_l^{mz}]$, and $B[{}_nT_l^{mz}]$ for a certain epoch. Setting the time derivatives at zero in equations (2.6), (2.7) and (2.8), we can solve the non-linear simultaneous algebraic equations by a Newton method. In calculating the corrections to initial values, terms associated with the first-order derivatives of Chebyshev polynomials appear in the coefficient matrix, as mentioned in Subsection 2.1. For example, the term $[B[T_\alpha]B[S_\beta]S_\gamma]$ in (2.8) is expressed as

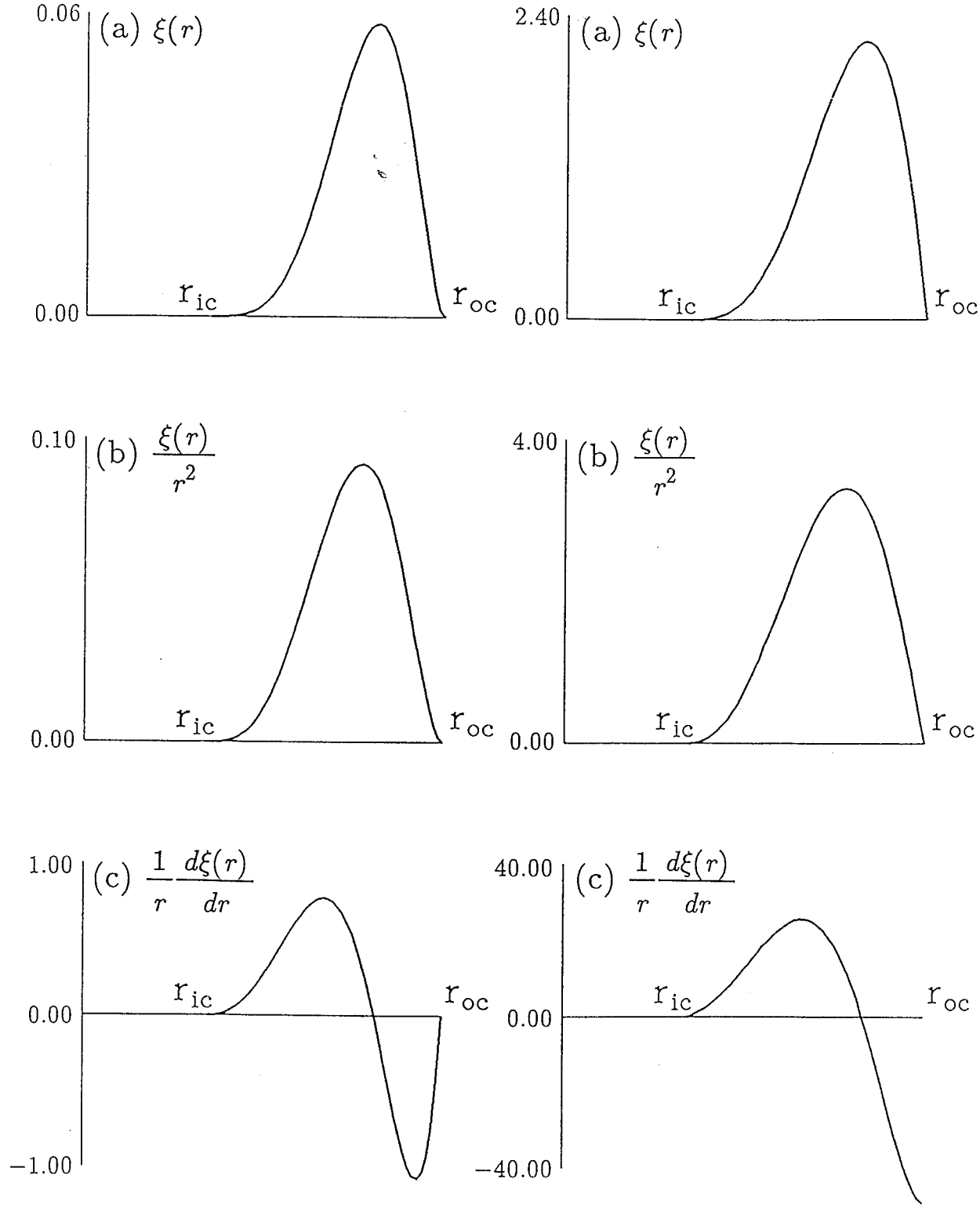

Fig. 2.1. Radial dependence of scalar function for the poloidal velocity field. Left-hand-side figures represent the scalar function given in (2.43), and right-hand-side figures the scalar function given in (2.44); (a) $\xi(r)$, (b) $\xi(r)/r^2$ and (c) $d\xi(r)/rdr$.

$$[B[T_\alpha]B[S_\beta]S_\gamma] = \frac{K_{\alpha\beta\gamma}}{N_\gamma}\left[\alpha(\alpha+1)\{\alpha(\alpha+1)-\beta(\beta+1)-\gamma(\gamma+1)\}B[T_\alpha]\frac{\partial B[S_\beta]}{\partial r}\right. \\ \left. + \beta(\beta+1)\{\alpha(\alpha+1)-\beta(\beta+1)+\gamma(\gamma+1)\}\frac{\partial B[T_\alpha]}{\partial r}B[S_\beta]\right], \tag{2.45}$$

as shown in Frazer (1974). Because of (2.18), however, no information is available on the first-derivative of maximum order N of Chebyshev polynomials. This is the reason why we use the equi-distant mesh-points defined in (2.19) rather than the Chebyshev mesh-points.

N_γ appearing in the interaction terms expressed by parenthesis and brackets in (2.6), (2.7) and (2.8), as in (2.45), is defined as

$$N_\gamma = N_l^m = \frac{2\pi l(l+1)}{2l+1}\frac{(l+m)!}{(l-m)!}(1+\delta_{m0}), \tag{2.46}$$

and can be calculated directly. With respect to the Gaunt integral $K_{\alpha\beta\gamma}$ and the Elsasser integral $L_{\alpha\beta\gamma}$, we use the method proposed by Kono (1990), in which the Gaunt integral is expressed by simple summation and the Elsasser integral by a combination of Gaunt integrals.

It is convenient to treat the equations in dimensionless form. In actual calculation, we scale the equations in terms of typical strength of magnetic field B_s, typical magnitude of velocity field V_s, and typical length L_s. In the present study, we adopt $B_s = 10^{-2}$ T, $V_s = 10^{-4}$ ms^{-1}, and $L_s = 3.485\times10^6$ m (outer core radius).

2.4. Magnetic field data

Secular variations in the geomagnetic field have been investigated in terms of time variations of Gauss coefficients. In particular, special emphasis has been put on the westward drift of non-dipole, to be exact, asymmetric with respect to the rotation axis of the Earth or non-axisymmetric, magnetic fields (Yukutake and Tachinaka,

1969; Wang and Qi, 1983; Yukutake, 1985; Shimizu and Honkura, 1986; Matsushima and Honkura, 1988). Yukutake and Tachinaka (1969) pointed out that the non-axisymmetric magnetic field can be separated into standing and drifting parts. Meanwhile, Matsushima and Honkura (1988) introduced fluctuations in the amplitude of the standing and also the drifting parts, in view of a non-linear nature of geodynamo process, and approximated them by periodic time variations.

Here, for the magnetic field data, we use model C of Matsushima and Honkura (1988), since $<\Delta Z^2>$ values, which are root-mean-square residuals of the vertical component of the magnetic field, are smaller in general than those for the Yukutake and Tachinaka model, the Wang and Qi model, models A and B of Matsushima and Honkura (1988). The total number of variables is different from one model to another, but the *AIC* values (Akaike, 1974), a criterion for judging which model is more significant in the case of uneven variables, are generally the smallest for model C. For $(l, m) = (6, 4)$ and $(6, 5)$, however, $<\Delta Z^2>$ values and *AIC* values in model C are larger than the corresponding ones in model B. This indicates that fluctuations are negligible for these modes of the standing part.

In model C, Gauss coefficients g_l^m and h_l^m are represented, respectively, as

$$\begin{aligned} g_l^m(t) &= \{F_l^m + E_l^m \sin\frac{2\pi}{T_{El}^m}(t-\tau_{El}^m)\}\cos\psi_l^m \\ &\quad + \{K_l^m + D_l^m \sin\frac{2\pi}{T_{Dl}^m}(t-\tau_{Dl}^m)\}\cos mv_l^m(t-\tau_l^m), \\ h_l^m(t) &= -\{F_l^m + E_l^m \sin\frac{2\pi}{T_{El}^m}(t-\tau_{El}^m)\}\sin\psi_l^m \\ &\quad - \{K_l^m + D_l^m \sin\frac{2\pi}{T_{Dl}^m}(t-\tau_{Dl}^m)\}\sin mv_l^m(t-\tau_l^m), \end{aligned} \tag{2.47}$$

where F_l^m and ψ_l^m denote the amplitude and the phase angle, E_l^m the amplitude of

periodic variation, T_{El}^m the period, and τ_{El}^m the phase in units of time, for the standing parts. Similarly, K_l^m and τ_l^m denote the amplitude and the phase in units of time, D_l^m the amplitude of periodic variation, T_{Dl}^m the period, and τ_{Dl}^m the phase in units of time, for the drifting parts. A positive value of velocity v_l^m corresponds to the westward drift. The time t is defined here as $t = (T-1800)/100$ with T indicating the year (A.D.). Parameter values used in the present study are shown in Table 2.1.

It should be noted that the secular variation model was derived from the geomagnetic field data spanning only some hundred years, and that the model can be applied only to non-axisymmetric magnetic fields of up to degree six of spherical harmonics.

With respect to axisymmetric meridional magnetic fields, we try to newly analyze secular variations in terms of time variations of Gauss coefficients. We use the same data as used by Shimizu and Honkura (1986) and Matsushima and Honkura (1988). Since axisymmetric magnetic fields have no longitudinal dependence, the drifting part is meaningless. In view of the previous analysis, however, in which fluctuations in the amplitudes of standing and drifting parts are taken into account, we express the time variation of Gauss coefficients g_l^0 as

$$g_l^0(t) = F_l^0 + E_l^0 \sin\frac{2\pi}{T_{El}^0}(t-\tau_{El}^0) + D_l^0 \sin\frac{2\pi}{T_{Dl}^0}(t-\tau_{Dl}^0), \qquad (2.48)$$

that is, two periods are considered; one of which is supposed, by analogy, to correspond to the drifting part. The non-linear inversion scheme which we used to determine variables is described in Shimizu and Honkura (1986). Parameter values which yield the smallest $<\Delta Z^2>$ values are shown in Table 2.2.

These models are useful when we try to calculate fluid motion in the core from geomagnetic field data, since the Earth's magnetic field and its time derivative are easily computed for any specific epoch. It should be noted, however, that the models

Table 2.1. Parameter values for the standing and the drifting parts (Matsushima and Honkura, 1988).

l	m	F (nT)	E (nT)	T_E (y)	τ_E	ψ (deg)	K (nT)	D (nT)	T_D (y)	τ_D	τ	v (deg/y)
1	1	12418	9141	3991	6.50	−122.5	1546	323	271	−0.53	2.21	0.542
2	1	786	826	519	1.17	33.8	2450	129	176	0.14	0.41	0.268
2	2	1365	822	535	2.04	92.3	2029	71	58	0.12	2.35	0.228
3	1	1528	702	643	0.82	−168.6	752	153	98	0.23	−4.57	0.139
3	2	1592	342	312	−0.75	24.6	914	268	268	−0.85	6.23	0.088
3	3	307	335	454	−2.09	−70.7	672	205	655	0.24	1.51	0.260
4	1	698	662	589	2.89	54.6	693	106	266	1.15	2.16	0.224
4	2	602	385	868	−3.30	49.2	308	88	148	0.60	1.81	0.380
4	3	83	54	153	0.71	145.9	317	61	404	1.34	−2.24	0.158
4	4	213	121	430	0.02	69.0	185	67	137	−0.43	1.86	0.232
5	1	328	170	418	−0.45	29.2	62	144	413	0.72	0.03	1.818
5	2	295	56	196	−0.28	3.5	35	117	246	1.11	−1.30	0.420
5	3	73	98	202	−0.46	120.4	77	107	263	−0.76	1.06	0.227
5	4	128	126	248	−0.90	−79.7	213	119	214	−0.85	−13.46	0.021
5	5	108	241	380	0.11	−74.0	185	113	247	0.47	−1.00	0.101
6	1	67	39	209	−0.35	−1.8	19	64	299	0.22	−0.88	1.711
6	2	49	41	242	−0.29	100.3	99	32	410	0.06	4.56	0.147
6	3	162	9	116	0.04	153.0	51	98	274	1.09	−0.66	0.340
6	4	69				151.5	84	130	773	1.91	−1.44	0.287
6	5	65				−92.5	22	53	495	0.46	0.92	0.243
6	6	55	24	55	0.11	173.8	61	23	47	0.15	0.75	0.339

Table 2.2. Parameter values for a secular variation model of meridional magnetic field.

l	m	F (nT)	E (nT)	T_E (y)	τ_E	D (nT)	T_D (y)	τ_D
1	0	−31275	1307	371	1.09	182	77	0.25
2	0	−1361	1379	483	−0.93	49	83	0.33
3	0	959	230	271	0.94	42	15	−0.05
4	0	680	261	503	0.45	21	11	−0.06
5	0	−133	118	317	−0.75	41	59	−0.20
6	0	59	23	82	0.35	21	11	0.00

are valid for a time scale comparable to the period for which data are available. For time variations with short periods, a few decades or so, the present models would be inappropriate and the International Geomagnetic Reference Field (IGRF) and the definitive IGRF (DGRF) are more suitable. DGRF is available for an interval of five years from 1945 to 1980. DGRF 1950, DGRF 1965 and DGRF 1980 (IAGA Division I Working Group 1, 1988) are shown in Table 2.3.

2.5. Physical constants and properties of the Earth and the core

Some physical constants and properties of the Earth and the core must be known in order for a realistic calculation of fluid motion in the core to be possible. The magnetic permeability would be taken as that of vacuum, μ_0. The constant of gravitation is not used in the present study since it is not included in the Navier-Stokes equation for toroidal velocity field.

Some parameters for properties of the Earth and the core are rather well determined from direct observations such as seismic observations; for example, the core radius, the mean density of the core, and the rotation rate of the Earth. Many others, however, are poorly known.

One unknown parameter is the electrical conductivity of the outer core σ, but it has been deduced in various ways. Elsasser (1946) took the value as $\sigma = 10^6$ Sm^{-1}, inferring from the electrical conductivity of iron under ordinary laboratory conditions, while Bullard (1949) took the value as $\sigma = 3\times10^5$ Sm^{-1}. Experiments made for core material at temperatures and pressures far lower than those in the core, indicate that $\sigma = 1\times10^5 \sim 6\times10^5$ Sm^{-1} (Gardiner and Stacey, 1971) and $\sigma = 2.7\times10^5$ Sm^{-1} (Johnston and Strens, 1973). Jain and Evans (1972) proposed $\sigma = 5\times10^5 \sim 1\times10^6$ Sm^{-1} from a model for electrical transport properties of core material. An upper limit, 10^6 Sm^{-1}, for the electrical conductivity of the core was imposed by considering

Table 2.3. The International Geomagnetic Reference Field. DGRF 1950, DGRF 1965 and DGRF 1980 are shown up to degree four, in nT.

		1950		1965		1980	
l	m	g_l^m	h_l^m	g_l^m	h_l^m	g_l^m	h_l^m
1	0	−30554		−30334		−29992	
1	1	−2250	5815	−2119	5776	−1956	5604
2	0	−1341		−1662		−1997	
2	1	2998	−1810	2997	−2016	3027	−2129
2	2	1576	381	1594	114	1663	−200
3	0	1297		1297		1281	
3	1	−1889	−476	−2038	−404	−2180	−336
3	2	1274	206	1292	240	1251	271
3	3	896	−46	856	−165	833	−252
4	0	954		957		938	
4	1	792	136	804	148	782	212
4	2	528	−278	479	−269	398	−257
4	3	−408	−37	−390	13	−419	53
4	4	303	−210	252	−269	199	−297

the amount of heat transferred from the outer core to the mantle (Stacey, 1972). Recent high-pressure experiments indicate that the electrical conductivity of the outer core is close to 1×10^6 Sm^{-1} (e.g. Knittle *el al.*, 1986).

Honkura and Matsushima (1988a) have estimated a lower limit for the electrical conductivity of the core, considering the magnetic Reynolds number R_m defined as $R_m = \mu_0\sigma L_c V_c$, where L_c and V_c denote the characteristic length and velocity, respectively. The evaluation of V_c relies on the method of estimating fluid motion in the outer core by Matsushima and Honkura (1989a). The estimation of velocity field magnitude depends on the value of the electrical conductivity of the core. Honkura and Matsushima (1988a) then took the value of σ as a parameter, derived the characteristic velocity V_c as mean magnitude of velocity field in the quasi-steady case, and examined R_m for various values of σ. The magnetic Reynolds number R_m provides information on magnetic field behavior (e.g. Rikitake and Honkura, 1985). If $R_m \gg 1$, the transport of magnetic lines of force dominates and the magnetic field is possibly maintained as long as the characteristic length for the magnetic field is comparable with that for the velocity field (e.g. Moffat, 1978). Then from the viewpoint of a steady dynamo, Honkura and Matsushima (1988a) claimed that the smallest possible R_m for dynamo action is the order of ten and concluded that the electrical conductivity of the outer core σ must be larger than about 1×10^5 Sm^{-1}. Thus the electrical conductivity of the core is supposed to be in the range of $10^5 \sim 10^6$ Sm^{-1}, and hence in the present study we adopt $\sigma = 3\times10^5$ Sm^{-1}.

The kinematic viscosity of the fluid core ν seems to be the most uncertain parameter. For example, Backus (1968) inferred the value as $\nu = 5\times10^{-3}$ m^2s^{-1}. Suzuki and Sato (1970) obtained the value as $\rho\nu = 3\times10^9 \sim 7\times10^9$ $Nm^{-2}s$ from attenuation of seismic waves. Gans (1972) theoretically derived the value as $\rho\nu = 3.7\times10^{-3} \sim 18.5\times10^{-3}$ $Nm^{-2}s$. If we take the mean density of the core as $\rho =$

1.1×10^4 kgm^{-3}, the kinematic viscosity of the core is in the range of $10^{-7} \sim 10^6$ m^{2}s^{-1}.

It is probable that smaller values correspond to molecular viscosity and larger ones to eddy viscosity. In usual description of dynamics of large-scale motions, the interaction between large-scale and smaller-scale motions is ignored, but it is necessary when the transfer of energy and momentum between the interest scale and the smaller scale is to be discussed (Pedlosky, 1986). For a meteorological phenomenon, eddy viscosity is usually used; for example, a cellular structure like Bénard convection and a vortex street similar to the Kármán vortex street seen in a photo of cloud pattern are explained in terms of eddy viscosity (Kimura, 1988). In this sense, eddy viscosity would be relevant to the present study, although it is beyond the present scope to consider the effect of smaller-scale motions like turbulence on magnetic field generation. Hence we tentatively take the value of the kinematic viscosity of the fluid core as $\nu = 1$ m^{2}s^{-1}.

Physical constants and properties of the Earth and the core used in the present study are summarized in Table 2.4.

Table 2.4. Physical constants and properties of the Earth and the core.

Physical Constants

Quantity	Symbol	Value
Magnetic permeability of vacuum	μ_0	$4\pi\times10^{-7}$ Hm^{-1}
Constant of gravitation	G	6.67×10^{-11} Nm^2kg^{-2}

Physical Properties of the Earth and the Core

Quantity	Symbol	Value
Equivolume sphere radius of Earth	r_e	6.371×10^6 m
Core radius	r_{oc}	3.485×10^6 m
Inner core radius	r_{ic}	1.217×10^6 m
Mean density of core	ρ	1.1×10^4 kgm^{-3}
Rotation rate of Earth	Ω	7.29×10^{-5} s^{-1}
Electrical conductivity	σ	3×10^5 Sm^{-1}
Kinematic viscosity	ν	1 m^2s^{-1}

3. Results

We derive fluid motion in the Earth's outer core from geomagnetic field data step by step for several cases. In Cases 1 and 2, inducing magnetic fields for the generation of non-axisymmetric poloidal magnetic fields are assumed to be zonal toroidal magnetic fields which are expected to be generated by the interaction between the axial dipole magnetic field and a zonal toroidal motion. It is then assumed that the non-axisymmetric poloidal magnetic fields are maintained simply by the interaction between poloidal velocity fields and the zonal toroidal magnetic fields. In Cases 3, 4 and 5, the axisymmetric poloidal magnetic fields are also considered as inducing magnetic fields. In Cases 6 and 7, non-zonal toroidal velocity and non-zonal toroidal magnetic fields are further taken into consideration. The inducing magnetic fields for the non-axisymmetric poloidal magnetic fields are then assumed to be the toroidal and the axisymmetric poloidal magnetic fields. In Cases 2, 5 and 7, an axisymmetric poloidal velocity field, which gives rise to zonal toroidal motions, is added with its magnitude varied variously. We first summarize the cases, for which fluid motion in the Earth's outer core is derived, and the inducing magnetic fields, which are assumed in the computation for respective cases, in Table 3.1.

As mentioned in Subsection 2.3, we must solve non-linear simultaneous algebraic equations, which do not generally guarantee the uniqueness of a solution. Therefore, we must somehow check the validity of solutions. One method would be to examine time-dependent behavior of the magnetic field with the derived velocity field fixed. If we derived an unrealistic fluid motion in the core, the magnetic field would diverge or decay within a short time, because some other induction terms, which should have been taken into account in deriving velocity field, must also be important in maintaining a steady magnetic field. The validity of solutions will be checked in Section

Table 3.1. The cases for which fluid motion in the Earth's outer core is derived, and the inducing magnetic fields which are assumed in the computation for respective cases.

Case	Inducing magnetic field	Additional velocity field
1	Zonal toroidal magnetic field $\boldsymbol{B}[T_\beta^0]$	
2	Zonal toroidal magnetic field $\boldsymbol{B}[T_\beta^0]$	Meridional circulation $\boldsymbol{V}[S_2^0]$
3	Zonal toroidal magnetic field $\boldsymbol{B}[T_\beta^0]$ Axial dipole magnetic field $\boldsymbol{B}[S_1^0]$	
4	Zonal toroidal magnetic field $\boldsymbol{B}[T_\beta^0]$ Axisymmetric poloidal magnetic field $\boldsymbol{B}[S_\beta^0]$	
5	Zonal toroidal magnetic field $\boldsymbol{B}[T_\beta^0]$ Axisymmetric poloidal magnetic field $\boldsymbol{B}[S_\beta^0]$	Meridional circulation $\boldsymbol{V}[S_2^0]$
6	Toroidal magnetic field $\boldsymbol{B}[T_\beta]$ Axisymmetric poloidal magnetic field $\boldsymbol{B}[S_\beta^0]$	
7	Toroidal magnetic field $\boldsymbol{B}[T_\beta]$ Axisymmetric poloidal magnetic field $\boldsymbol{B}[S_\beta^0]$	Meridional circulation $\boldsymbol{V}[S_2^0]$

4.

3.1. Reexamination of preliminary calculation

3.1.1. The results of Matsushima and Honkura

As mentioned in Section 1, Matsushima and Honkura (1989a) derived fluid motion in the core based on the presumption that a strong toroidal magnetic field $\boldsymbol{B}[T_2^0]$ is generated by the interaction between a differential rotation $\boldsymbol{V}[T_1^0]$ and the axial dipole magnetic field $\boldsymbol{B}[S_1^0]$ in the core. The factors taken into account in the calculation are $\boldsymbol{V}[T_1^0]\times\boldsymbol{B}[S_1^0]$ (the ω-effect), $\boldsymbol{V}[S_l^m]\times\boldsymbol{B}[T_2^0]$ as induction processes, and the balance, in spherical shells, between the electromagnetic torque due to the Lorentz force $(\mu_0)^{-1}(\nabla\times\boldsymbol{B}[T_2^0])\times\boldsymbol{B}[S_1^0]$ and the effective torque due to the angular momentum transfer expected from virtual displacement of fluid particles. The torque balance yielded the differential rotation $\boldsymbol{V}[T_1^0]$. Matsushima and Honkura (1989b) further expanded the method and took into account the meridional dependence of differential rotation; that is, $\boldsymbol{V}[T_l^0]$ and $\boldsymbol{B}[T_l^0]$ ($l \leq 6$) were all considered.

We first show the results of Matsushima and Honkura (1989b; unpublished result) in Fig. 3.1; (a) the distribution of angular velocity, (b) the distribution of strength of zonal toroidal magnetic field, and (c) the poloidal velocity field on the equatorial and the two meridional planes at the epoch of 1980 AD. For geomagnetic field data, model C of Matsushima and Honkura (1988) has been used except for $(l, m) = (6, 4)$ and $(6, 5)$, as mentioned in Subsection 2.4.

It is clearly seen from Fig. 3.1(a) that the differential rotation cannot be represented by $\boldsymbol{V}[T_1^0]$, even in an approximate sense, contrary to Matsushima and Honkura (1989a), and the meridional dependence is striking. The zonal toroidal motion is westward near the equator and eastward near the poles. This feature is similar to the result of Olson (1989), although the magnitude of rotation rate is

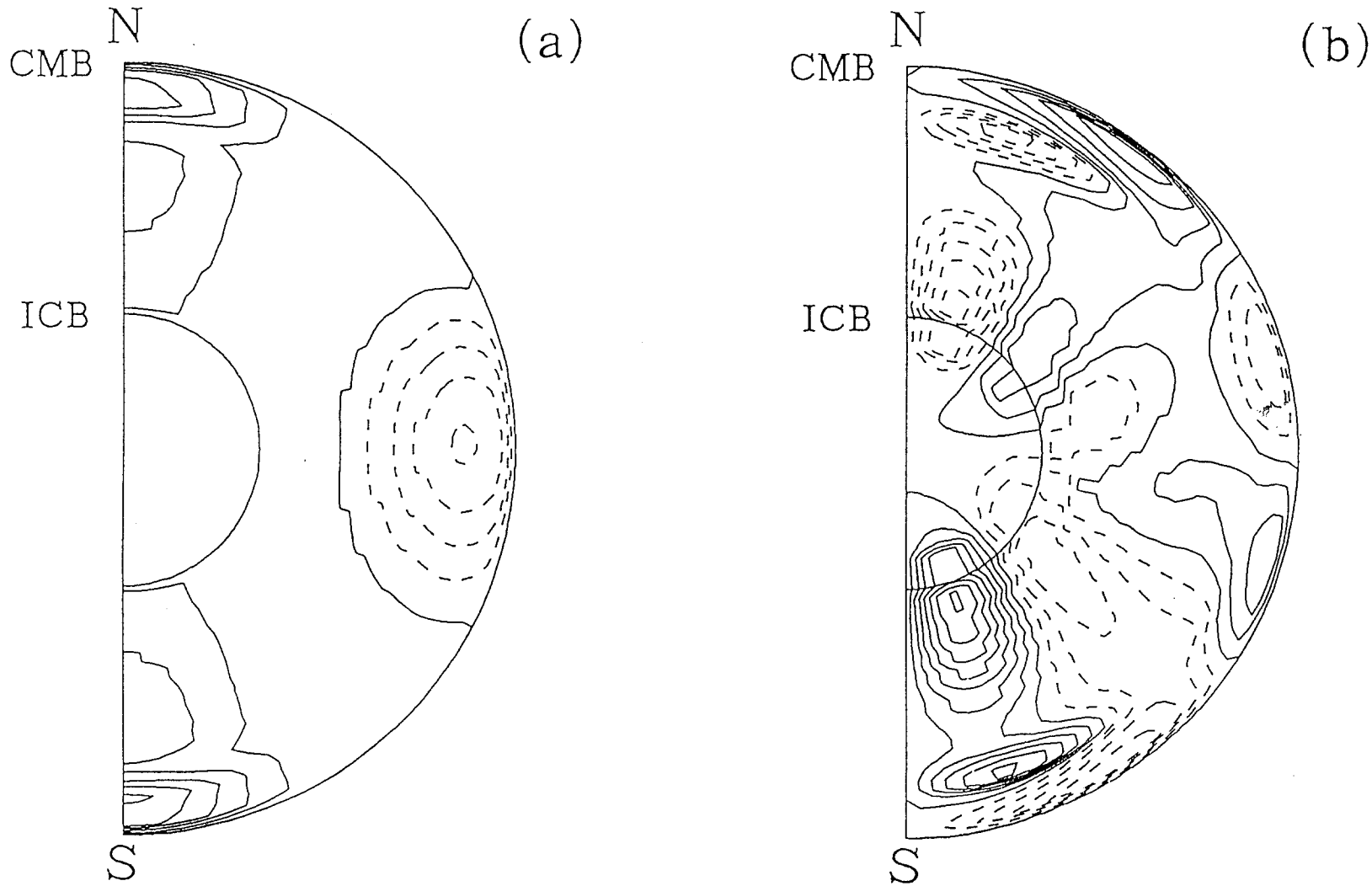

Fig. 3.1. (a) Distribution of angular velocity in the outer core. Solid contours indicate positive (eastward) values in units of 10^{-9} rad·s^{-1} and broken contours negative (westward) values. (b) Distribution of zonal toroidal magnetic fields. Solid contours indicate positive values in units of 2×10^{-3} T and broken contours negative values.

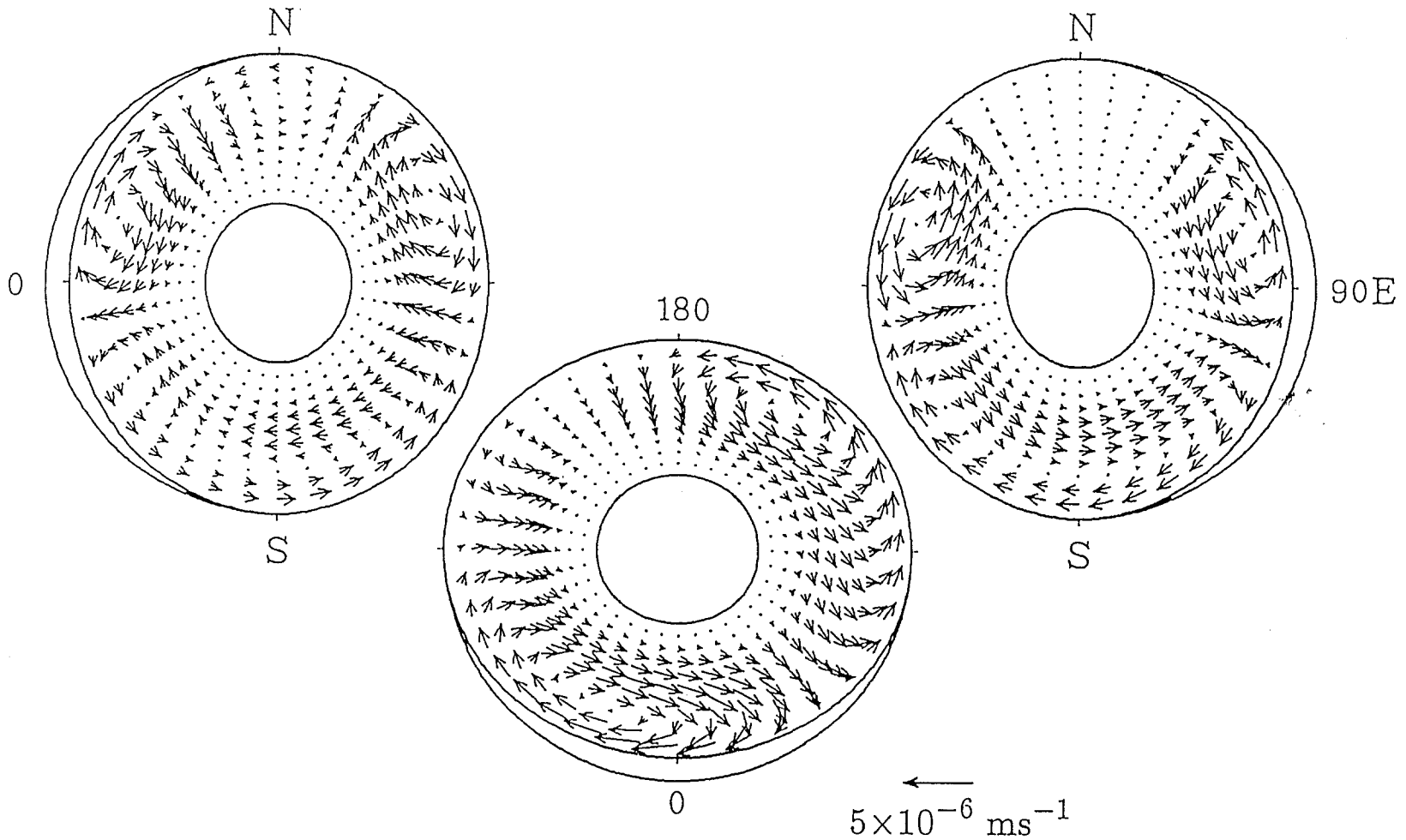

Fig. 3.1. (c) Poloidal velocity fields on the equatorial plane and on the meridional planes for the epoch of 1980 AD. The arrow for scale length corresponds to 5×10^{-6} ms^{-1}.

generally larger in this case; about 5° year^{-1} in maximum. The zonal toroidal magnetic field generated by the interaction between the axial dipole magnetic field and the differential rotation mainly consists of $\boldsymbol{B}[T_2^0]$ and $\boldsymbol{B}[T_4^0]$ with magnitude of the order of $10^{-3} \sim 10^{-2}$ T, as seen in Fig. 3.1(b). The magnitude of poloidal velocity field shown in Fig. 3.1(c) is much smaller than that of Matsushima and Honkura (1989a). This discrepancy is interpreted as follows.

We may define the magnetic Reynolds number characteristic of the ω-effect R_ω as

$$R_\omega = \omega_c L_c^2 / \nu_m, \tag{3.1}$$

where ω_c is a characteristic angular velocity and L_c a characteristic length. The radial motion which induces poloidal magnetic fields from toroidal magnetic fields tends to become weaker with increasing R_ω (Roberts and Gubbins, 1987). In Matsushima and Honkura (1989a), only $\boldsymbol{B}[T_2^0]$ was taken as the inducing magnetic field and strong toroidal magnetic field regions were located in the deeper parts of the core. In the case shown in Fig. 3.1, the inducing magnetic fields are $B[T_l^0]$ $(l \leq 6)$ and some of the strong toroidal magnetic field regions are located near the CMB. It is then expected that a poloidal magnetic field is easily induced by a weak poloidal velocity field in the presence of such a strong toroidal magnetic field. This represents one class of typical velocity field in $\alpha\omega$-dynamos; that is, a strong ω-effect due to a strong zonal toroidal motion combined with a weak poloidal motion.

3.1.2. Case 1

We here reexamine the results of Matsushima and Honkura (unpublished work) as Case 1. In the induction equation, we take into account $\boldsymbol{V}[T_l^0] \times \boldsymbol{B}[S_1^0]$ and $\boldsymbol{V}[S_\alpha] \times \boldsymbol{B}[T_l^0]$ as in Matsushima and Honkura (1989b), whereas in the Navier-Stokes

equation for toroidal motion, the Lorentz force $(\mu_0)^{-1}(\nabla\times\boldsymbol{B}[T_l^0])\times\boldsymbol{B}[S_1^0]$ and the advection terms are both considered, since a differential rotation would arise from the non-linear momentum transport of the convection (Busse, 1970).

No information is available on the radial dependence of the axial dipole magnetic field $\boldsymbol{B}[S_1^0]$ in the core. Here we simply adopt the radial dependence for the longest free-decay mode as in Matsushima and Honkura (1989a). The free-decay time is given by $\mu_0\sigma r_{oc}^2/\pi^2$ (Elsasser, 1946) and amounts to 1.5×10^4 years for $\sigma = 3\times10^5$ Sm^{-1} taken in the present study. This time is much longer than the characteristic time for non-dipole magnetic fields, and hence the dipole magnetic field is assumed to be steady. The scalar function is expressed as

$$B[S_1^0](r) = B_{S10}r^{1/2}J_{3/2}(\pi r/r_{oc}), \tag{3.2}$$

where $J_{3/2}(z)$ is a Bessel function. B_{S10} is a constant determined by the boundary condition at $r = r_{oc}$.

It is assumed that both the CMB and the ICB are rigid boundaries as in Matsushima and Honkura (1989a), and the radial dependence of poloidal velocity field given in (2.43) is used. We tentatively set the truncation levels L and N at 4 and 9, respectively. Unknowns are zonal toroidal velocity fields $V[_nT_l^0]$, non-axisymmetric poloidal velocity fields $U[S_l^{mz}]$, zonal toroidal magnetic fields $B[_nT_l^0]$, and non-axisymmetric poloidal magnetic fields $B[_nS_l^{mz}]$. The total number of unknowns in this case is $L(L+3)(N+1)+L(L+1) = 300$.

The result is completely different from the previous one when we solve both the induction and the Navier-Stokes equations in order to derive fluid motion in the core. Figure 3.2 shows an example obtained in the present study; (a) the distribution of angular velocity and (b) the distribution of zonal toroidal magnetic field at the epoch of 1980 AD. The pattern of zonal toroidal velocity field is similar to that shown in

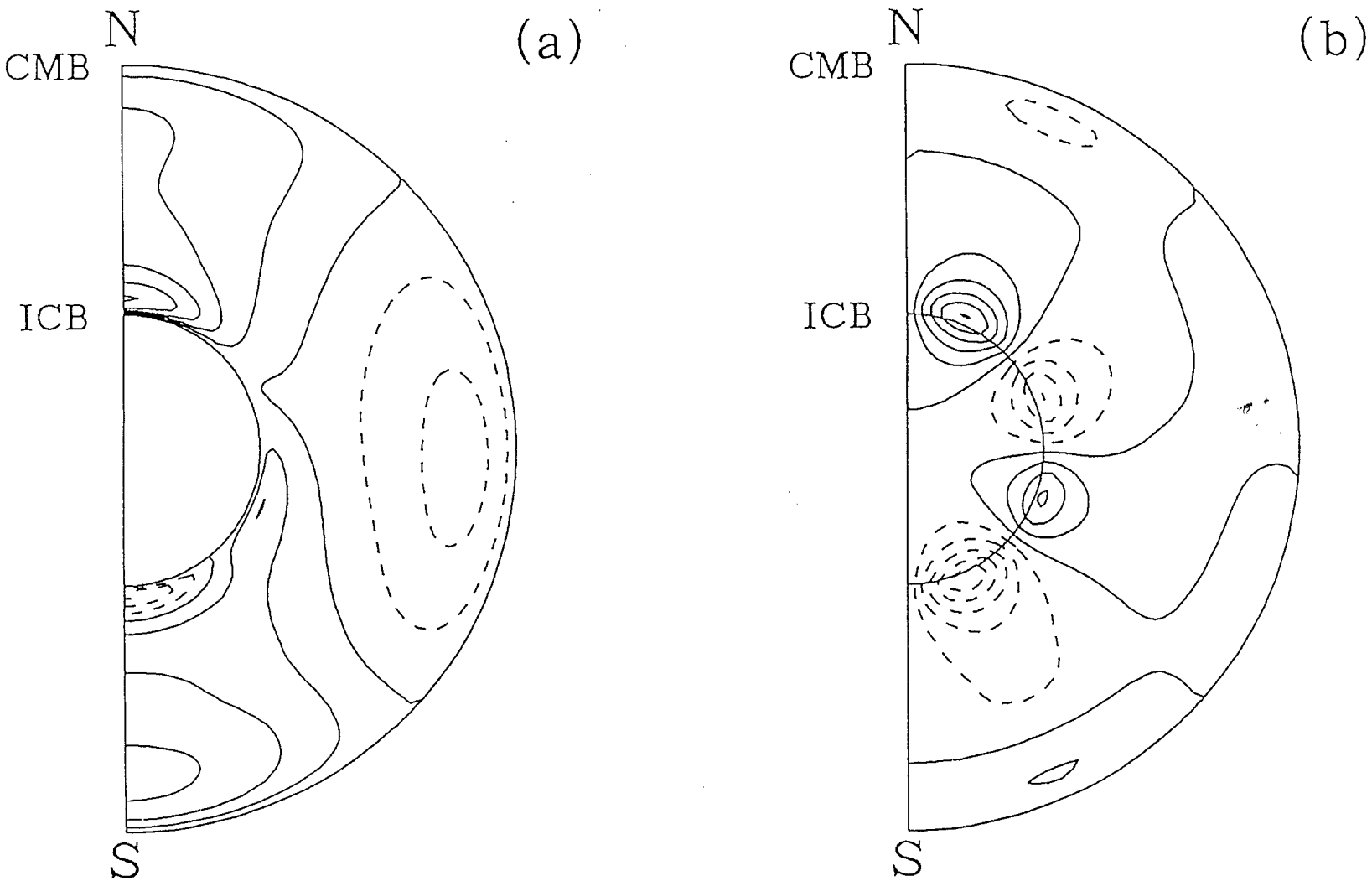

Fig. 3.2. (a) Distribution of angular velocity in the outer core. Solid contours indicate positive (eastward) values in units of 2×10^{-12} rad·s^{-1} and broken contours negative (westward) values. (b) Distribution of zonal toroidal magnetic fields. Solid contours indicate positive values in units of 2×10^{-5} T and broken contours negative values. These were derived for Case 1.

Fig. 3.1(a); that is, the flow is westward near the equator and eastward near the poles, although we see a strange flow pattern, which is not seen in Fig. 3.1(a), near the ICB.

The most notable difference is that the magnitude of zonal toroidal motion is much smaller than that of zonal toroidal motion shown in Fig. 3.1(a). It has been supposed that a strong zonal toroidal magnetic field would be generated by the interaction between the dipole magnetic field and the differential rotation (shear motion). However a slow zonal toroidal motion results in insufficient shear, and hence the strength of zonal toroidal magnetic field, generated by the ω-effect, shown in Fig. 3.2(b) is much weaker than that in Fig. 3.1(b). The magnitude of poloidal velocity field is accordingly much larger than that in Fig. 3.1(c); we should recall the assumption that non-axisymmetric poloidal magnetic fields are generated only by the interaction between poloidal convective motions and zonal toroidal magnetic fields.

The overall velocity field is shown in Fig. 3.3; one velocity vector is plotted, in Fig. 3.3(a), at each point of a regular grid in colatitude θ and longitude ϕ on a cylindrical equidistant projection. The length of each vector is linearly proportional to the flow speed at the mesh point, and the arrow for scale length is plotted at lower right of the figure. The outlines of the continents are shown only for reference. In Fig. 3.3(b), the velocity fields on the equatorial plane (center) and on the meridional planes passing through $\phi = 0°-180°$ (left) and $\phi = 90°-270°$ (right) are shown. The arrow for scale length is plotted as in Fig. 3.3(a). It is clearly seen from Fig. 3.3 that the poloidal velocity field is dominant. Judging from the result that zonal toroidal magnetic fields are not so strong, the presumption that non-axisymmetric poloidal magnetic fields are generated only by the interaction between zonal toroidal magnetic fields and poloidal convective motions will fail under the condition we imposed for Case 1. Thus modification of the method is required.

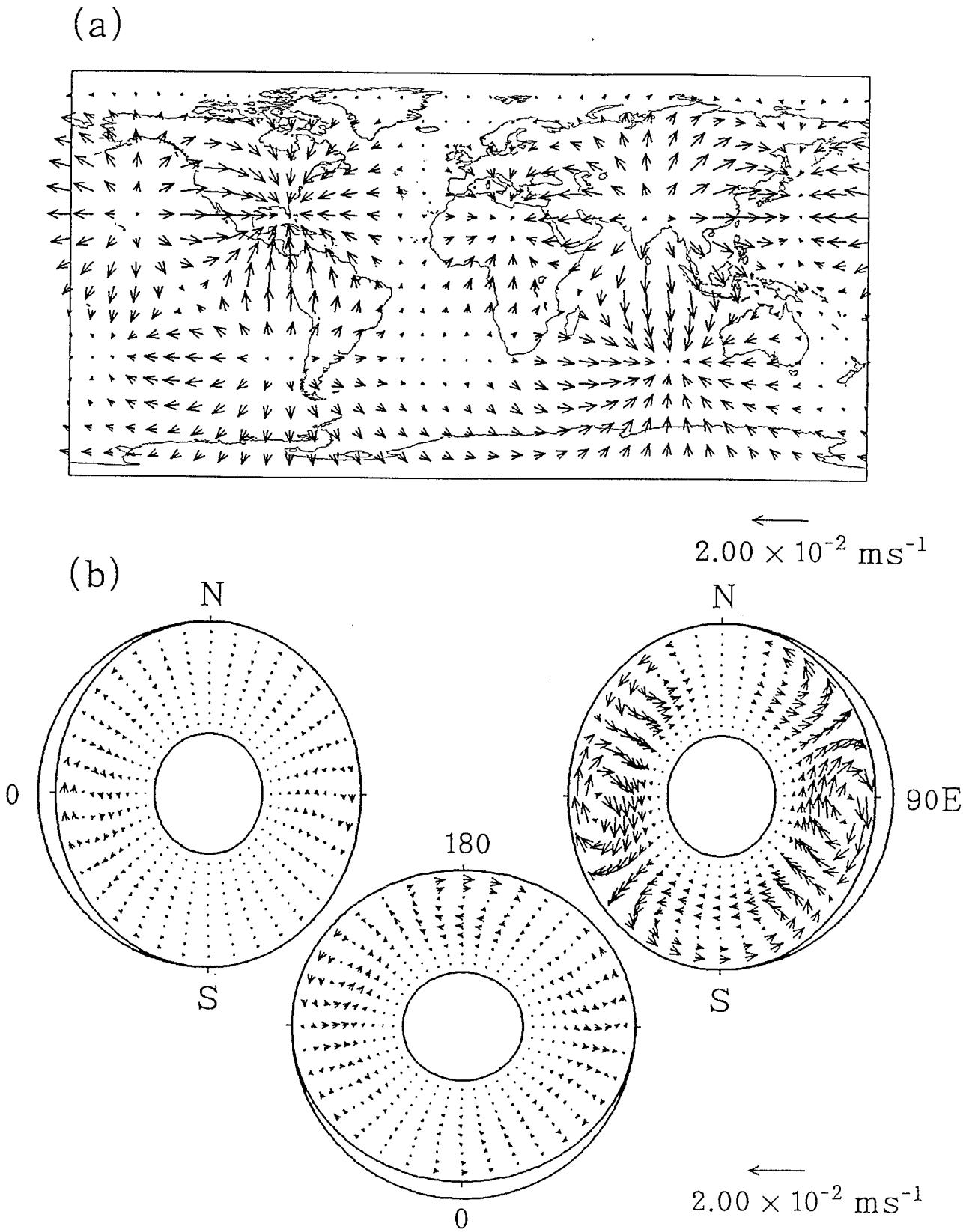

Fig. 3.3. (a) Horizontal velocity field at $r = 0.95r_{oc}$ and (b) the overall velocity fields on the equatorial plane and on the meridional planes for the epoch of 1980 AD in Case 1. The arrow for scale length corresponds to 2×10^{-2} ms^{-1}.

3.2. Introduction of meridional circulation (Case 2)

So far meridional circulation has not been taken into consideration in deriving fluid motion in the core. The poloidal motion can create a zonal toroidal motion through the interaction term $(V[S_\alpha]S_1^\Omega S_\gamma)$ in (2.8). We here add a meridional poloidal velocity field $\boldsymbol{V}[S_2^0]$, which is related to $\boldsymbol{V}[T_1^0]$ and $\boldsymbol{V}[T_3^0]$. This meridional motion possesses only one convection cell in the Northern and the Southern Hemispheres, respectively. The magnitude $U[S_2^0]$ is unknown, however, as long as the derivation of fluid motion in the core is based on the presumption that inducing magnetic fields are strong zonal toroidal magnetic fields alone, generated by the ω-effect. This is because the interaction of meridional motion with zonal toroidal magnetic field $\boldsymbol{V}[S_\alpha^0]\times\boldsymbol{B}[T_\beta^0]$ generates no poloidal magnetic field, as verified from one of the selection rules given in Bullard and Gellman (1954). We put the superscript 0 explicitly, to emphasize the field of order $m = 0$ of spherical harmonics, in spite of our abbreviation that Greek letters appearing as a subscript denote the set of (l, m, z). We here take the magnitude $U[S_2^0]$ as a parameter to examine the effect of meridional circulation. This is Case 2.

In a model considered by Roberts and Stix (1972), for example, the value of $U[S_2^0]$ is negative when dynamo action occurs most easily. A negative value of $U[S_2^0]$ corresponds to a meridional flow in which the fluid rises near the equator and sinks near the poles. Here we tentatively consider only negative values of $U[S_2^0]$, although the above result would depend on models.

For $U[S_2^0] = -10^{-5}$ with the radial dependence given in (2.43), we show the distributions of angular velocity and zonal toroidal magnetic field derived for Case 2 in Fig. 3.4. Contour intervals in Fig. 3.4 are the same as in Fig. 3.2. It is found that too slow meridional circulation little affects zonal toroidal motion. The overall velocity field shown in Fig. 3.5 is also nearly the same as that shown in Fig. 3.3.

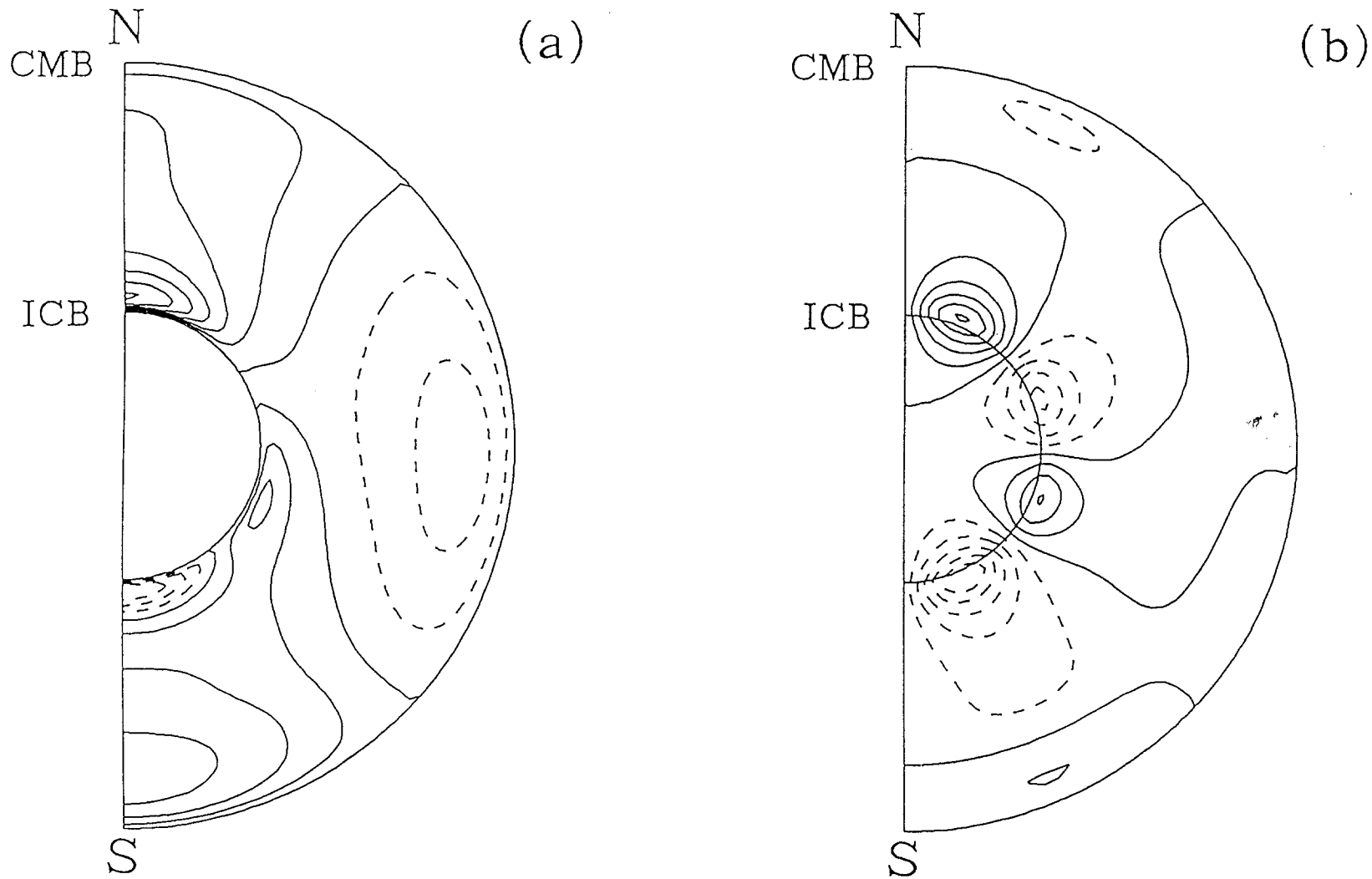

Fig. 3.4. (a) Distribution of angular velocity in the outer core. Solid contours indicate positive (eastward) values in units of 2×10^{-12} rad·s^{-1} and broken contours negative (westward) values. (b) Distribution of zonal toroidal magnetic fields. Solid contours indicate positive values in units of 2×10^{-5} T and broken contours negative values. These were derived for Case 2.

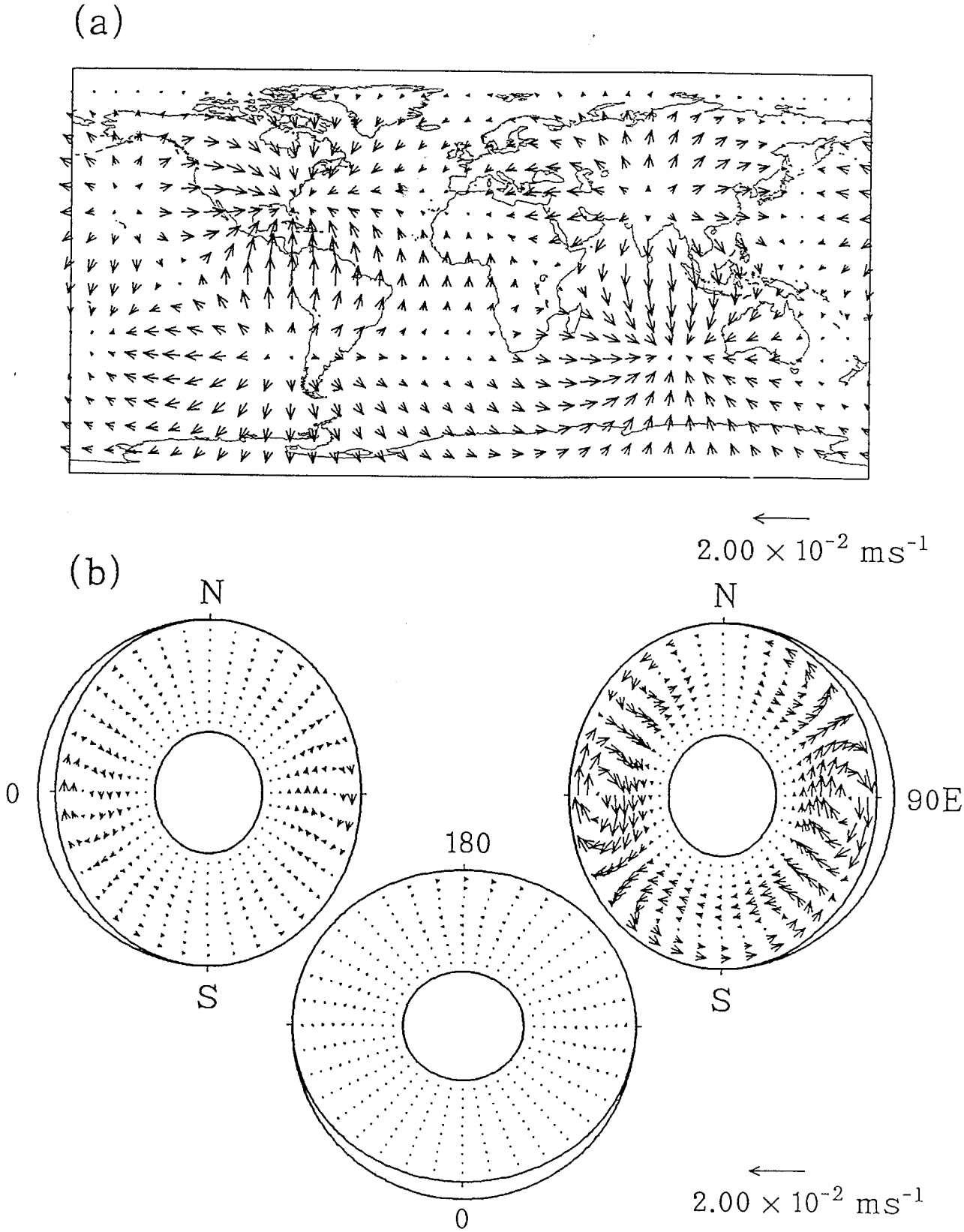

Fig. 3.5. (a) Horizontal velocity field at $r = 0.95 r_{oc}$ and (b) the overall velocity fields on the equatorial plane and on the meridional planes for the epoch of 1980 AD in Case 2. The arrow for scale length corresponds to 2×10^{-2} ms^{-1}.

Once we take a larger value such as $U[S_2^0] = -10^{-3}$, however, the results are different. Figure 3.6 shows the distributions of angular velocity and zonal toroidal magnetic field in the core for the case $U[S_2^0] = -10^{-3}$. Contour intervals are five times larger than those in Fig. 3.4. It is then expected that the magnitude of derived poloidal velocity field is reduced, since inducing magnetic fields are enhanced than in Case 1.

Figure 3.7 shows the overall velocity field, the pattern of which is different from previous results, but the magnitude is not significantly different. This may be a result of non-linearity of the problem or a slight difference in the zonal toroidal magnetic field distribution from the previous ones. Whichever is the case, a problem remains; that is, even if a meridional poloidal motion is taken into consideration, the strength of zonal toroidal magnetic field is very weak, of the order of 10^{-4} T. Hence we must not rely on the presumption that strong zonal toroidal magnetic fields, generated by the ω-effect, are the primary inducing magnetic fields, at least under the condition we imposed in Case 2.

In addition, we must consider another problem. We have so far employed rigid boundary conditions at the CMB and the ICB. These conditions may not be reasonable. The Ekman number E, defined as $E = \nu/\Omega L^2$, is of the order of 10^{-9} for a value of kinematic viscosity, $\nu = 1$ m^{2}s^{-1}, taken in the present study. If we take the value as $\nu = 10^{-6}$ m^{2}s^{-1}, which would correspond to the molecular viscosity, E amounts to 10^{-15}. This suggests that an Ekman layer $10^{-1} \sim 10^2$ m thick would be set up, and in this layer, fluid flow would adjust itself to the physical boundary condition imposed through the contact with a solid. It is impossible to resolve the boundary layer with the truncation level for Chebyshev polynomials, $N = 9$ or so. It would be better to impose stress-free boundary conditions.

If both the CMB and the ICB are stress-free, however, a problem arises for a

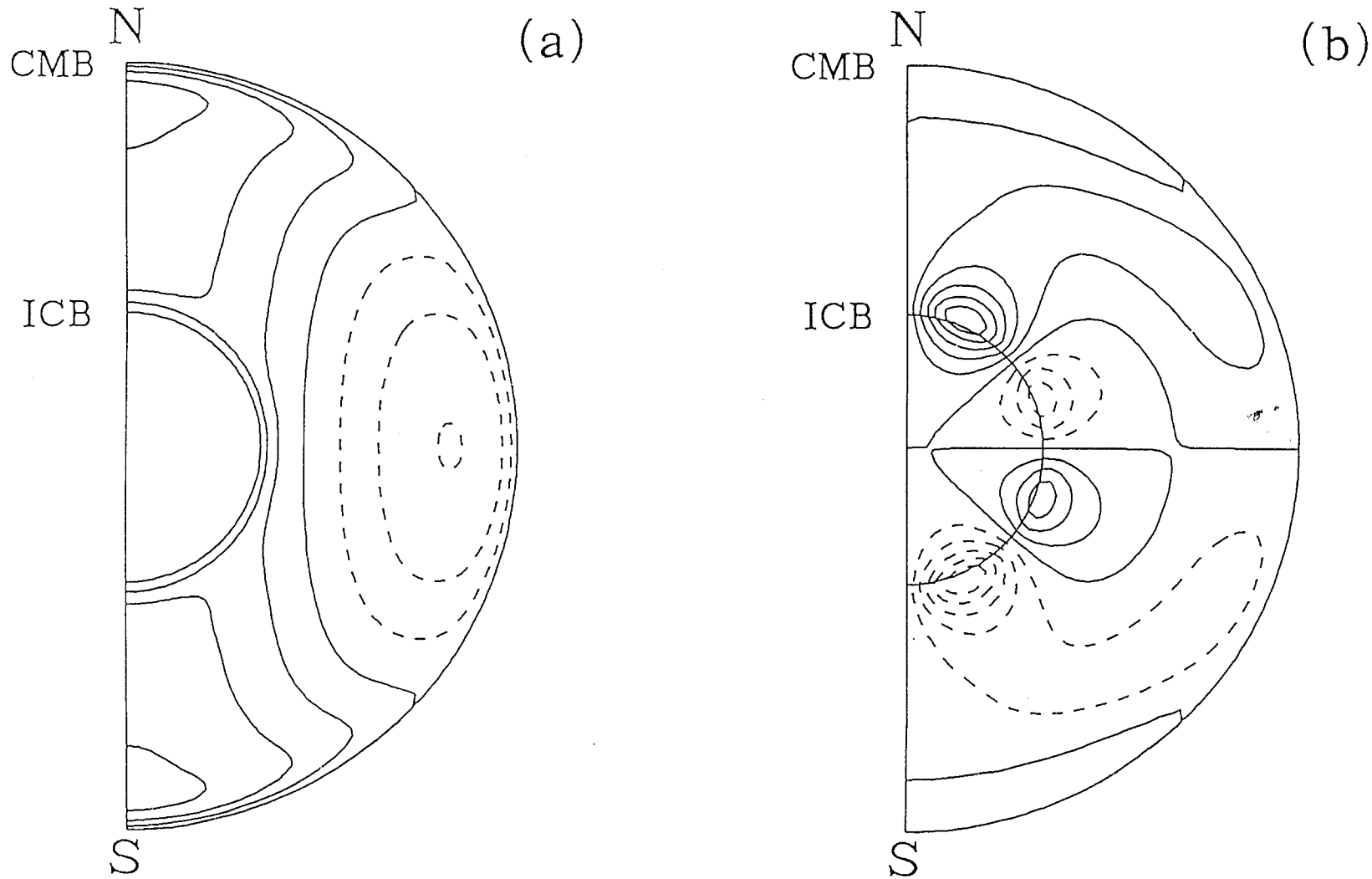

Fig. 3.6. (a) Distribution of angular velocity in the outer core. Solid contours indicate positive (eastward) values in units of 1×10^{-11} rad·s^{-1} and broken contours negative (westward) values. (b) Distribution of zonal toroidal magnetic fields. Solid contours indicate positive values in units of 1×10^{-4} T and broken contours negative values. These were derived for Case 2.

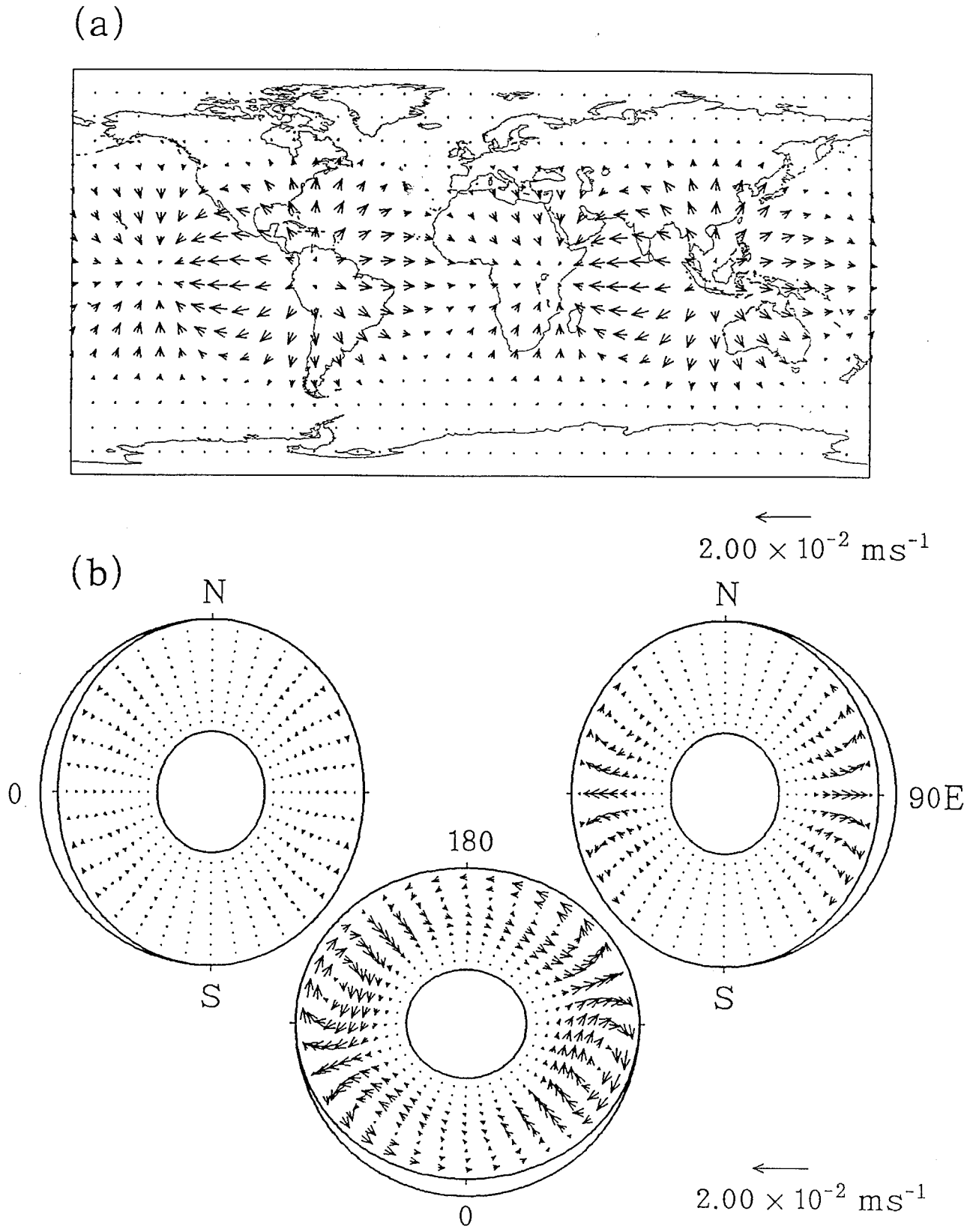

Fig. 3.7. (a) Horizontal velocity field at $r = 0.95r_{oc}$ and (b) the overall velocity fields on the equatorial plane and on the meridional planes for the epoch of 1980 AD in Case 2. The arrow for scale length corresponds to 2×10^{-2} ms^{-1}.

zonal toroidal velocity field $V[T_1^0]$. We have expressed the radial dependence, $V[T_1^0](r)$, in Chebyshev polynomials. Alternatively it is possible to expand it into power series with respect to r. These are equivalent to each other. For the term of r^2 in $V[T_1^0]$, the diffusion term vanishes; that is,

$$\left[\frac{d^2}{dr^2} - \frac{2}{r^2}\right] r^2 = 0.$$

Moreover, in the equation governing the boundary condition for free surfaces, the coefficient for the term of r^2 is always equal to zero; see equation (2.41). If we do not take into account meridional circulation and non-zonal toroidal motion, the advection term $[V[T_\alpha]\, V[S_\beta] S_\gamma]$ also vanishes for zonal toroidal motion. Even in this case, the coefficient matrix, which appears in the equation to be solved by a Newton method, is not singular, since the matrix elements, corresponding to the ω-effect in the induction equation for zonal toroidal magnetic fields, do not vanish. When we are to consider a steady state, we need some terms to restrict time evolution such as a viscous force term, but we can find nothing. As a result, a nearly free-body rotation of the outer core is permitted. This may be allowed at the CMB because the mantle is insulating. By contrast, strong shear at the ICB would generate a strong magnetic field, which is expected to inhibit the zonal motion. Hence, in the present study, we may presume that the CMB is free but the ICB is rigid.

From now on we will take the radial dependence of poloidal velocity field given in (2.44).

3.3. The cases including the dipole magnetic field as an inducing magnetic field

3.3.1. Case 3

In the above, we have found that zonal toroidal magnetic fields are not so strong

as long as we take into consideration the interactions as considered so far. Here we direct our attention toward the poloidal magnetic field. The strongest one is obviously the axial dipole magnetic field $\boldsymbol{B}[S_1^0]$. For example, Yokoyama and Yukutake (1990) examined general characteristics of induced magnetic fields in the steady state, taking the dipole magnetic field $\boldsymbol{B}[S_1^0]$ and the toroidal magnetic field $\boldsymbol{B}[T_2^0]$ as inducing magnetic fields. As the next step, then, we extend the previous approach so as to include the dipole magnetic field as one of the inducing magnetic fields.

In this case (Case 3), we add the interaction term $\boldsymbol{V}[S_\alpha]\times\boldsymbol{B}[S_1^0]$ to the induction equation for the poloidal magnetic field in order to derive fluid motion in the core. The scalar function for the axial dipole magnetic field is given in (3.2). The total number of unknowns is the same as in Cases 1 and 2.

As shown in Fig. 3.6, the strength of zonal toroidal magnetic field may be comparable with that of the dipole magnetic field. We therefor include not only the dipole field but also zonal toroidal magnetic fields as inducing magnetic fields.

We show the distributions of angular velocity and zonal toroidal magnetic field in Fig. 3.8 and the overall velocity field in Fig. 3.9 at the epoch of 1980 AD in Case 3. The distribution of angular velocity is clearly different from that shown in Fig. 3.2(a), whereas the distribution of zonal toroidal magnetic field is similar to that shown in Fig. 3.2(b), although the strength in Fig. 3.9(b) is weaker than that shown in Fig. 3.2(b). These arise from the free CMB condition. In order to confirm this, we show, in Fig. 3.10, the distributions of angular velocity and zonal toroidal magnetic field obtained in Case 1 under the free CMB condition. If Fig. 3.10 is compared with Fig. 3.2, the strength of zonal toroidal magnetic field in Fig. 3.10 is twice that shown in Fig. 3.2, although the angular velocity in Fig. 3.10 is hundred times larger than that shown in Fig. 3.2. This implies that the distribution of angular velocity in the core under the free CMB condition hampers the generation of strong zonal toroidal

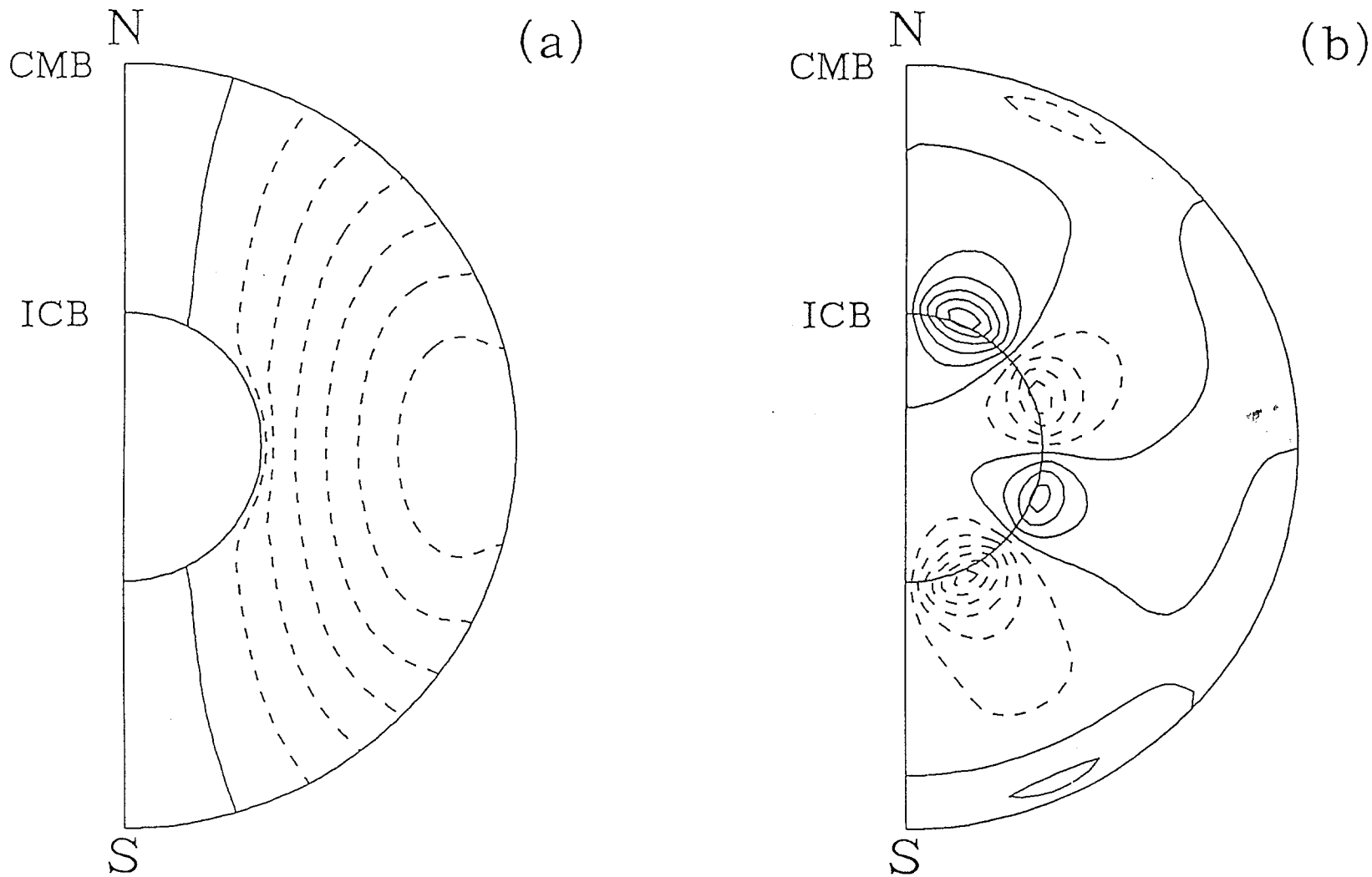

Fig. 3.8. (a) Distribution of angular velocity in the outer core. Solid contours indicate positive (eastward) values in units of 5×10^{-12} rad·s^{-1} and broken contours negative (westward) values. (b) Distribution of zonal toroidal magnetic fields. Solid contours indicate positive values in units of 1×10^{-6} T and broken contours negative values. These were derived for Case 3.

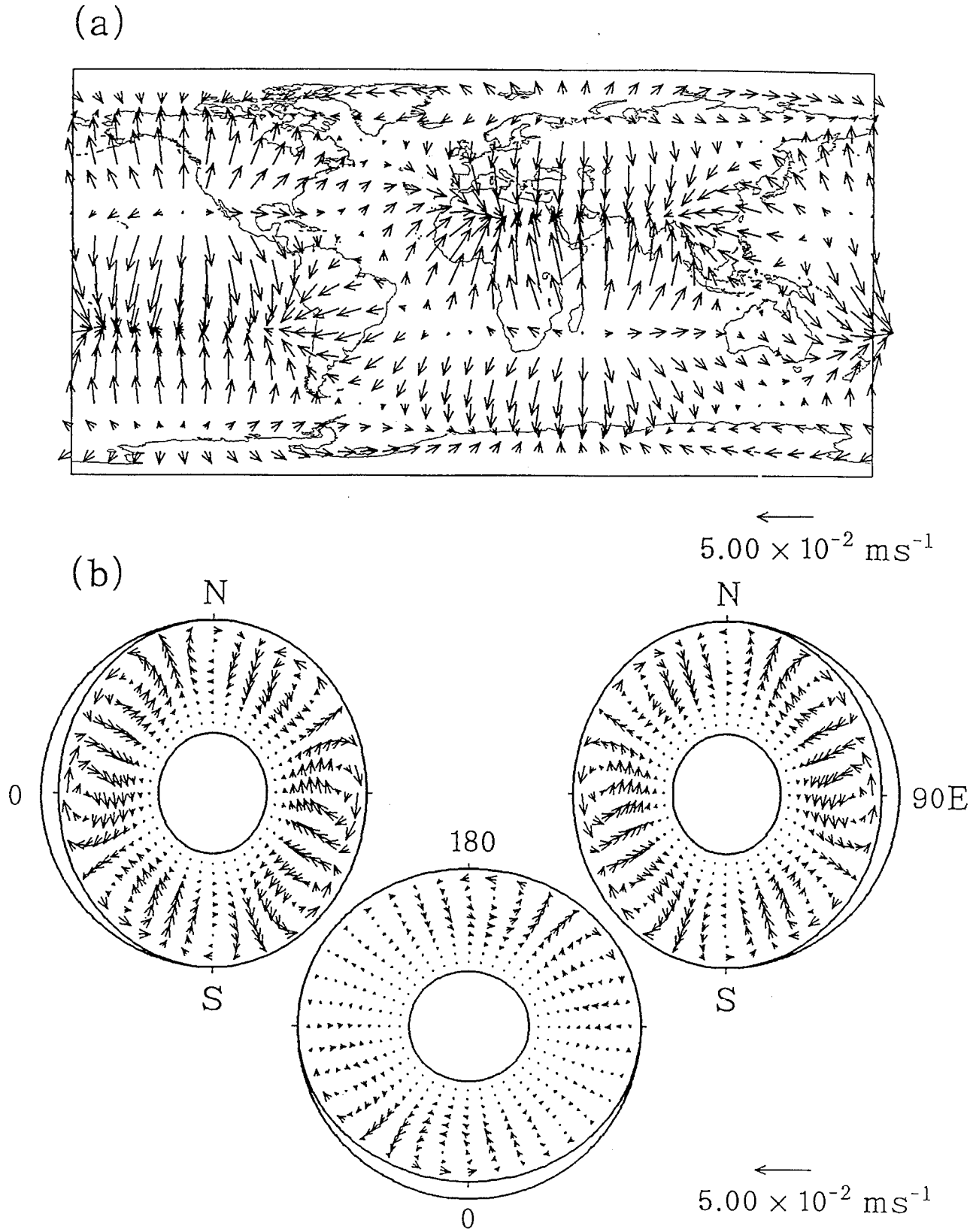

Fig. 3.9. (a) Horizontal velocity field at the core surface and (b) the overall velocity fields on the equatorial plane and on the meridional planes for the epoch of 1980 AD in Case 3. The arrow for scale length corresponds to 5×10^{-2} ms^{-1}.

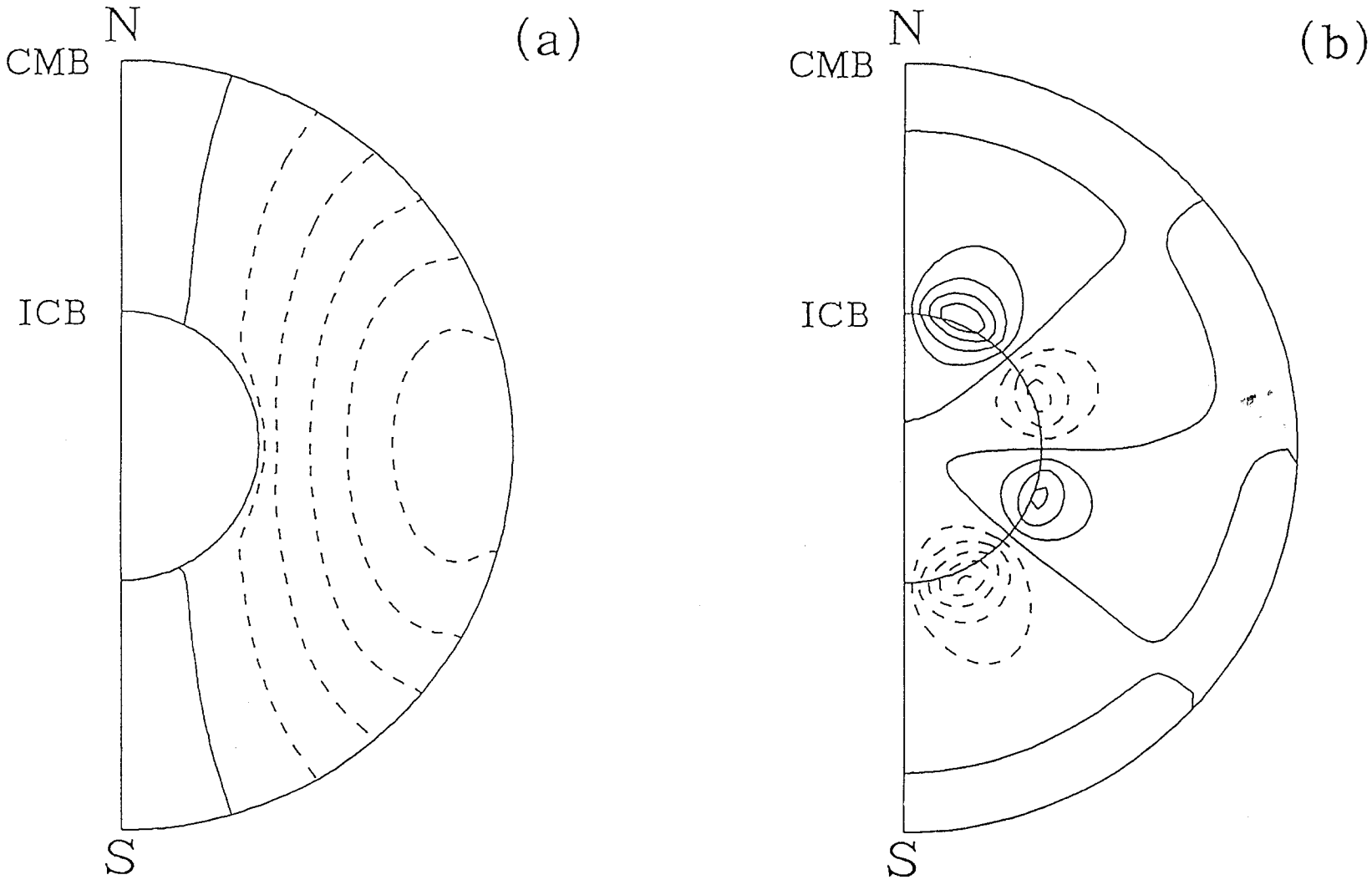

Fig. 3.10. (a) Distribution of angular velocity in the outer core. Solid contours indicate positive (eastward) values in units of 2×10^{-10} rad·s^{-1} and broken contours negative (westward) values. (b) Distribution of zonal toroidal magnetic fields. Solid contours indicate positive values in units of 4×10^{-5} T and broken contours negative values. These were derived for Case 1 under the free CMB condition.

magnetic field. On the other hand, contour intervals in Fig. 3.10 is forty times larger than those in Fig. 3.8, but characteristics of the distributions are similar to each other. This implies that the assumption made to derive fluid motion in the core strongly controls the magnitude of zonal toroidal velocity field and strength of zonal toroidal magnetic field, but the characteristics of the distributions are little affected by the assumption. Then it is likely that the weaker zonal toroidal magnetic field is due not to the assumption made in Case 3 but to the free CMB condition.

For Case 3, we show another solution in Figs. 3.11 and 3.12, where the distributions of angular velocity and zonal toroidal magnetic field in the core and the overall velocity field are shown, respectively. So far we have obtained zonal toroidal flow which is westward near the equator and eastward near the poles. The zonal toroidal flow shown in Fig. 3.11(a) is opposite; that is, the flow is eastward near the equator, as is the case for the Sun's surface. Contour intervals in Fig. 3.11 are hundred times larger than those in Fig. 3.8. It may be expected then that the magnitude of poloidal velocity field is smaller than that shown in Fig. 3.9, but this is not the case. This result arises from competition between dominant inducing magnetic fields. We will discuss this feature in Section 5.

3.3.2. Case 4

We next take other axisymmetric poloidal magnetic fields as inducing magnetic fields in order to examine their effect on the solution (Case 4). The radial dependence of the axisymmetric poloidal magnetic fields in the core is not known, and we again assume the longest free-decay mode for each degree of spherical harmonics as in the case of the axial dipole magnetic field. The scalar function of free-decay mode for the poloidal magnetic field with degree l is expressed as (Elsasser, 1946)

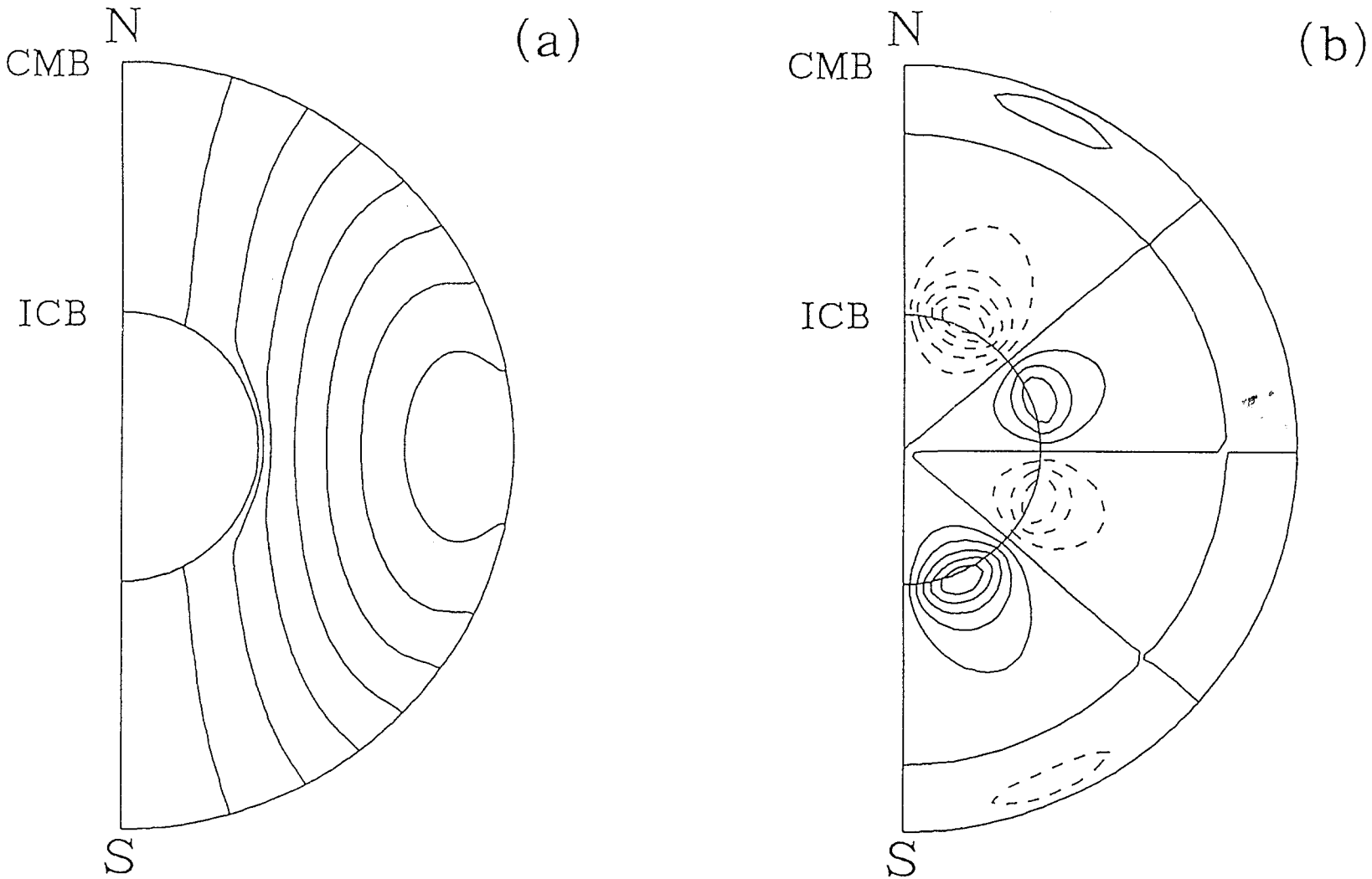

Fig. 3.11. (a) Distribution of angular velocity in the outer core. Solid contours indicate positive (eastward) values in units of 5×10^{-10} rad·s^{-1} and broken contours negative (westward) values. (b) Distribution of zonal toroidal magnetic fields. Solid contours indicate positive values in units of 1×10^{-4} T and broken contours negative values. These were derived for Case 3.

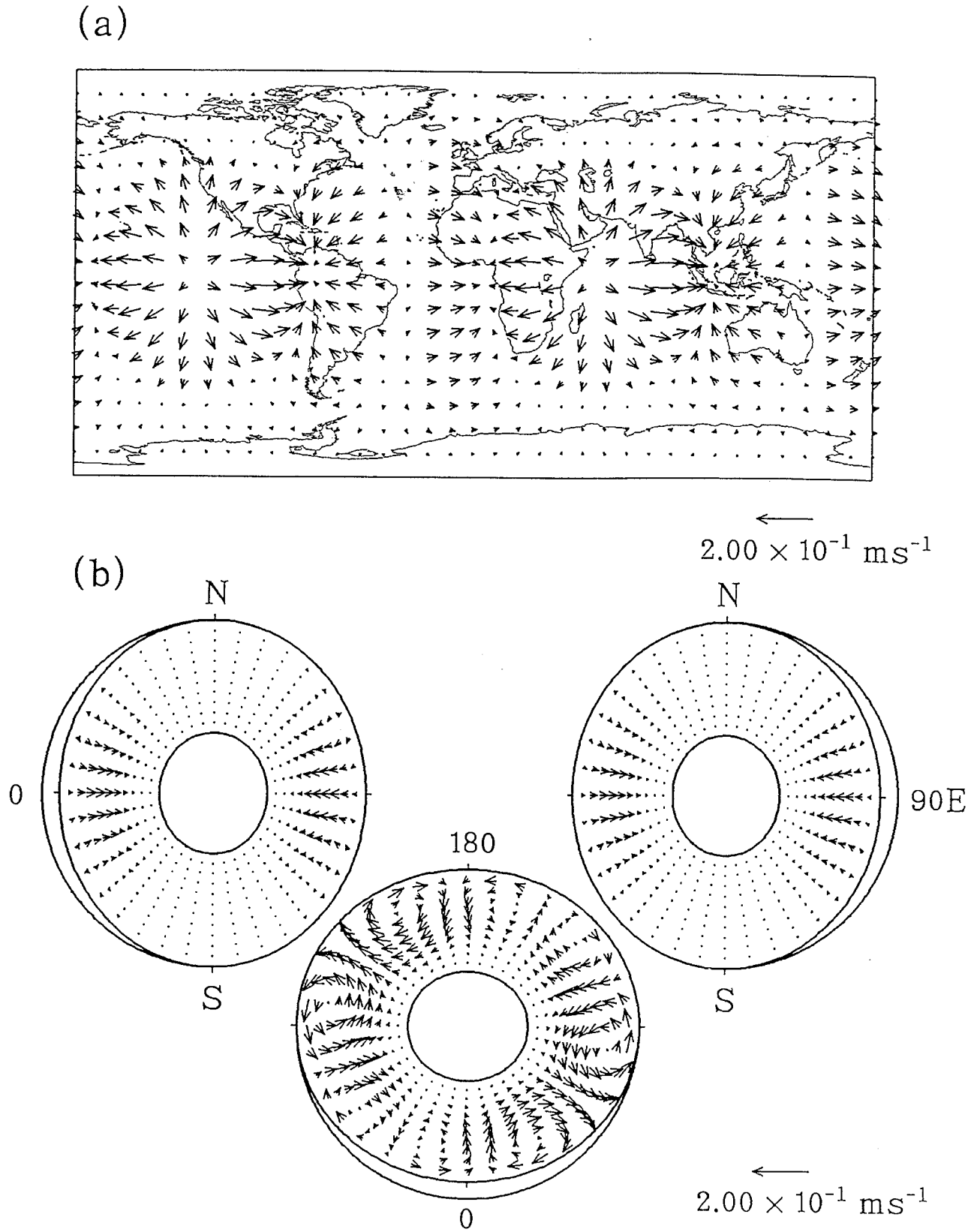

Fig. 3.12. (a) Horizontal velocity field at the core surface and (b) the overall velocity fields on the equatorial plane and on the meridional planes for the epoch of 1980 AD in Case 3. The arrow for scale length corresponds to 2×10^{-1} ms^{-1}.

$$B[S_l^0](r) = \frac{r_{oc}^{3/2}(r_e/r_{oc})^{l+2} g_l^0}{l\, J_{l+1/2}(k_l r_{oc})} r^{1/2} J_{l+1/2}(k_l r) \tag{3.3}$$

with the condition

$$J_{l-1/2}(k_l r_{oc}) = 0, \tag{3.4}$$

where k_l is defined as

$$(k_l)^2 = \lambda \mu_0 \sigma \tag{3.5}$$

if the magnetic field decays as $\exp[-\lambda t]$. Then k_l should correspond to the smallest positive solution, since we are to consider the longest free-decay mode. Magnetic lines of force are shown in Fig. 3.13; for $l = 1$ (upper left), for $l = 2$ (upper right), for $l = 3$ (lower left), for $l = 4$ (lower right), and for the synthesis (center). It should be noted here that in the figures of upper left and center, line-intervals are ten times larger and contours are drawn by thin lines. Assuming that the axisymmetric meridional magnetic fields and the zonal toroidal magnetic fields are the inducing magnetic fields for the generation of the non-axisymmetric poloidal magnetic fields, we make calculations for fluid motion in the outer core.

Figures 3.14 and 3.15 show the distributions of angular velocity and zonal toroidal magnetic fields in the core and the overall velocity field at the epoch of 1980 AD in Case 4. The distribution of angular velocity shown in Fig. 3.14(a) is different from that shown in Fig. 3.8(a). However, the distribution of zonal toroidal magnetic field and the pattern of overall velocity field are similar to those in Figs. 3.8(b) and 3.9, respectively, although the magnitude is smaller. The difference in the magnitude may be ascribed to either the non-linear nature or the truncation level L for spherical harmonics, or both.

If we do not introduce meridional circulation, zonal toroidal magnetic fields are weaker than the axial dipole magnetic field and occasionally than axisymmetric non-

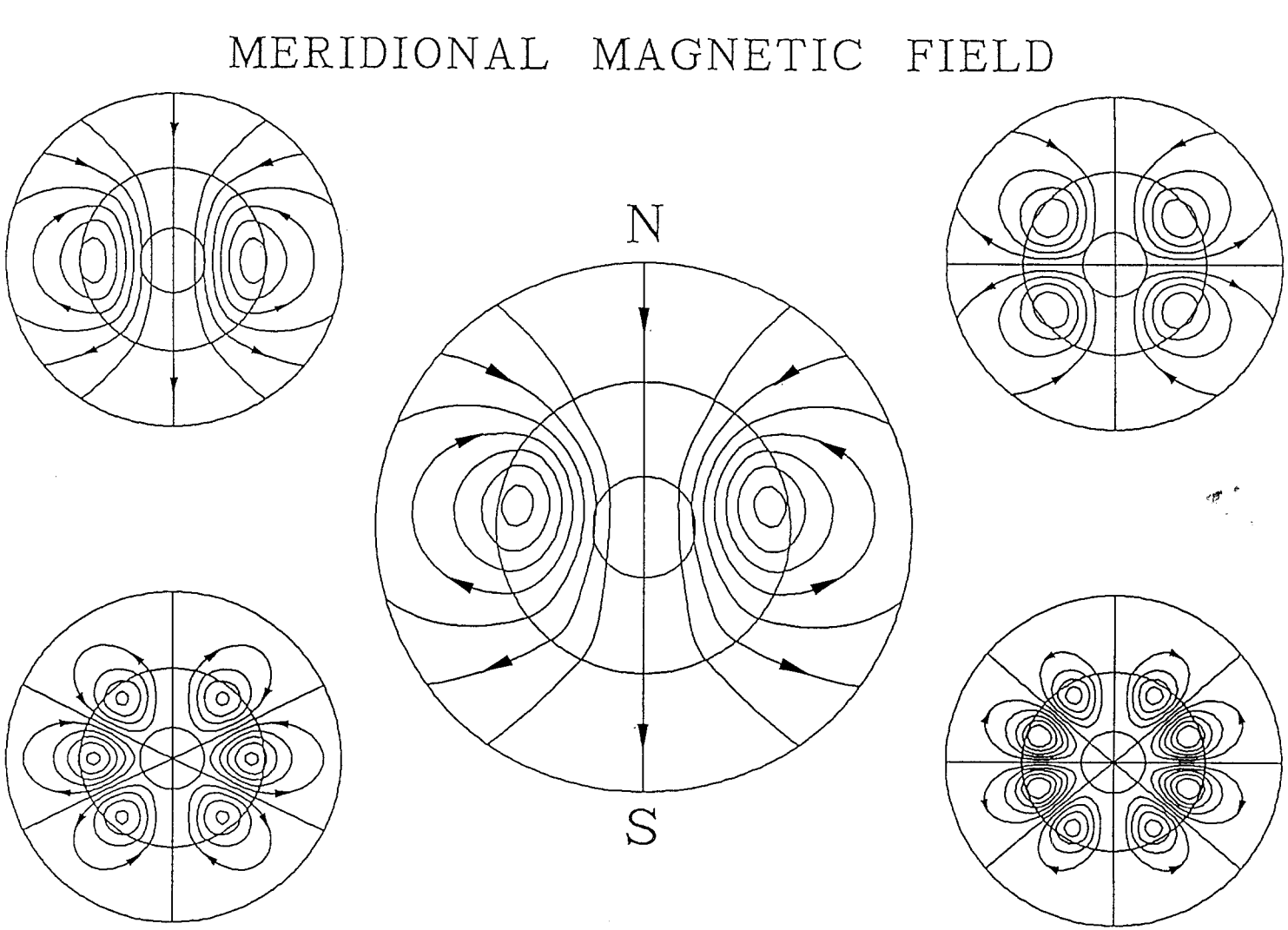

Fig. 3.13. Magnetic lines of force for axisymmetric meridional magnetic fields: upper left for degree $l = 1$, upper right for $l = 2$, lower left for $l = 3$, lower right for $l = 4$, and center for $l = 1 \sim 4$. The line interval unit is ten times larger in the upper left and the center.

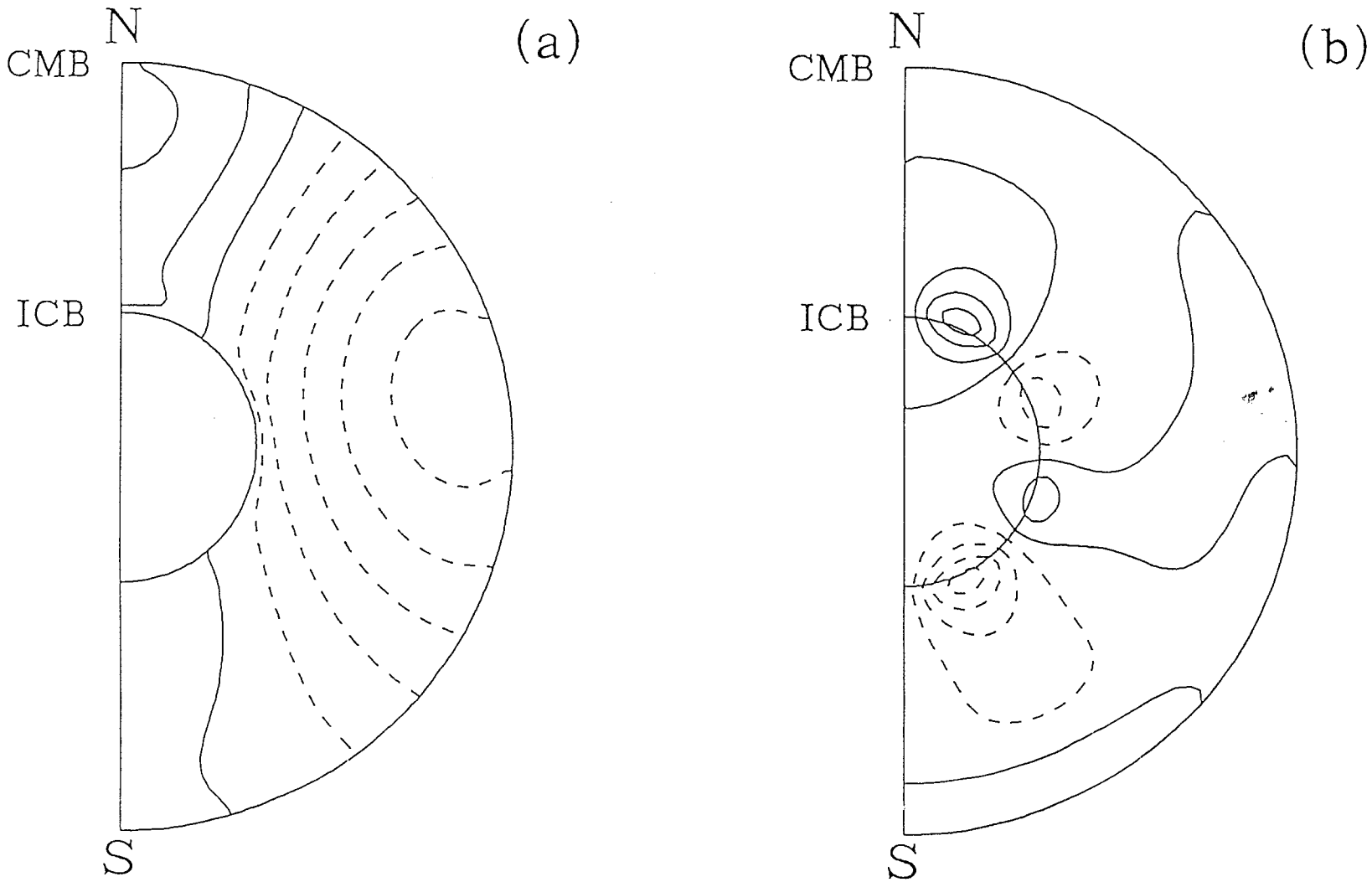

Fig. 3.14. (a) Distribution of angular velocity in the outer core. Solid contours indicate positive (eastward) values in units of 2×10^{-12} rad·s^{-1} and broken contours negative (westward) values. (b) Distribution of zonal toroidal magnetic fields. Solid contours indicate positive values in units of 1×10^{-6} T and broken contours negative values. These were derived for Case 4.

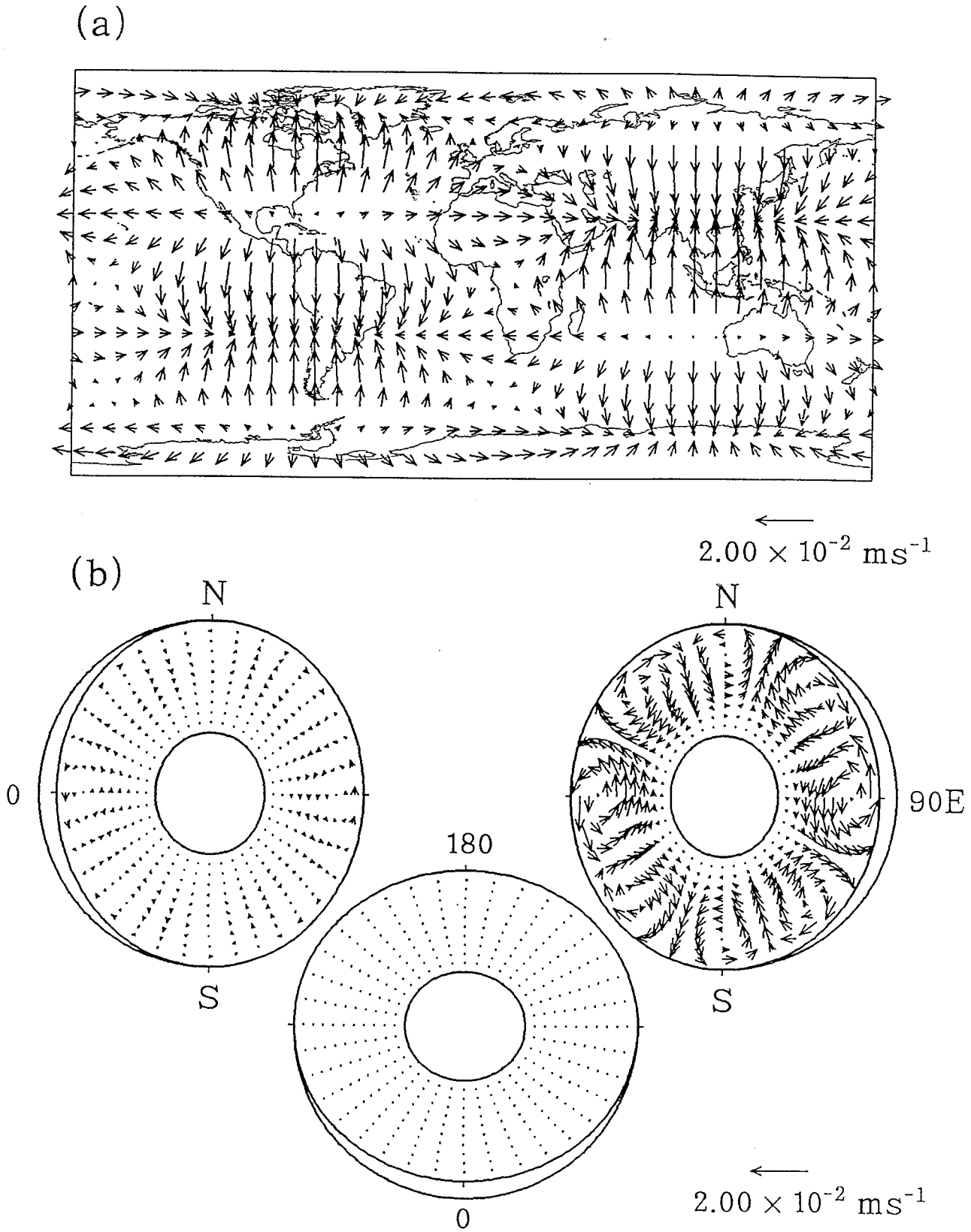

Fig. 3.15. (a) Horizontal velocity field at the core surface and (b) the overall velocity fields on the equatorial plane and on the meridional planes for the epoch of 1980 AD in Case 4. The arrow for scale length corresponds to 2×10^{-2} ms^{-1}.

dipole magnetic fields. If the inducing magnetic field is the axial dipole magnetic field alone, it is impossible to determine the poloidal velocity field of maximum degree and order $U[S_L^{Lz}]$, because the induction term $\boldsymbol{V}[S_L^{Lc}] \times \boldsymbol{B}[S_1^0]$, for example, induces only a poloidal magnetic field $\boldsymbol{B}[S_{L+1}^{Lc}]$, which is truncated. In actual calculations, we could derive fluid motion in the core, since zonal toroidal magnetic fields are also taken into consideration. In this sense, we cannot simply conclude that the introduced non-dipole magnetic fields have a strong effect on the determination of fluid motion in the core. However, the characteristics of derived flow pattern do not seem to be much affected by the introduction of axisymmetric non-dipole magnetic fields.

3.3.3. Case 5

We further add meridional circulation as in Case 2. This is Case 5. For $U[S_2^0] = -10^{-5}$, the distributions of angular velocity and zonal toroidal magnetic field in the core and the overall velocity field are shown in Figs. 3.16 and 3.17, respectively. It should be noted that the value of $U[S_2^0]$ is the same as in Case 2 but the radial dependence is different. Then the magnitude of corresponding poloidal velocity field becomes different. If we compare it in terms of the root-mean-square (rms) velocity defined as

$$V_{\rm rms} = \left[\frac{\int V^2 dv}{\int dv} \right]^{1/2}, \tag{3.6}$$

where the volume integral is performed for the outer core, with $U[S_2^0] = -10^{-5}$, the radial dependence (2.43) leads to $V_{\rm rms}[S_2^0] = 3.90 \times 10^{-10}$ ms^{-1}, while (2.44) leads to $V_{\rm rms}[S_2^0] = 1.54 \times 10^{-8}$ ms^{-1}; about forty times difference.

As in Case 2, the introduction of meridional circulation enhances the magnitude

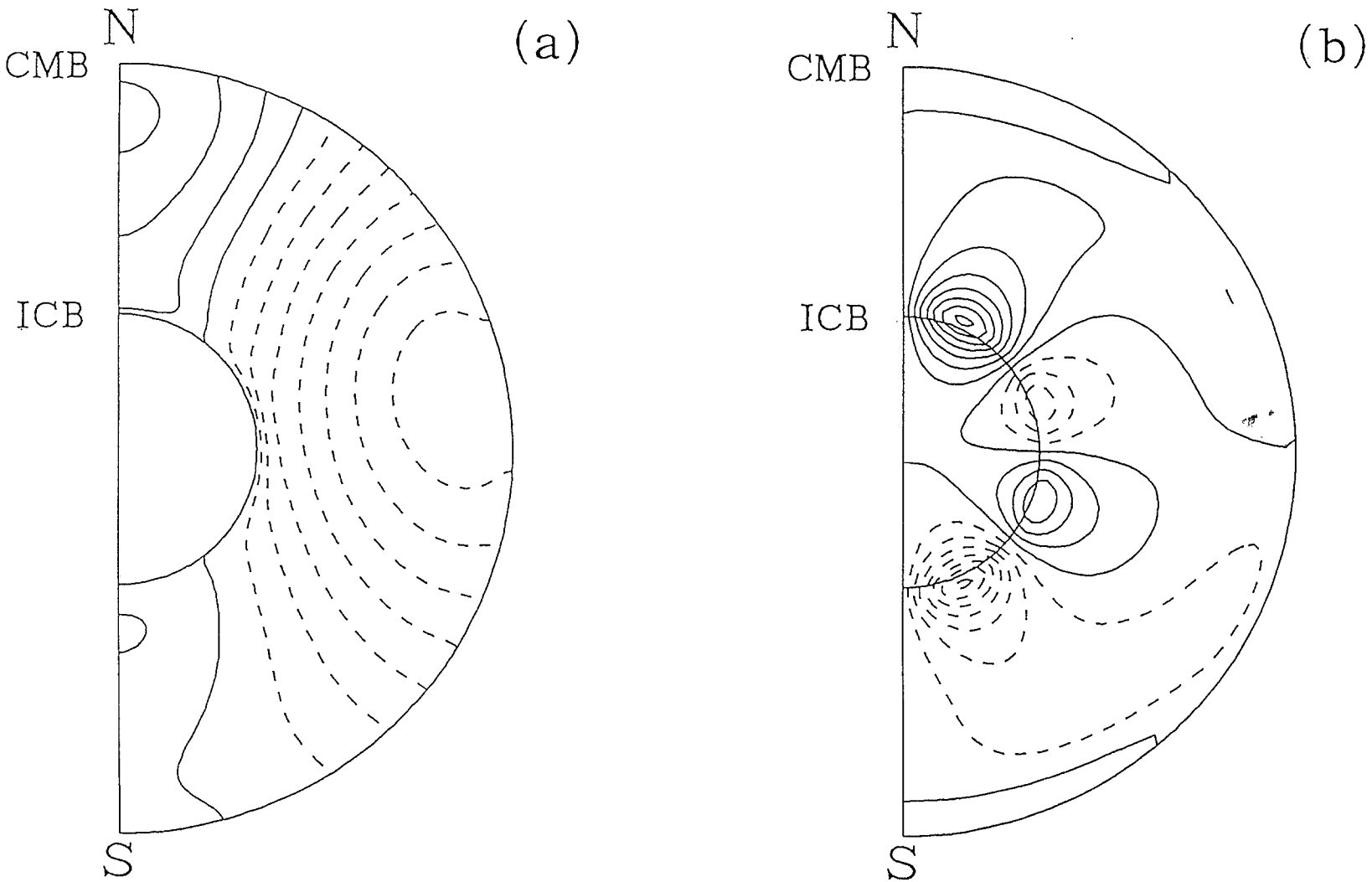

Fig. 3.16. (a) Distribution of angular velocity in the outer core. Solid contours indicate positive (eastward) values in units of 1×10^{-10} rad·s^{-1} and broken contours negative (westward) values. (b) Distribution of zonal toroidal magnetic fields. Solid contours indicate positive values in units of 4×10^{-5} T and broken contours negative values. These were derived for Case 5.

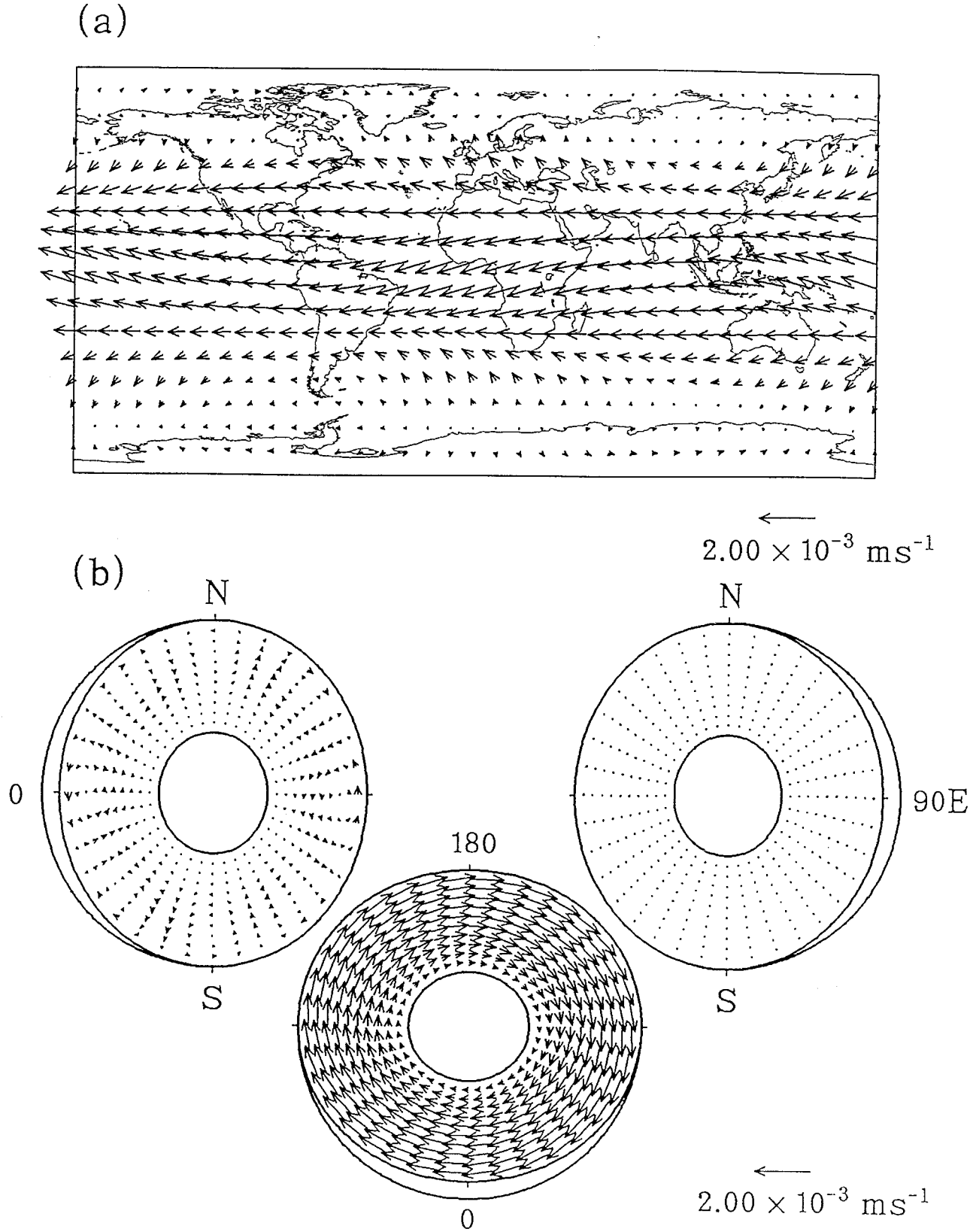

Fig. 3.17. (a) Horizontal velocity field at the core surface and (b) the overall velocity fields on the equatorial plane and on the meridional planes for the epoch of 1980 AD in Case 5. The arrow for scale length corresponds to 2×10^{-3} ms^{-1}.

of zonal toroidal motion, and then zonal toroidal magnetic fields are strengthened. As clearly seen in Fig. 3.17, the zonal toroidal motion is dominant. This may represent one class of velocity fields in $\alpha\omega$-dynamos, although the strength of zonal toroidal magnetic field is not strong, of the order of 10^{-4} T. The poloidal constituent of the velocity field is shown in Fig. 3.18. The pattern is similar to that shown in Fig. 3.15, although the magnitude is smaller. This reflects that zonal toroidal magnetic fields as inducing magnetic fields are stronger than those shown in Fig. 3.14(b), whereas axisymmetric poloidal magnetic fields as inducing magnetic fields remain unchanged. In other words, the derived poloidal velocity fields are controlled by the competition between the dominant inducing magnetic fields.

3.4. Introduction of non-zonal toroidal motion

3.4.1. Case 6

So far we have neglected non-zonal toroidal velocity fields which may be dominant, at least near the CMB, as pointed out by Whaler (1980) and Bloxham (1989). We here take into account a non-zonal toroidal motion, which is derived by solving the Navier-Stokes equation under the condition that the poloidal constituent of velocity field is known. If the non-zonal toroidal velocity field is dominant, strong non-zonal toroidal magnetic fields would be generated. We then take the non-zonal toroidal magnetic fields as inducing magnetic fields. This is Case 6, where unknowns are toroidal velocity fields $V[_nT_l^{mz}]$, non-axisymmetric poloidal velocity fields $U[S_l^{mz}]$, toroidal magnetic fields $B[_nT_l^{mz}]$, and non-axisymmetric poloidal magnetic fields $B[_nS_l^{mz}]$. The total number of unknowns is $L(3L+5)(N+1)+L(L+1) = 700$ with the truncation levels $L = 4$ and $N = 9$. We first attempted to include all the interaction terms and derive fluid motion in the core by solving the induction and the Navier-Stokes equations. However, we could obtain no converged solutions through the

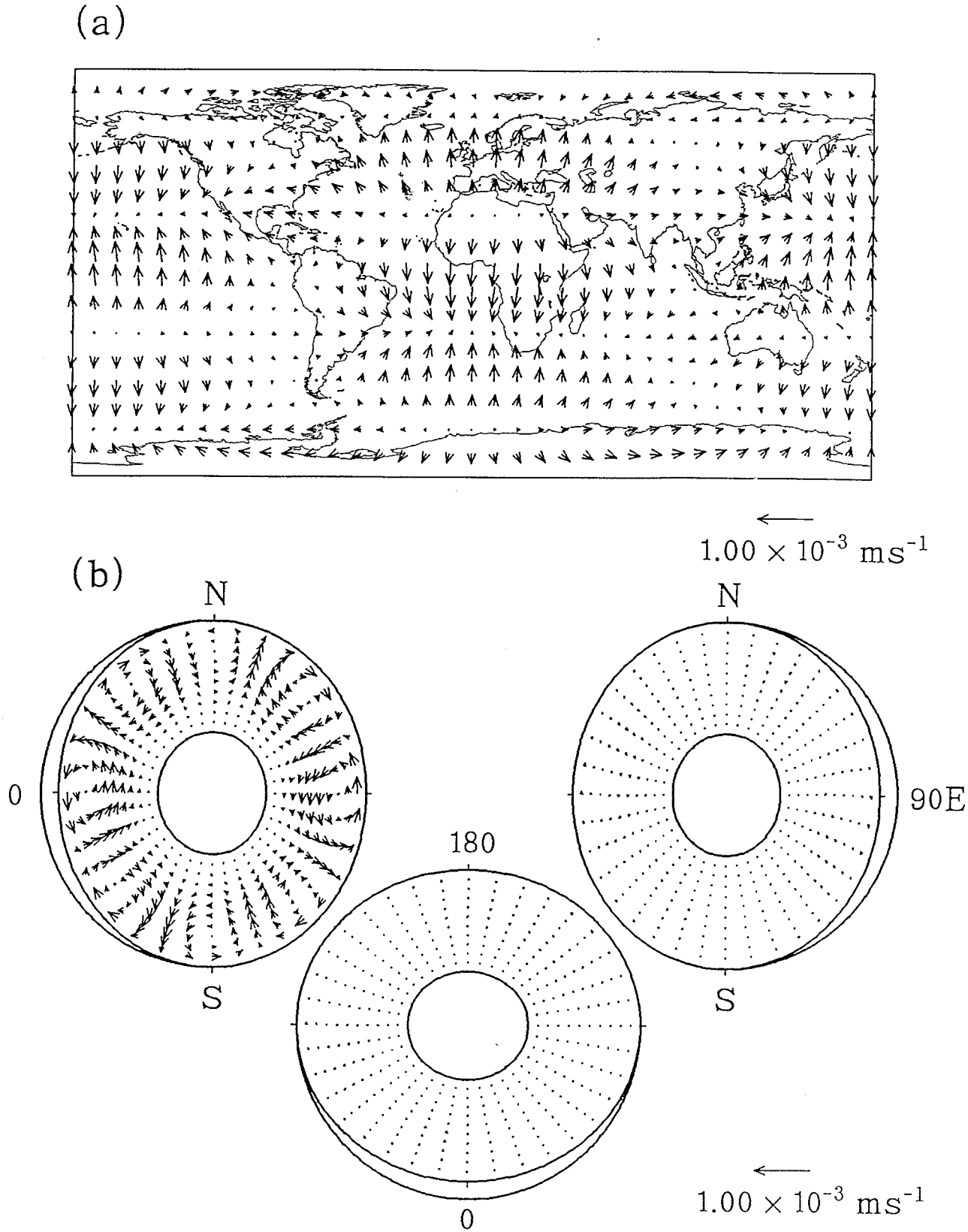

Fig. 3.18. (a) Horizontal velocity field for the poloidal constituent at the core surface and (b) the poloidal velocity fields on the equatorial plane and on the meridional planes for the epoch of 1980 AD in Case 5. The arrow for scale length corresponds to 1×10^{-3} ms^{-1}.

iterative calculation based on a Newton method.

In the following we consider some possible reasons. In particular, we examine the assumed radial dependence for poloidal velocity field, truncation levels, and non-linear nature of the problem, respectively. We have arbitrarily assumed the radial dependence, which satisfies boundary conditions, of scalar function for poloidal velocity field, as in a kinematic dynamo problem. The assumed radial dependence would somehow control the toroidal velocity field, the toroidal and the poloidal magnetic fields. Non-linear terms are expected to have an effect of feedback to the original field and the radial dependence for the poloidal velocity field would be altered by such a feedback effect or the Lorentz force, even when the Navier-Stokes equation for the poloidal velocity field is not taken into consideration. Nevertheless, however, the radial dependence has been fixed in the present study. This could be one reason why no solutions are derived. Another factor would be the truncation level N for Chebyshev polynomials. However, we could not obtain converged solutions even for $N = 19$; the number of unknowns for a set of (l, m, z) is twice.

Furthermore, as implied by non-linear equations for a dynamo problem, complicated variations of the Earth's magnetic field arising from its non-linear nature would be an essential feature of the geodynamo. Based on coupled-disk dynamo models, Shimizu and Honkura (1985) claimed that the non-linear nature is essential in polarity reversals of the Earth's magnetic field. Meanwhile, Honkura and Matsushima (1988b) examined the Cox model (Cox, 1968, 1969) in order to search for a mechanism of polarity reversals of the Earth's magnetic field. They represented the Cox model using a disk dynamo (Bullard, 1955) with external perturbations, and pointed out that irregularity in fluctuations of the non-dipole field plays an important role in the Cox model. In this sense, fluctuations of the Earth's magnetic field would really be an inherent property, and the constraint of a steady state may be misleading.

We, therefore, simplify the problem.

As an extension of the previous methods, we tentatively take $\boldsymbol{V}[T_\alpha] \times \boldsymbol{B}[S_\beta^0]$ into consideration in the induction equation for toroidal magnetic fields, $\boldsymbol{V}[S_\alpha] \times \boldsymbol{B}[T_\beta]$ and $\boldsymbol{V}[S_\alpha] \times \boldsymbol{B}[S_\beta^0]$ in the induction equation for poloidal magnetic fields, and the advection, the Coriolis force and the Lorentz force terms in the Navier-Stokes equation for toroidal velocity fields. We consider only the linear terms in Lorentz force; that is, $[B[S_\alpha^0]B[S_\beta]S_\gamma]$, $[B[S_\alpha]B[S_\beta^0]S_\gamma]$ and $[B[T_\alpha]B[S_\beta^0]S_\gamma]$ as expressed in (2.8).

Now we examine the magnitude of the Lorentz force term which we neglected in deriving fluid motion in the core. For non-zonal toroidal velocity fields, the Coriolis force term is dominant in (2.8). At most of the mesh-points x_k, the Coriolis force term is one to three orders of magnitude larger than the Lorentz force term. At some mesh-points, the magnitude of the Lorentz force term is comparable, at most, to that of the Coriolis force term. Therefore, the non-zonal toroidal velocity field derived on the assumption tentatively made in Case 6 would not change significantly, even if the Lorentz force terms, which have not been taken into consideration, are included in the calculation; that is, the derivation of fluid motion in the core is justified. For zonal toroidal velocity fields, however, the Lorentz force term must be small at all the mesh-points, since the advection term is small and meridional circulation has not been taken into consideration; that is, from (2.8),

$$\nu\left\{r^2\frac{d^2V[T_\gamma^0]}{dr^2} - \gamma(\gamma+1)\,V[T_\gamma^0]\right\}$$

$$+\frac{1}{\rho\mu_0}\sum_\alpha\sum_\beta\{[B[S_\alpha]B[S_\beta]S_\gamma^0] + [B[T_\alpha]B[S_\beta]S_\gamma^0] + [B[T_\alpha]B[T_\beta]S_\gamma^0]\} \qquad (3.7)$$

$$- \sum_{\alpha}\sum_{\beta}\{[V[S_\alpha]V[S_\beta]S_\gamma^0] + [V[T_\alpha]V[S_\beta]S_\gamma^0] + [V[T_\alpha]V[T_\beta]S_\gamma^0]\} = 0.$$

When all the Lorentz force terms are included in the calculation, no solution can be found. Since the viscous and the advection terms are small compared with the Lorentz force term, (3.7) can be rewritten, for the zonal toroidal velocity fields, as

$$\int_0^{2\pi} \frac{1}{\rho\mu_0}[(\nabla \times \boldsymbol{B}) \times \boldsymbol{B}]_\phi d\phi \sim 0, \tag{3.8}$$

where the integrand is the ϕ-component of the Lorentz force. Equation (3.8) is a more severe condition than Taylor's condition (Taylor, 1963), which is known as a dynamical constraint for a steady, slow, and inviscid fluid motion, given as

$$\int_{C(s)} \frac{1}{\mu_0}[(\nabla \times \boldsymbol{B}) \times \boldsymbol{B}]_\phi dS = 0, \tag{3.9}$$

where the surface integral is performed for $C(s)$ which is the side surface of the co-axial cylinder of radius s and length $2z_1 = 2(r_{oc}^2 - s^2)^{1/2}$.

Now we assume that the Coriolis force due to the axisymmetric poloidal velocity field is balanced with the Lorentz force and derive the axisymmetric poloidal velocity field. It turns out that the axisymmetric poloidal velocity field thus derived is by no means dominant. The rms velocities before and after taking the axisymmetric poloidal velocity field into consideration amount to 3.31×10^{-5} ms^{-1} and 3.35×10^{-5} ms^{-1}, respectively. We show the two estimates of velocity fields thus derived in Figs. 3.19 and 3.20, respectively, where no significant difference is recognized. Thus we will consider the axisymmetric poloidal velocity field, which is related to the Coriolis force balanced with the Lorentz force acting on the zonal toroidal velocity field.

The pattern of the fluid motion shown in Fig. 3.20 is different considerably from those derived so far. This is a result of the introduction of non-zonal toroidal motion,

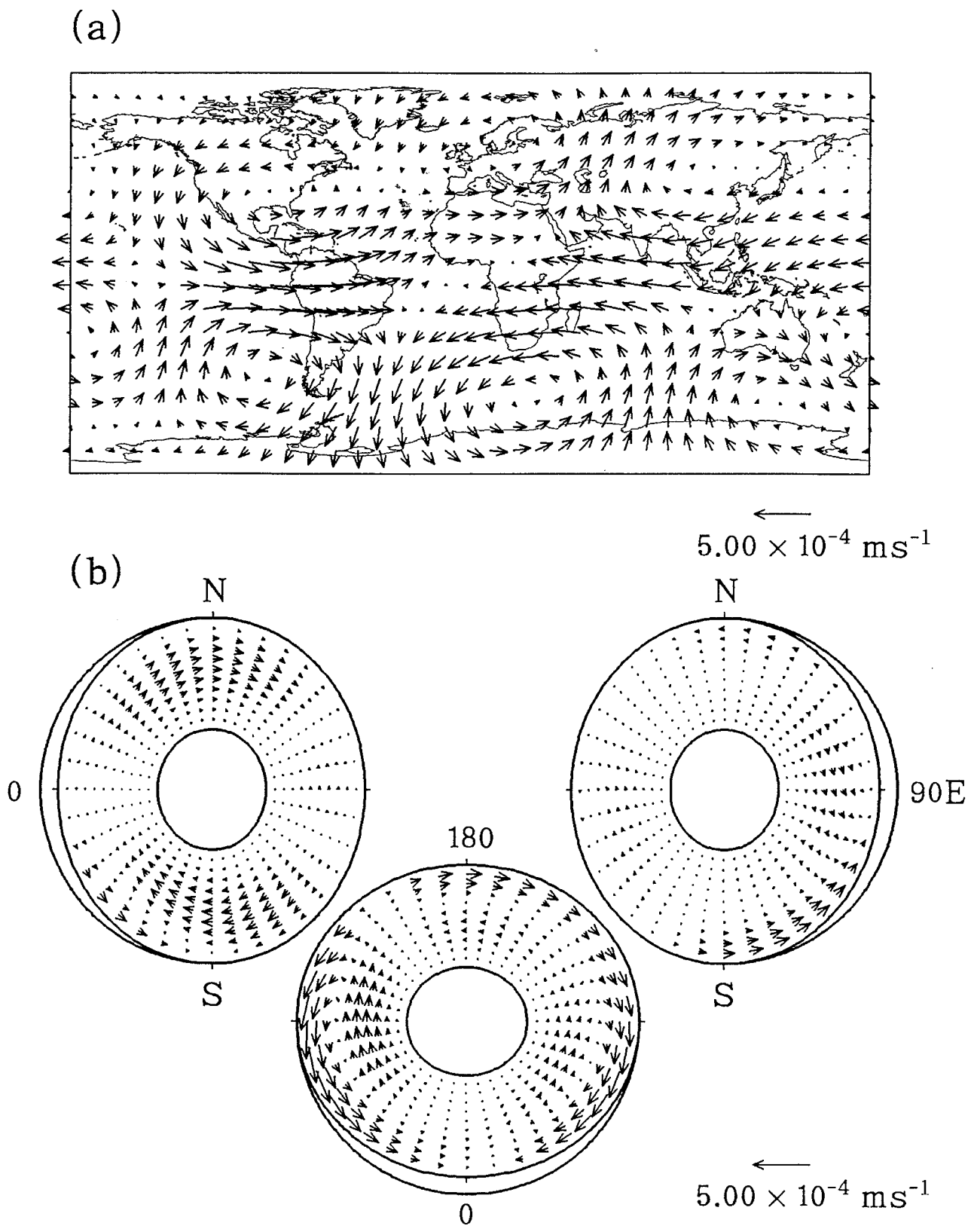

Fig. 3.19. (a) Horizontal velocity field at the core surface and (b) the overall velocity fields on the equatorial plane and on the meridional planes for the epoch of 1980 AD, derived for Case 6 but without considering the balance between the Coriolis and the Lorentz forces. The arrow for scale length corresponds to 5×10^{-4} ms^{-1}.

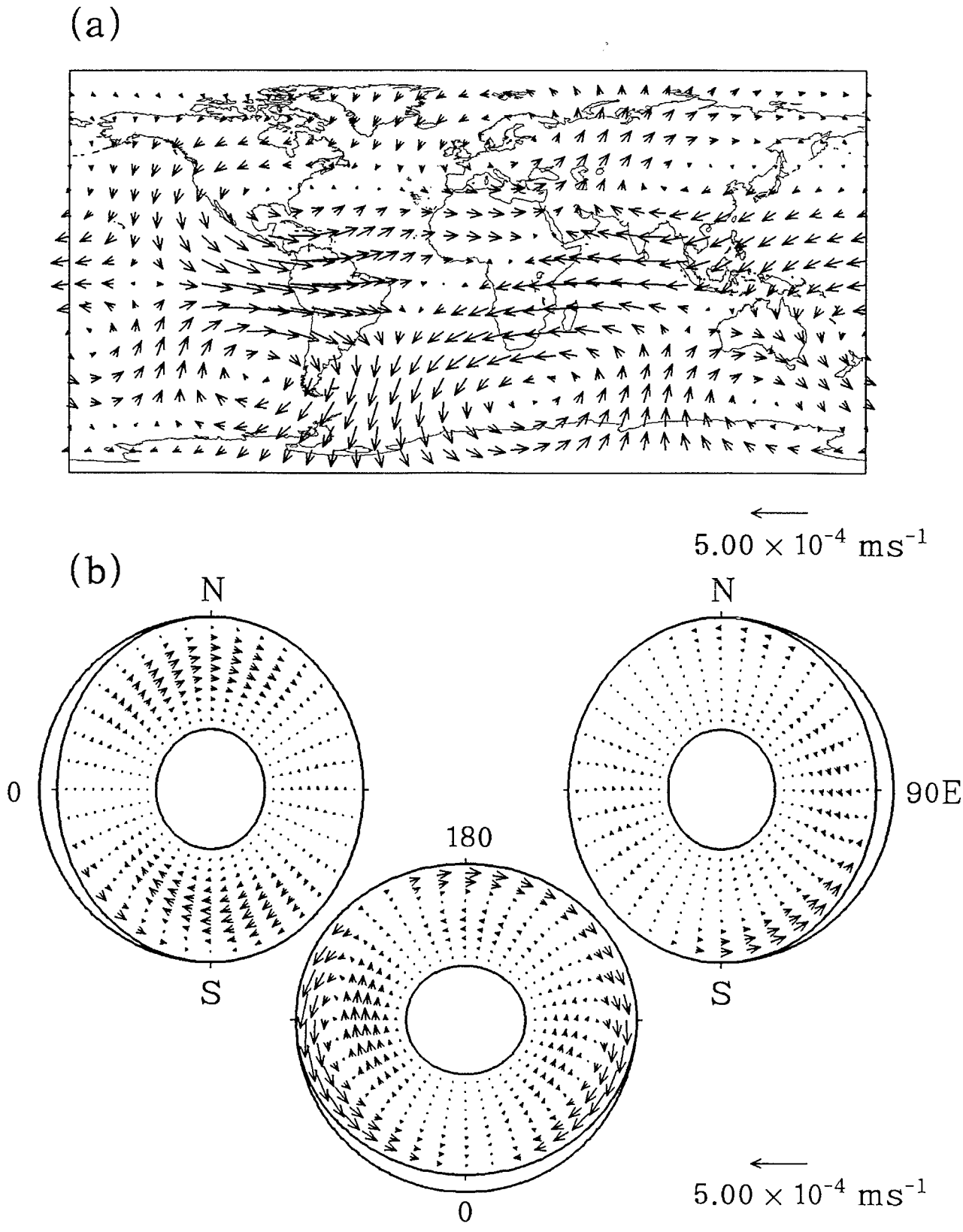

Fig. 3.20. (a) Horizontal velocity field at the core surface and (b) the overall velocity fields on the equatorial plane and on the meridional planes for the epoch of 1980 AD in Case 6. The arrow for scale length corresponds to 5×10^{-4} ms^{-1}.

as clearly seen in Fig. 3.20. The main feature of the flow is four vortices; two at around 90° W are nearly symmetric with respect to the equator, while the other two at around 30° E antisymmetric. Westward motion prevails largely in a zone near the equator from around 150° W to 0° in longitude. The fluid flow near the CMB, as shown in Fig. 3.20, does not coincide with those derived with the frozen-flux approximation by Le Mouël *et al.* (1985), Voorhies (1986), Whaler and Clarke (1988), Bloxham (1989), Gire and Le Mouël (1990), Hulot *el al.* (1990), and Lloyd and Gubbins (1990).

In the present approach, fluid motion in the core is derived under the condition that non-axisymmetric poloidal magnetic fields at the CMB are maintained in such a way that the steady state is realized through induction processes within the core. In the frozen-flux approximation, on the other hand, fluid motion at the core surface is derived to explain the secular variation of the geomagnetic field, using poloidal magnetic fields and their time variations at the CMB. The present approach is entirely different from that based on the frozen-flux approximation, and it is therefore not surprising that the velocity shown in Fig. 3.20 is different from those derived for the frozen-flux approximation. Nevertheless, some common features can be found; the vortex at around 30° E in the Southern Hemisphere, consisting of currents from near the South Pole toward the equator at around 90° E, the westward flow under equatorial Africa and the Indian Ocean, and the flow from the equator toward the South Pole.

The toroidal and poloidal constituents of the derived velocity field are shown in Figs. 3.21(a) and (b), respectively. It should be noticed that the scale length for arrows in Fig. 3.21(b) is different from that in Fig. 3.21(a). Comparing Fig. 3.21(a) with Fig. 3.20(a), it is clearly recognized that the toroidal constituent of the derived velocity field at the CMB is dominant. If we compare the magnitudes of toroidal and

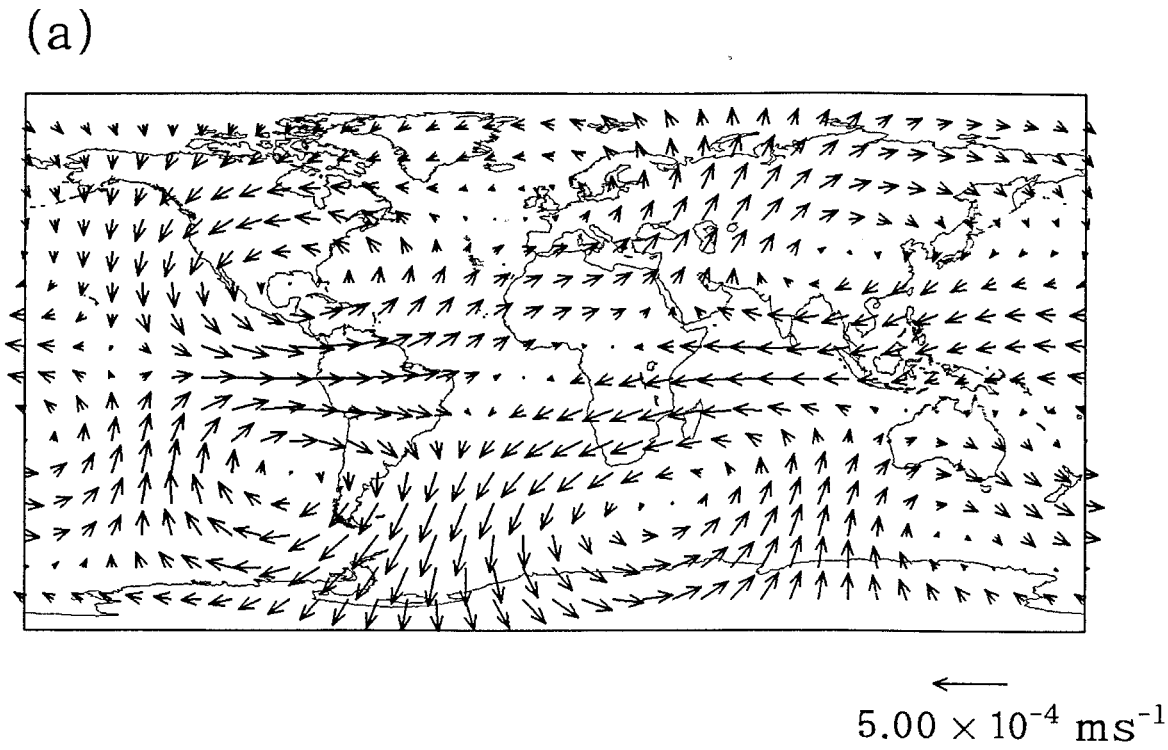

Fig. 3.21. (a) The toroidal constituent and (b) the poloidal constituent of the velocity field shown in Fig. 3.20. The arrow for scale length in (b) is different from that in (a).

poloidal constituents in terms of the rms velocity as defined in (3.6), we obtain $V_{\rm rms}[T] = 9.96\times10^{-5}$ ms^{-1} and $V_{\rm rms}[S] = 3.35\times10^{-5}$ ms^{-1}. The toroidal velocity is therefore dominant throughout the outer core by a factor of 3.

The derived poloidal velocity field shown in Fig. 3.21(b) is characterized by upwelling flows near the Hawaii Islands and in the east of the Indian Ocean, and also by a downwelling flow at the Atlantic. It also seems that two columnar convective motions are composed of the poloidal velocity field; one along 90° W and the other along the (60° S, 30° E)–(60° N, 90° E) line. In order to clarify this, we show, in Fig. 3.22, the poloidal velocity field on some planes parallel to the equatorial plane. Locations of the planes are at $z = \frac{i}{6} r_{oc}$, where i = 4, 3, 2, 1, and 0 from the upper left to the lower left, and i = 0, −1, −2, −3, and −4 from the upper right to the lower right. It is clearly seen that the center of one columnar convective motion situated at around 90° W stays at the same position in longitude, whereas the center of the other does not. Such columnar motions are also pointed out by Hulot *et al.* (1990), who derived fluid motion at the CMB based on the frozen-flux and the tangentially geostrophic approximations. They claimed that the non-zonal toroidal motion, which is symmetric with respect to the equator, represents a surface flow within the core organized into cylindrical pillars as proposed by Busse (1975), although the scale in their result is also larger.

We here examine the effect of the truncation N. So far we have set the truncation level at N = 9; that is, Chebyshev polynomials of the order zero to nine have been employed to express the radial dependence of a scalar function for a toroidal or a poloidal field. We now increase the truncation level to N = 19 with the total number of variables for a set of (l, m, z) being twice; that is, the total number of unknowns is 1380 in this case with the truncation level L = 4. The velocity field

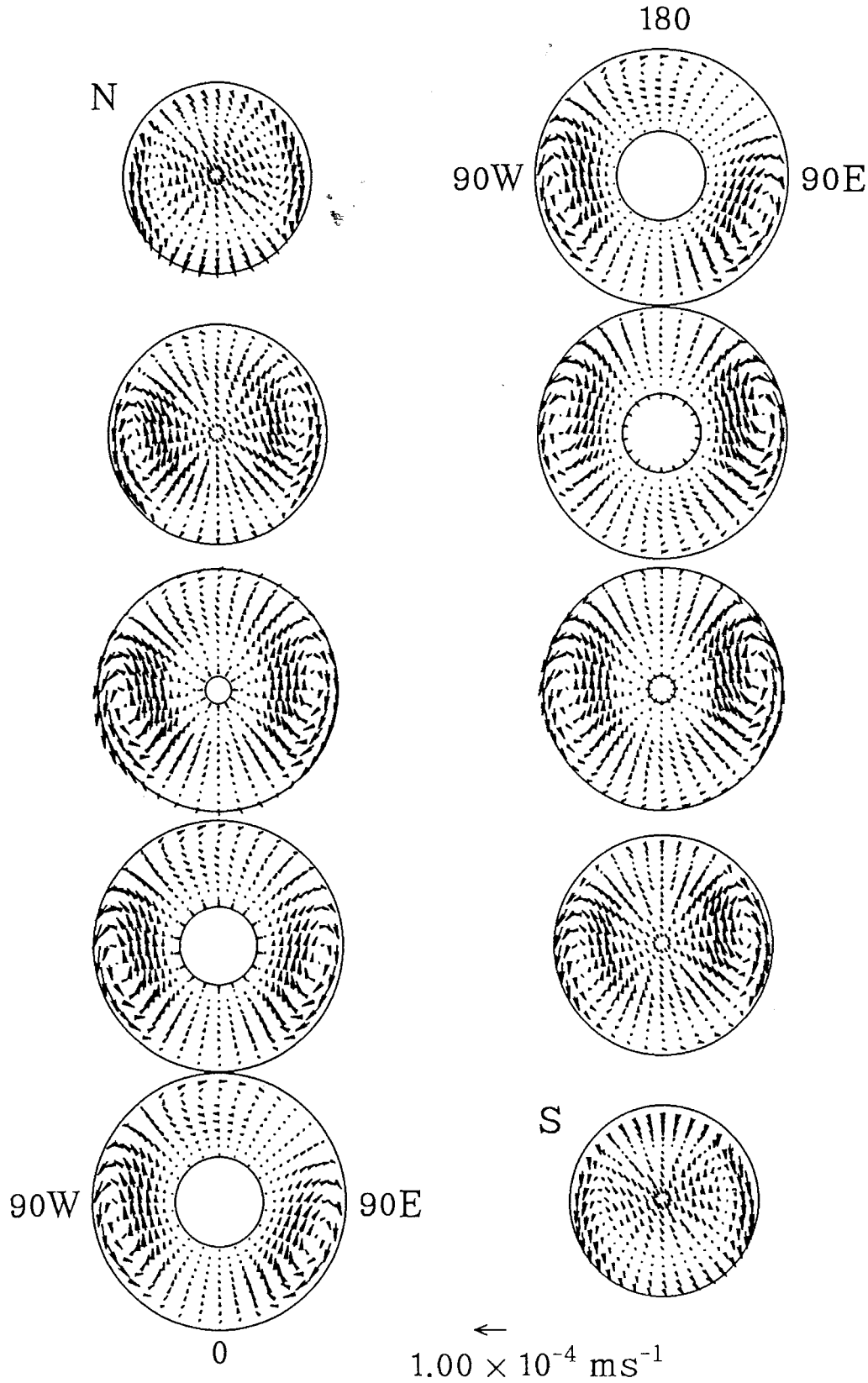

Fig. 3.22. The poloidal constituent of the velocity field shown in Fig. 3.20 on the planes, parallel to the equatorial plane, at $z = (i/6)r_{oc}$ (i = 4, 3, 2, 1, and 0, from upper to lower for the left column; i = 0, −1, −2, −3, and −4, from upper to lower for the right column).

obtained with the new truncation levels is shown in Fig. 3.23. No significant difference can be seen between Figs. 3.20 and 3.23. Table 3.2 shows the rms velocities for the overall, the toroidal and the poloidal velocity fields for $N = 9$, 13 and 19, respectively, although the figure of the velocity field for $N = 13$ is not shown. The quantitative difference among them may be recognized in this table. If we wish to discuss quantitative nature of the derived fluid motion in detail, we should set the truncation level for Chebyshev polynomials at least at $N = 13$. As far as qualitative nature is concerned, however, the truncation level $N = 9$ would be sufficient. This problem is obviously related to CPU time for computation, since we must solve a large size matrix equation iteratively. This is the reason why the truncation level $N = 9$ is taken. With regard to the truncation level L, we will discuss in Section 5.

Table 3.2. The root-mean-square velocities for the overall, toroidal and poloidal velocity fields with the truncation levels $N = 9$, 13 and 19.

N	$V_{\rm rms}$ (ms^{-1})	$V_{\rm rms}[T]$ (ms^{-1})	$V_{\rm rms}[S]$ (ms^{-1})
9	9.66×10^{-5}	9.06×10^{-5}	3.35×10^{-5}
13	1.20×10^{-4}	1.14×10^{-4}	4.16×10^{-5}
19	1.22×10^{-4}	1.14×10^{-4}	4.29×10^{-5}

3.4.2. Case 7

We further add meridional circulation $V[S_2^0]$ to Case 6; this is Case 7. For $U[S_2^0] = -10^{-6}$ and $U[S_2^0] = -3\times10^{-6}$, the derived overall velocity fields are shown in Figs. 3.24 and 3.25, respectively. The axisymmetric poloidal velocity field, which is related to the Coriolis force balance with the Lorentz force acting on the zonal toroidal velocity field, is to be derived in the same way as in Case 6 after calculating fluid motion in the core for the additional axisymmetric poloidal velocity field $V[S_2^0]$. The

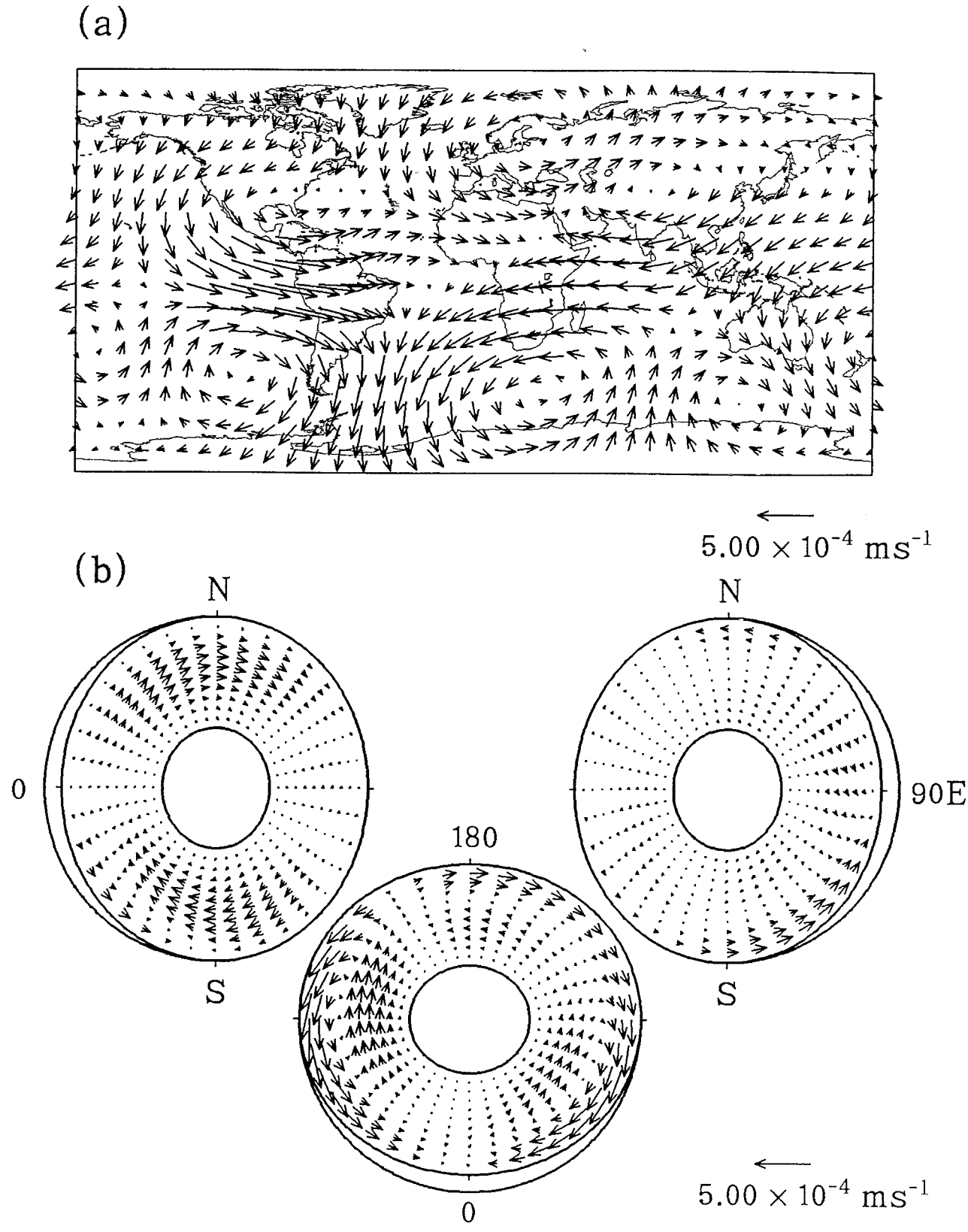

Fig. 3.23. (a) Horizontal velocity field at the core surface and (b) the overall velocity fields on the equatorial plane and on the meridional planes for the epoch of 1980 AD in Case 6. The arrow for scale length corresponds to 5×10^{-4} ms^{-1}.

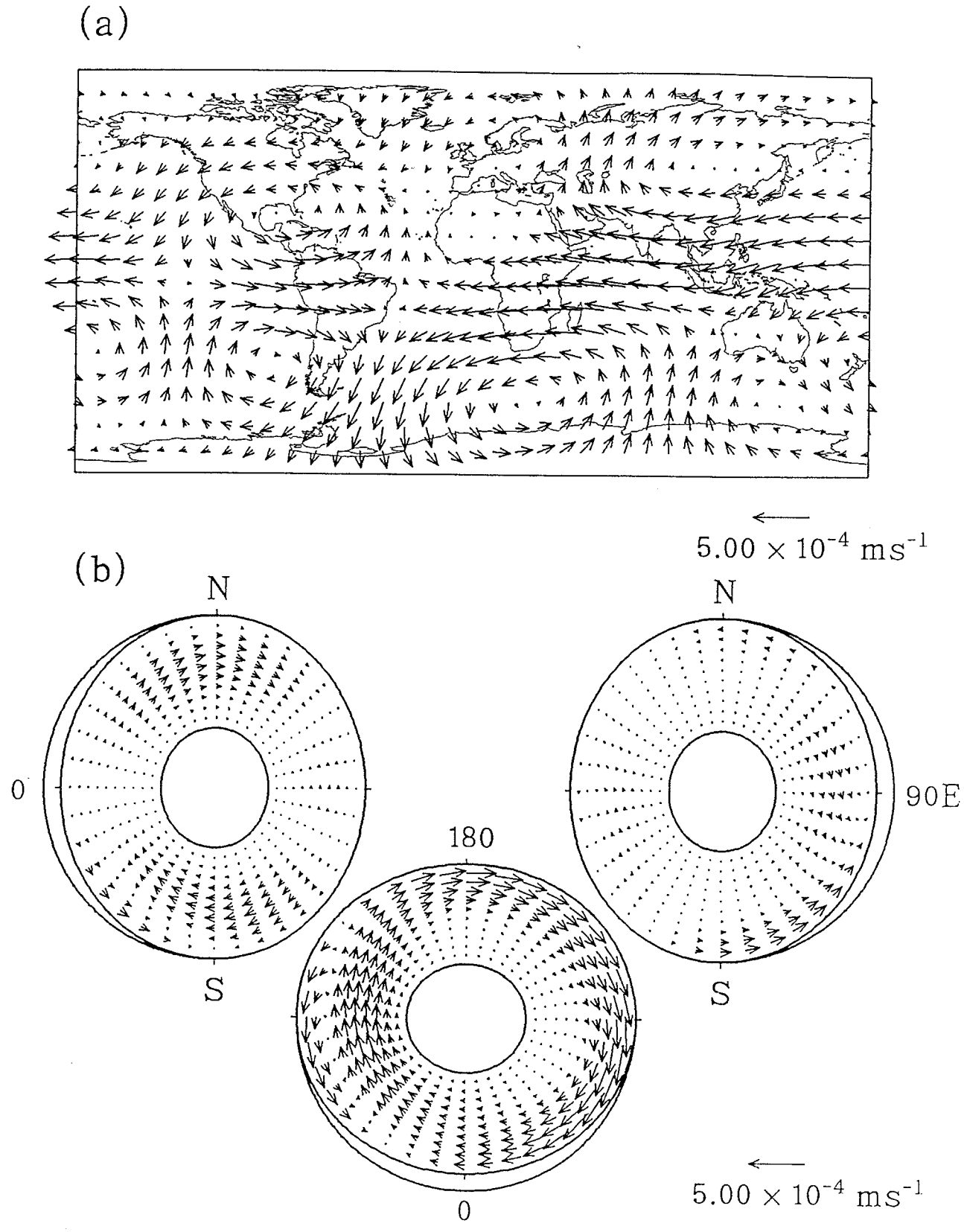

Fig. 3.24. (a) Horizontal velocity field at the core surface and (b) the overall velocity fields on the equatorial plane and on the meridional planes for the epoch of 1980 AD in Case 7. The arrow for scale length corresponds to 5×10^{-4} ms^{-1}.

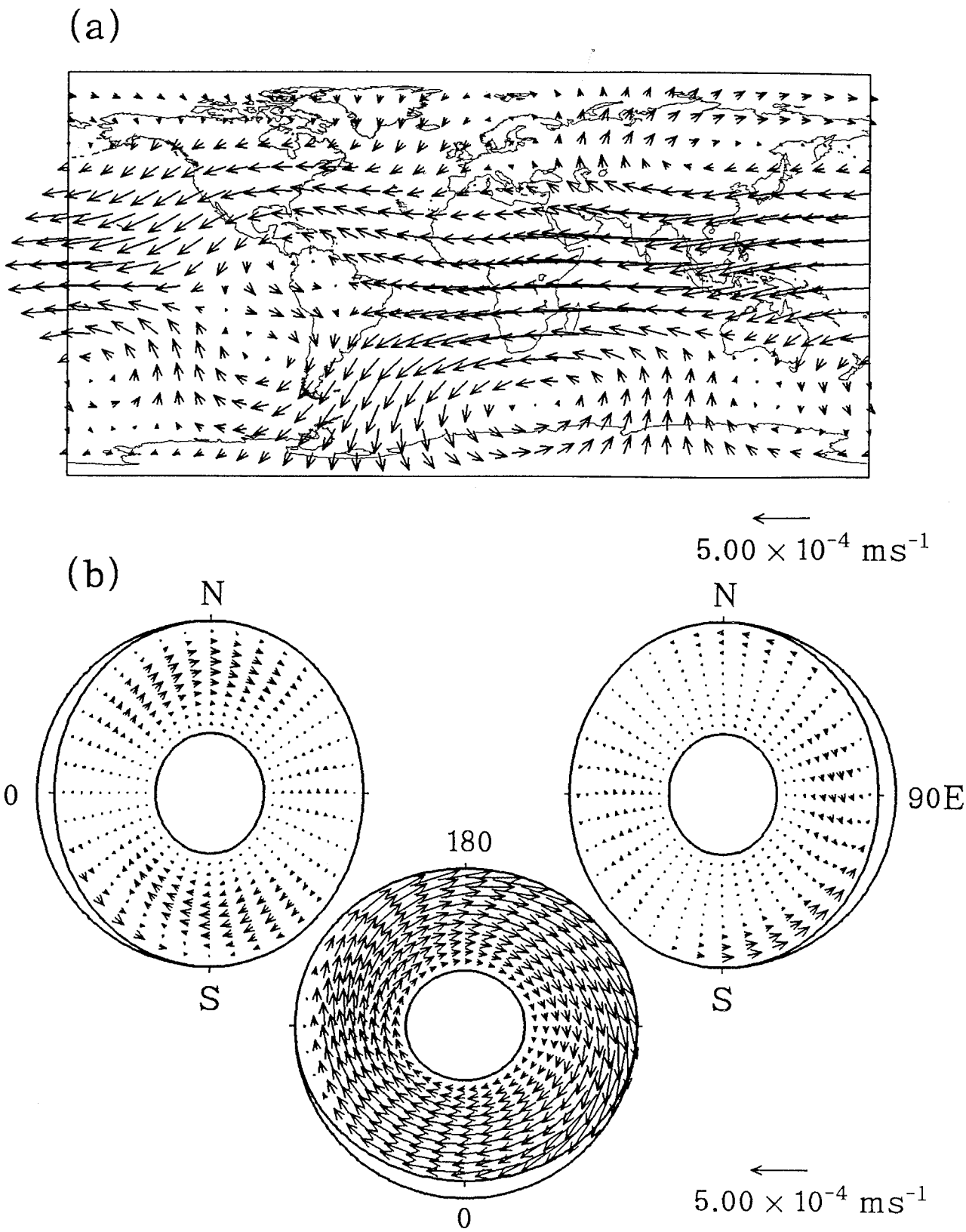

Fig. 3.25. (a) Horizontal velocity field at the core surface and (b) the overall velocity fields on the equatorial plane and on the meridional planes for the epoch of 1980 AD in Case 7. The arrow for scale length corresponds to 5×10^{-4} ms^{-1}.

westward flow in a zone near the equator is dominant in both figures. The columnar convective motions in Fig. 3.25 are therefore indistinct. Nevertheless, the vortex situated at around (60° S, 30° E) is noticeable. It seems that the additional meridional circulation affects only the zonal toroidal motion. Therefore, the vortex flow may be an essential one in the Earth's outer core.

4. Time-Dependent Behavior of the Magnetic Field

In this section we examine the results obtained so far from a different point of view. Respective results have been obtained by solving the induction and the Navier-Stokes equations for the steady-state case on various assumptions made in Cases 1 to 7. Whether the magnetic field is in fact steady under the conditions we imposed can be tested by examining time-dependent behavior of the magnetic field with the derived velocity field fixed.

As mentioned in Section 3, we should somehow check the validity of solutions. If the assumption made in deriving fluid motion in the core is inappropriate, the magnetic field would diverge or decay within a short time, because some induction terms, which are important in maintaining a steady magnetic field, must have been omitted. Rikitake and Hagiwara (1968), for example, examined time-dependent behavior of the magnetic field for the Bullard-Gellman dynamo model. Uno (1972) also examined the Bullard-Gellman-Lilley dynamo model. The steady state is realized for specific magnetic Reynolds numbers, corresponding to eigenvalues in kinematic dynamo problems (e.g. Bullard and Gellman, 1954; Lilley, 1970). Since the magnetic Reynolds number specifies the magnitude of velocity field in kinematic dynamos, we can check the validity through the magnitude.

4.1. The numerical method

We employ the same mathematical formulation as described in Section 2; the velocity and magnetic fields are expressed in terms of toroidal and poloidal vector fields, and the scalar functions are expanded in spherical surface harmonics for the θ- and ϕ-dependence and in Chebyshev polynomials for the r-dependence as given in (2.5) and (2.10). Equations (2.6) and (2.7) obtained by the orthogonality of toroidal

and poloidal fields and of spherical harmonics are satisfied at the mesh-points given in (2.19) except the boundaries, where boundary conditions given in (2.25) to (2.30) are imposed. The electrical conductivity of the inner core has been assumed to be the same as that of the outer core. In addition, the magnetic field must be finite at $r = 0$, and we obtain

$$B^{(i)}[T_\gamma](0,\ t) = 0, \tag{4.1}$$

$$B^{(i)}[S_\gamma](0,\ t) = 0. \tag{4.2}$$

There is no motion inside the solid inner core, and the induction equation is reduced to the diffusion equation. The scalar functions for magnetic fields inside the inner core $B^{(i)}[T_\gamma](r,\ t)$ and $B^{(i)}[S_\gamma](r,\ t)$ are also expanded in spherical harmonics and Chebyshev polynomials. The radial coordinate r in the inner core is transformed into coordinate x by

$$x = \frac{2r - r_{ic}}{r_{ic}}. \tag{4.3}$$

Since we have expanded all the scalar functions $B[T_\gamma](r,\ t)$, $B^{(i)}[T_\gamma](r,\ t)$, $B[S_\gamma](r,\ t)$, and $B^{(i)}[S_\gamma](r,\ t)$ in Chebyshev polynomials, the partial differential equations (2.6) and (2.7) are reduced to ordinary differential equations with respect to t for $B[{}_nT_l^{mz}](t)$, $B^{(i)}[{}_nT_l^{mz}](t)$, $B[{}_nS_l^{mz}](t)$ and $B^{(i)}[{}_nS_l^{mz}](t)$. We have then $2(N+1)$ variables and $2(N+1)$ equations for a set of $(l,\ m,\ z)$ of toroidal or poloidal magnetic field; $2(N-1)$ equations correspond to the induction equations at the mesh-points x_k, given in (2.19) and (4.3), for $k = 1$ to $k = N-1$, and the other four are the boundary conditions. The $2(N+1)$ equations are combined into one matrix equation. The diffusion and induction terms on the right-hand-side of the matrix equation are calculated at each mesh-point. The matrix, $2(N+1)$ by $2(N+1)$, is independent of order m of spherical harmonics and time t, since the matrix for the poloidal magnetic field

depends only on degree l of spherical harmonics through the boundary condition. Then one matrix for each degree l of toroidal or poloidal magnetic field is subjected to LU decomposition and stored onto the memory. We use the fourth-order Runge-Kutta scheme for time integration. In order to guarantee the stability of numerical calculation, the time step Δt should be less than

$$\left|\frac{\Delta r}{V_r}\right|_{\min}, \qquad \left|\frac{r}{\{L(L+1)(V_\theta^2+V_\phi^2)\}^{1/2}}\right|_{\min}, \tag{4.4}$$

where Δr is the distance between mesh-points, V_r, V_θ and V_ϕ denote r-, θ- and ϕ-components of velocity field, respectively (e.g. Glatzmaier, 1984); that is, Δt is the time during which a fluid particle at a mesh-point does not proceed beyond the next mesh-point. Furthermore we should pay attention to the limit Δt originating from the diffusion term.

In actual calculations, the induction equation is expressed in non-dimensional form. As mentioned in Section 2, we scale the equation by measuring the magnetic field $\boldsymbol{B}$ in units of typical strength of magnetic field B_s, the velocity field $\boldsymbol{V}$ in units of typical magnitude of velocity field V_s, length in units of typical length L_s. Time t is measured in units of the magnetic diffusion time L_s^2/ν_m. Then the induction equation, in vector form, becomes

$$\frac{\partial \boldsymbol{B}}{\partial t} = R_m \nabla \times (\boldsymbol{V} \times \boldsymbol{B}) + \nabla^2 \boldsymbol{B}, \tag{4.5}$$

where R_m is the magnetic Reynolds number defined as $R_m = V_s L_s/\nu_m$. We take the values as $B_s = 10^{-2}$ T, $V_s = 10^{-4}$ ms^{-1}, and $L_s = r_{oc} = 3.485\times10^6$ m. Then one magnetic diffusion time unit is about 1.45×10^5 years and $R_m \sim 130$.

4.2. Preliminary result

As a preliminary calculation, we attempt to examine time-dependent behavior of the magnetic field in Case 1; that is, the initial values are given from the result for Case 1, and only the same induction terms as adopted in Case 1 are considered; $(V[T_\alpha^0]B[S_\beta^0]T_\gamma)$ and $(V[S_\alpha]B[T_\beta^0]S_\gamma)$. The time step Δt is taken as $\Delta t = 6.92\times10^{-7}$. The results of time integration up to $1000\Delta t$ for $B[S_1^{1s}]$, $B[S_2^{1s}]$, $B[S_2^{2s}]$, $B[S_3^{1s}]$, $B[S_3^{2c}]$, $B[S_3^{3c}]$, $B[T_1^0]$, and $B[T_4^0]$, with the velocity field fixed, are shown in Fig. 4.1, where the values of scalar function at $x = 1.0$ $(r = r_{oc})$ are plotted for the dimensionless poloidal magnetic field, while those at $x = 0.8$ $(r = 0.93r_{oc})$ are plotted for the toroidal magnetic field. It is obviously seen in Fig. 4.1 that the steady state is actually realized as long as the same induction terms as adopted in Case 1 are taken into consideration.

4.3. Application to the results obtained in Cases 1 to 7

We apply the program code to the results obtained so far and examine time-dependent behavior of the magnetic field; that is, we regard the derived magnetic field in each case as the initial values, where the steady state has been realized, and examine a time-dependent kinematic dynamo for the derived velocity field.

In respective cases, we have neglected some interaction terms when we derive fluid motion in the core. If such terms are actually insignificant as presumed, a steady state, or a nearly steady state, would be realized in the calculation. If not, either one of the two following possibilities would be responsible. One is that the obtained result is not a plausible one; it might have been derived on inappropriate assumptions. The other is that other interaction terms are also responsible for secular variations of the Earth's magnetic field; we have assumed that both the magnetic and the velocity fields are in a steady state and have not considered the effect on

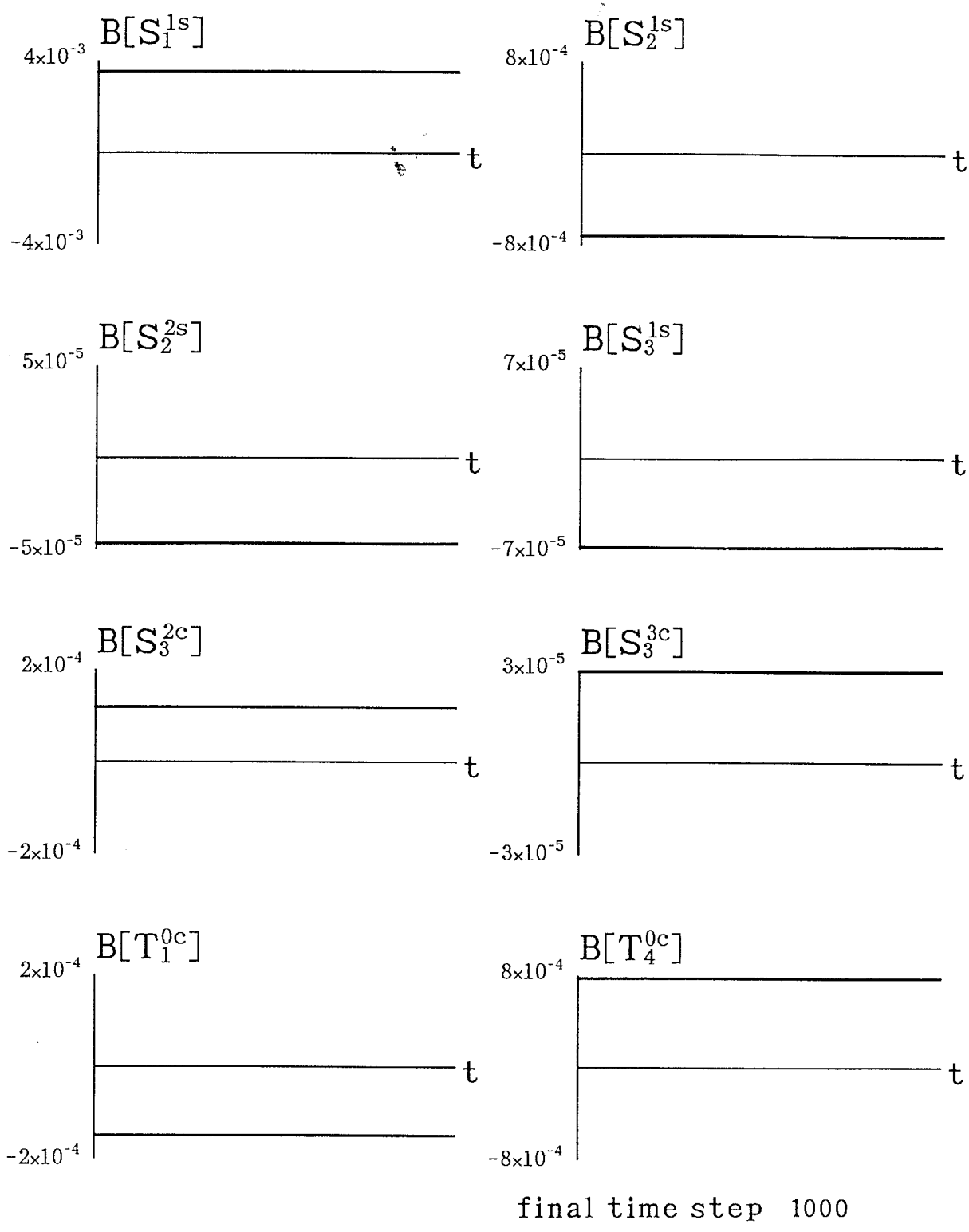

Fig. 4.1. Time-dependent behavior of magnetic fields for Case 1 up to $1000\Delta t$ (the time step $\Delta t = 6.92\times10^{-7}$). The lines indicate non-dimensional values of radial functions at $x = 1$ ($r = r_{oc}$) for poloidal fields and at $x = 0.8$ ($r = 0.93r_{oc}$) for toroidal fields. In this kinematic dynamo calculation, only the induction terms assumed in Case 1 are taken into consideration.

time variations in the equations to be solved.

We should recall that the present approach to fluid motion in the core from geomagnetic field data is completely different from the approaches based on the frozen-flux approximation. Time variations of the magnetic field due to the interactions between surface fluid motion and the magnetic field are taken into consideration in the frozen-flux approximation, but the magnetic diffusion term is neglected, on the ground that only short time-scale variations, say, some tens of years, are considered. In the present approach, the magnetic diffusion inside the core is taken into consideration, but time variations are not considered.

4.3.1. Case 1

First, we examine time evolution of the magnetic field, using the result obtained in Case 1. The velocity field to be considered in the calculation is shown in Fig. 3.3. Time integration is performed for a time step $\Delta t = 6.92\times10^{-7}$. The result is shown in Fig. 4.2, which indicates the scalar functions for poloidal and toroidal magnetic fields at the same r as in Fig. 4.1. The total time $100\Delta t$ corresponds to 10 years, during which the magnetic fields vary considerably. It is indeed unreasonable that within such a short time interval the sectorial dipole magnetic field $B[S_1^{1c}]$ becomes stronger than the axial dipole magnetic field $B[S_1^0]$ and also other magnetic fields vary rapidly. This would not result from numerical instability, since we have chosen the time step Δt so as to guarantee numerical stability. In fact, even for the time step $\Delta t = 6.92\times10^{-8}$, one tenth of the previous one, we obtained the same result.

This result indicates that the velocity field derived on the assumption in Case 1 is inappropriate. The time-dependent behavior of the magnetic field shown in Fig. 4.2 obviously relies on the assumption that strong zonal toroidal magnetic fields are generated by the interaction between the axial dipole magnetic field and the zonal

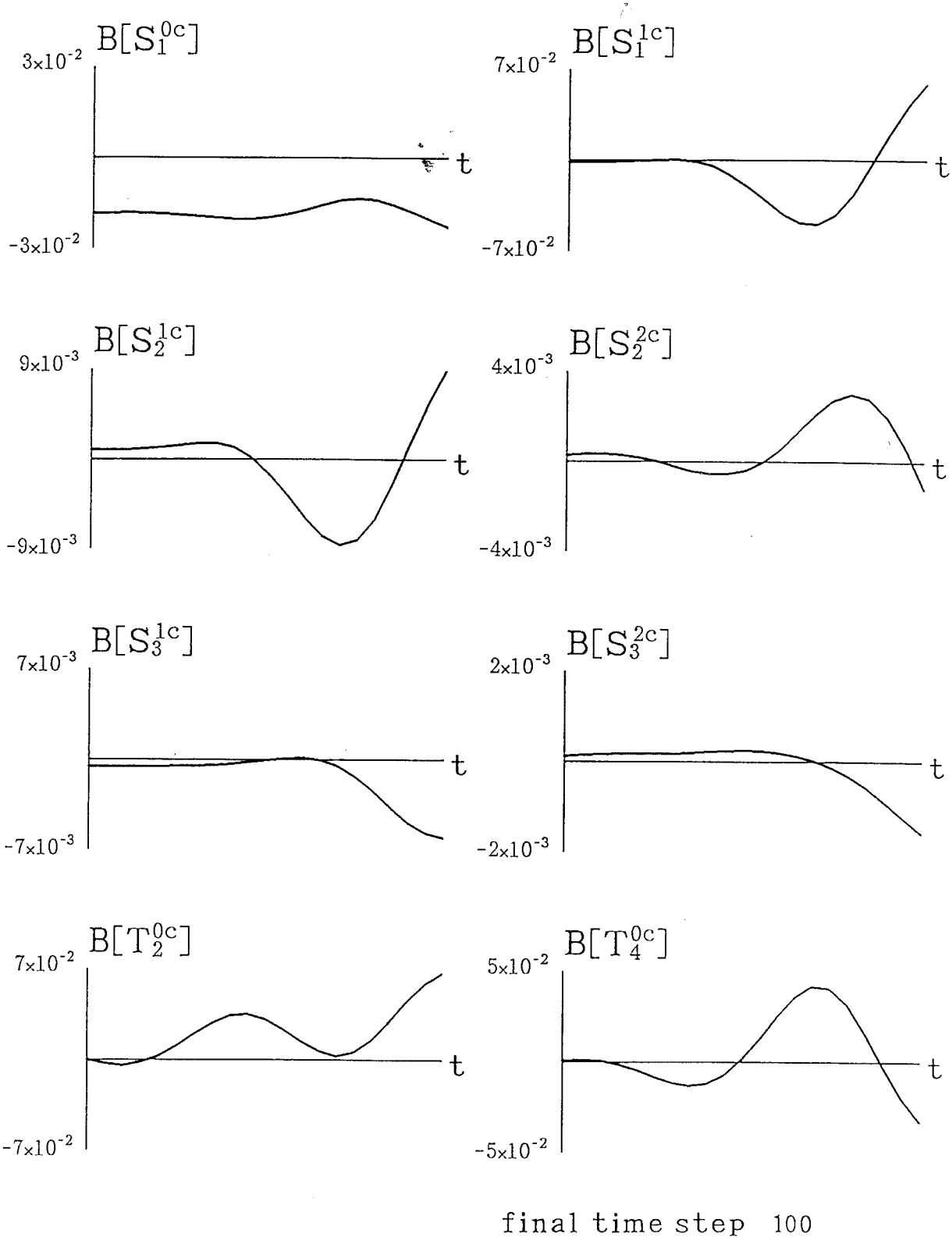

Fig. 4.2. Time-dependent behavior of magnetic fields for Case 1 up to $100\Delta t$ (the time step $\Delta t = 6.92\times10^{-7}$). The lines indicate non-dimensional values of radial functions at $x = 1$ ($r = r_{oc}$) for poloidal fields and at $x = 0.8$ ($r = 0.93r_{oc}$) for toroidal fields.

toroidal motion. However, the calculated zonal toroidal magnetic field turned out to be much weaker than we have expected, resulting in a too large velocity field. In actual time evolution of the magnetic field, other magnetic fields must also be primary inducing magnetic fields. In other words, the reason why magnetic fields vary considerably with time is that such magnetic fields are neglected. It is concluded, therefore, that the assumption made in Case 1 is not reasonable.

If the velocity field is also allowed to vary according to the induction, the Navier-Stokes, and the energy equations, time evolution of the magnetic field would not tend to diverge. If a strong magnetic field is induced in the core, the Lorentz force due to the magnetic field would also become stronger and eventually weaken the velocity field. In this way the non-linear terms effectively suppress the growth of magnetic field and time evolution is stabilized. It is known, however, that the effect of such non-linear terms depends on the initial state. A good example of initial value dependence in the non-linear effect is demonstrated in disk dynamo models (Bullard, 1955; Shimizu and Honkura, 1985). Judging from the time evolution shown in Fig. 4.2, the magnetic and velocity fields derived on the assumption in Case 1 are likely to be far from the equilibrium state. It is expected, therefore, that even solutions of the magnetohydrodynamic equations would unrealistically oscillate if the result derived in Case 1 is adopted as the initial state.

4.3.2. Case 2

Second, time evolution of the magnetic field is examined, using the result derived on the assumption in Case 2. The velocity field used in the calculation is shown in Fig. 3.7; that is, the result for $U[S_2^0] = -10^{-3}$ is adopted here, since there is no significant difference between the velocity fields derived for $U[S_2^0] = 0$ and $U[S_2^0] = -10^{-5}$ shown in Figs. 3.3 and 3.5, respectively. Time integration is performed up to $200\Delta t$

with the same time step $\Delta t = 6.92\times10^{-7}$ as in the previous calculation, and the result is shown in Fig. 4.3. During the time interval $200\Delta t$, corresponding to 20 years, the magnetic fields tend to diverge in this case. During 20 years, the axial dipole magnetic field $B[S_1^0]$ grows by three times the initial value. This also indicates that the velocity field derived on the assumption made in Case 2 is inappropriate. The reason would be the same as for Case 1. We conclude that the assumption made in Case 2 is also inappropriate.

4.3.3. Case 3

Third, we examine time evolution of the magnetic field, using the result derived in Case 3. The velocity field used in the calculation is shown in Fig. 3.9. In this case, we take the time step as $\Delta t = 6.92\times10^{-8}$, which is shorter than those taken in the previous calculations. Time integration is performed up to $200\Delta t$, corresponding to only 2 years. The result is shown in Fig. 4.4. During such a very short time span, the magnetic fields also tend to diverge. Therefore, the velocity field derived on the assumption made in Case 3 is not plausible.

4.3.4. Case 4

Next, we examine time-dependent behavior of the magnetic field for Case 4. The velocity field is shown in Fig. 3.15. Time integration for magnetic fields is performed up to $200\Delta t$ with the time step $\Delta t = 6.92\times10^{-8}$. Figure 4.5 shows the result. The magnetic fields eventually tend to diverge after only 2 years. The velocity field derived on the assumption made in Case 4 is not plausible.

4.3.5. Case 5

Next, we calculate time evolution of the magnetic field, using the result for Case

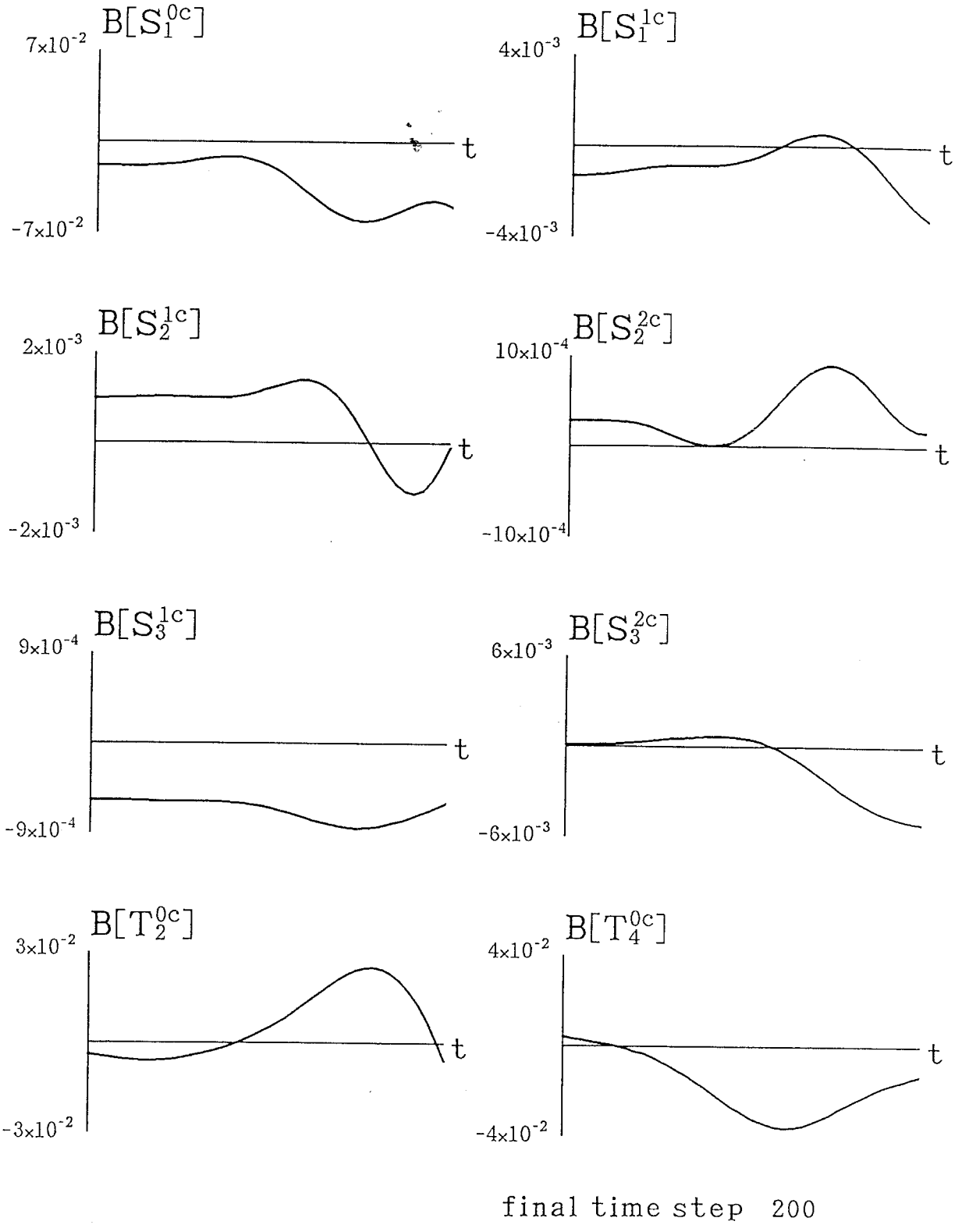

Fig. 4.3. Time-dependent behavior of magnetic fields for Case 2 up to $200\Delta t$ (the time step $\Delta t = 6.92\times10^{-7}$). The lines indicate non-dimensional values of radial functions at $x = 1$ ($r = r_{oc}$) for poloidal fields and at $x = 0.8$ ($r = 0.93r_{oc}$) for toroidal fields.

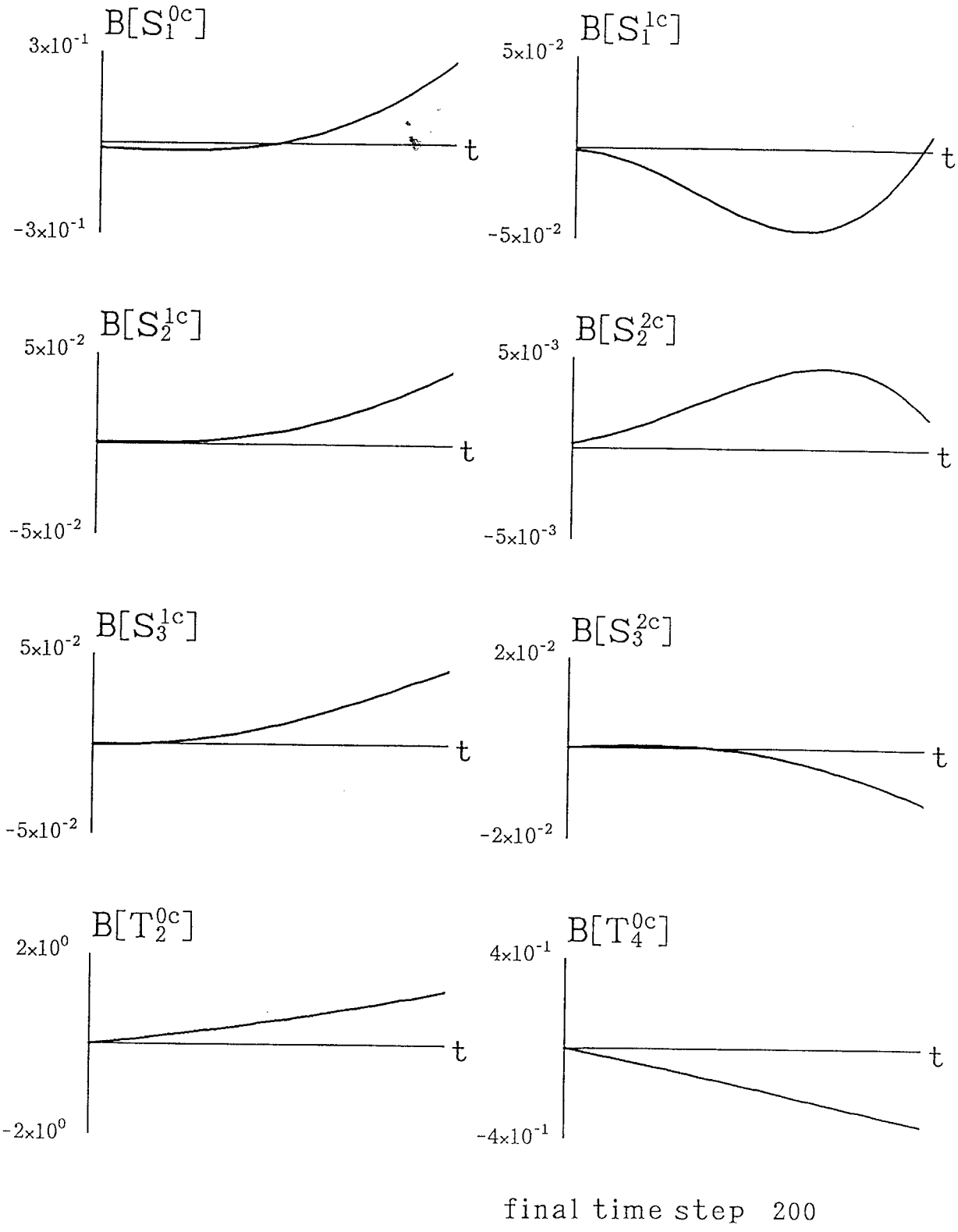

Fig. 4.4. Time-dependent behavior of magnetic fields for Case 3 up to $200\Delta t$ (the time step $\Delta t = 6.92\times10^{-8}$). The lines indicate non-dimensional values of radial functions at $x = 1$ ($r = r_{oc}$) for poloidal fields and at $x = 0.8$ ($r = 0.93r_{oc}$) for toroidal fields.

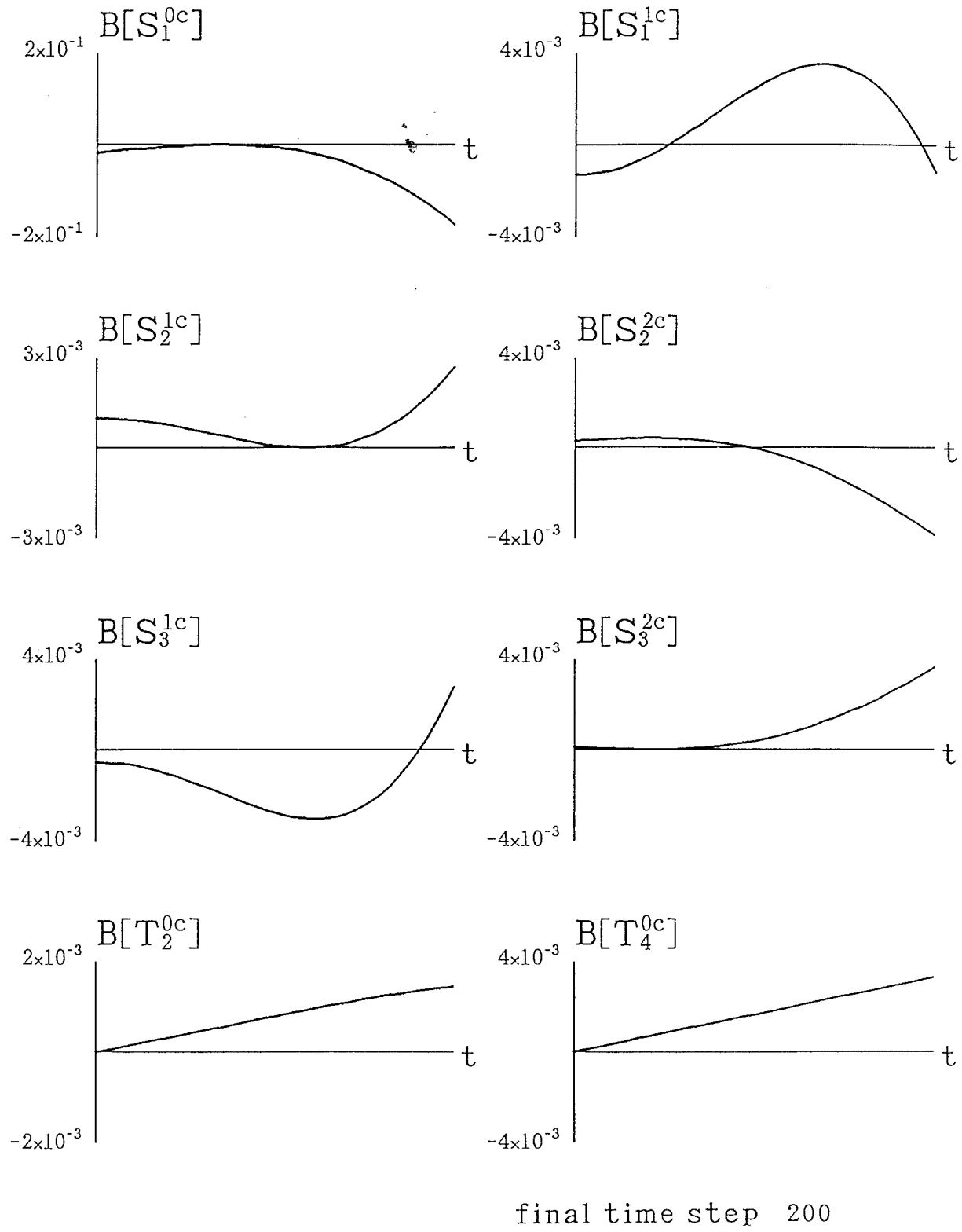

Fig. 4.5. Time-dependent behavior of magnetic fields for Case 4 up to $200\Delta t$ (the time step $\Delta t = 6.92\times10^{-8}$). The lines indicate non-dimensional values of radial functions at $x = 1$ ($r = r_{oc}$) for poloidal fields and at $x = 0.8$ ($r = 0.93r_{oc}$) for toroidal fields.

5. The velocity field is shown in Fig. 3.17. The result of time integration is shown in Fig. 4.6, where the calculation was performed up to $500\Delta t$ with the time step $\Delta t = 6.92\times10^{-6}$.

In this case, the stability seems to be rather promising, compared with the previous results, and the fluctuations of the magnetic fields are apparently close to those near an equilibrium state. If we examine magnetic energy, however, we recognize magnetic fields growing with time. The magnetic energy in the core is defined as

$$E_B = \frac{1}{2\mu_0}\int B^2 dv, \tag{4.6}$$

where volume integral is performed for the whole core. Since fluid motion exists only in the outer core and the volume of the inner core is very small, about 4 % of the whole core, we calculate the quantity defined as

$$E_b = \int B^2 dv, \tag{4.7}$$

where volume integral is performed only for the outer core and dimensionless values are used. Hereafter we will simply call E_b the magnetic energy. We show time-dependent behavior of E_b in Fig. 4.7. The magnetic energy E_b turns out to grow exponentially with time. The value of E_b at $t = 500\Delta t$ is nearly nineteen times the value at $t = 0$.

This type of time-dependent behavior is generally seen in kinematic dynamos for the given velocity field which is too large to maintain a steady magnetic field. Since the velocity field is fixed, the equation governing the magnetic field is linear. Assuming that the magnetic fields depend on time as $\exp[\lambda t]$, the induction equation (4.5) is written as

$$\lambda \boldsymbol{B} = R_m \nabla \times (\boldsymbol{V} \times \boldsymbol{B}) + \nabla^2 \boldsymbol{B}. \tag{4.8}$$

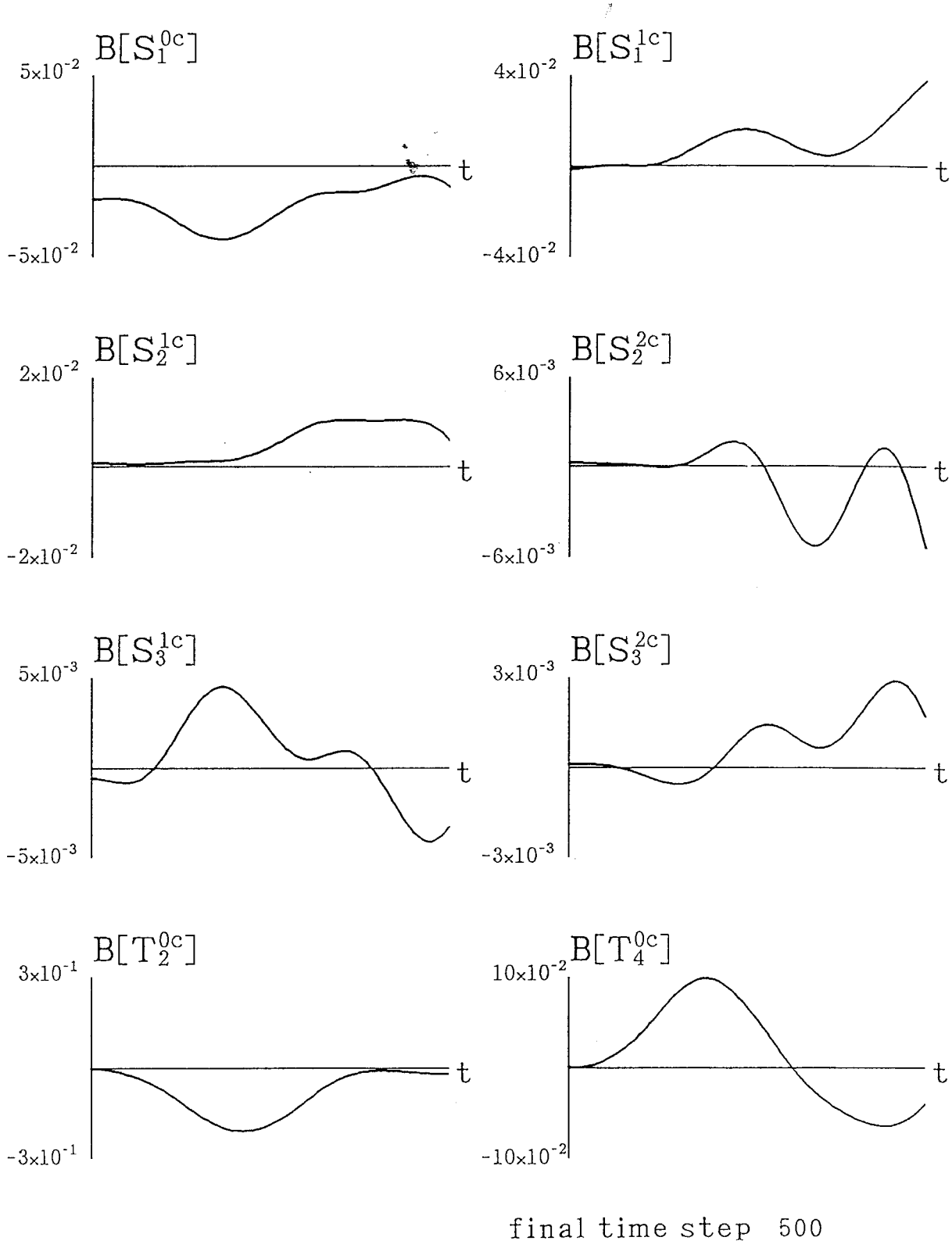

Fig. 4.6. Time-dependent behavior of magnetic fields for Case 5 up to $500\Delta t$ (the time step $\Delta t = 6.92\times10^{-6}$). The lines indicate non-dimensional values of radial functions at $x = 1$ ($r = r_{oc}$) for poloidal fields and at $x = 0.8$ ($r = 0.93r_{oc}$) for toroidal fields.

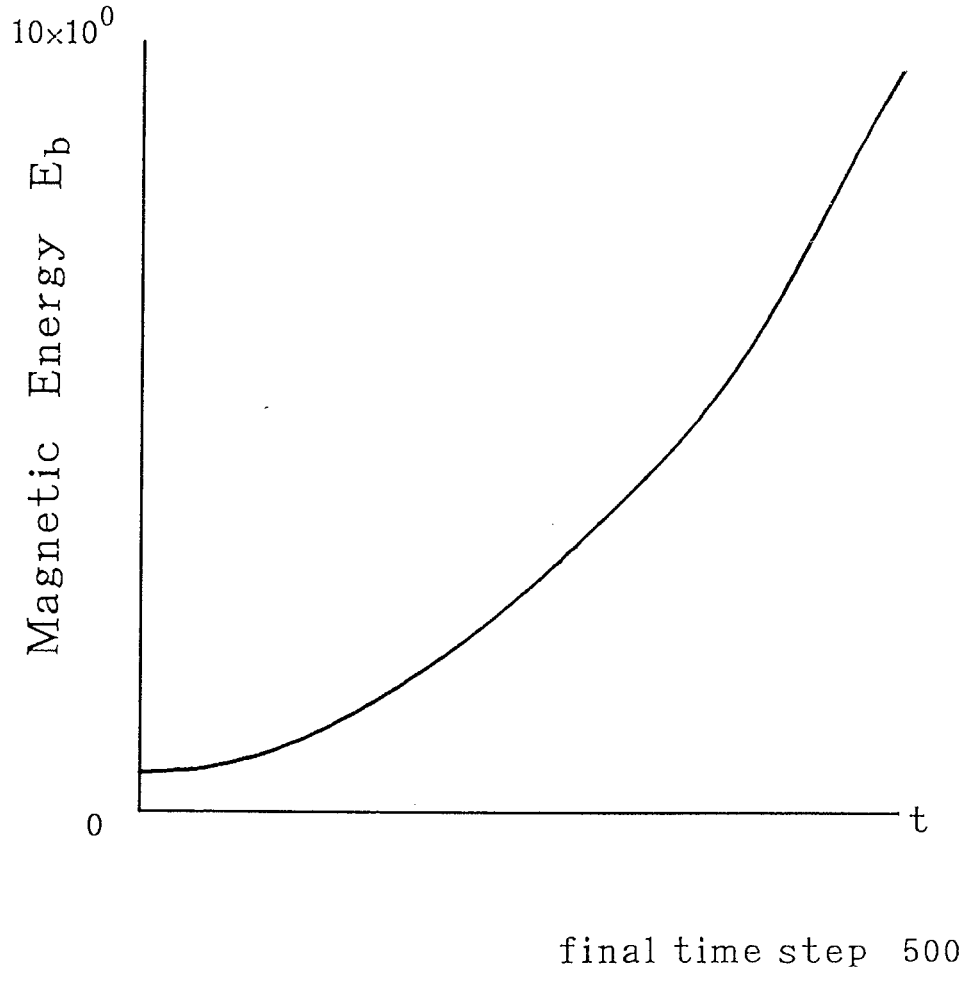

Fig. 4.7. Time-dependent behavior of magnetic energy E_b, defined in (4.7), for Case 5.

In Bullard and Gellman (1954), under the condition $\lambda = 0$, (4.8) was solved as an eigenvalue problem for the magnetic Reynolds number R_m. Alternatively, (4.8) can be solved as an eigenvalue problem for λ with R_m specified (e.g. Roberts, 1972). The eigenvalues λ's are generally complex numbers. The eigenvalue $\lambda_{\max}$ which has the largest real part corresponds to the mode showing the maximum growth rate in time. If Re $\lambda_{\max} = 0$ and Im $\lambda_{\max} = 0$, the magnetic field is steady. If Re $\lambda_{\max} = 0$ and Im $\lambda_{\max} \neq 0$, time-dependent behavior of the magnetic field is oscillatory. Figure 4.7 suggests that if we solve the eigenvalue problem with respect to λ for the velocity field derived in Case 5 and R_m taken in the present study, we will obtain Re $\lambda_{\max} > 0$.

4.3.6. Case 6

Next, we examine time-dependent behavior of the magnetic field, using the result derived for Case 6. The velocity field is shown in Fig. 3.20. In this case, the initial state is different from those in Cases 1 to 5 in the sense that non-zonal toroidal magnetic fields and non-zonal toroidal velocity fields are taken into consideration, whereas there are no non-zonal toroidal magnetic and non-zonal toroidal velocity fields in Cases 1 to 5; that is, the magnetic and velocity fields up to the truncation level L of spherical harmonics are all taken into consideration in Case 6. It turns out then that the result obtained in Case 6 seems to represent a possible state in the core, at least in that magnetic fields do not diverge during a short time with the velocity field fixed. Taking the time step as $\Delta t = 6.92 \times 10^{-6}$, time integration for the magnetic field was preformed up to $500\Delta t$, which corresponds to 500 years. The results of time evolution of poloidal and toroidal magnetic fields are shown in Figs. 4.8 and 4.9, respectively, for some modes.

It is clearly seen from the figures that the magnetic fields are by no means

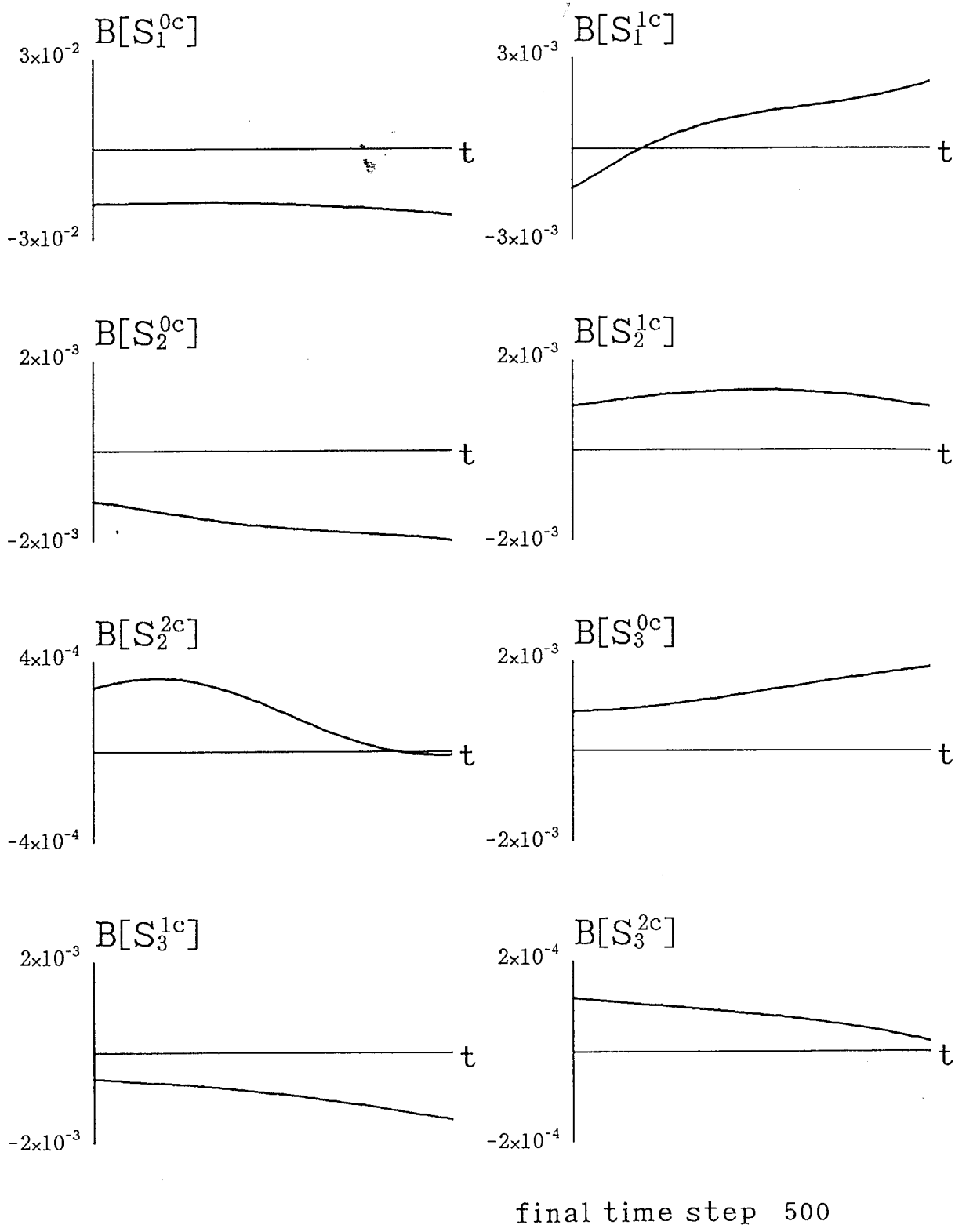

Fig. 4.8. Time-dependent behavior of poloidal magnetic fields for Case 6 up to $500\Delta t$ (the time step $\Delta t = 6.92\times10^{-6}$). The lines indicate non-dimensional values of radial functions at $x = 1$ ($r = r_{oc}$).

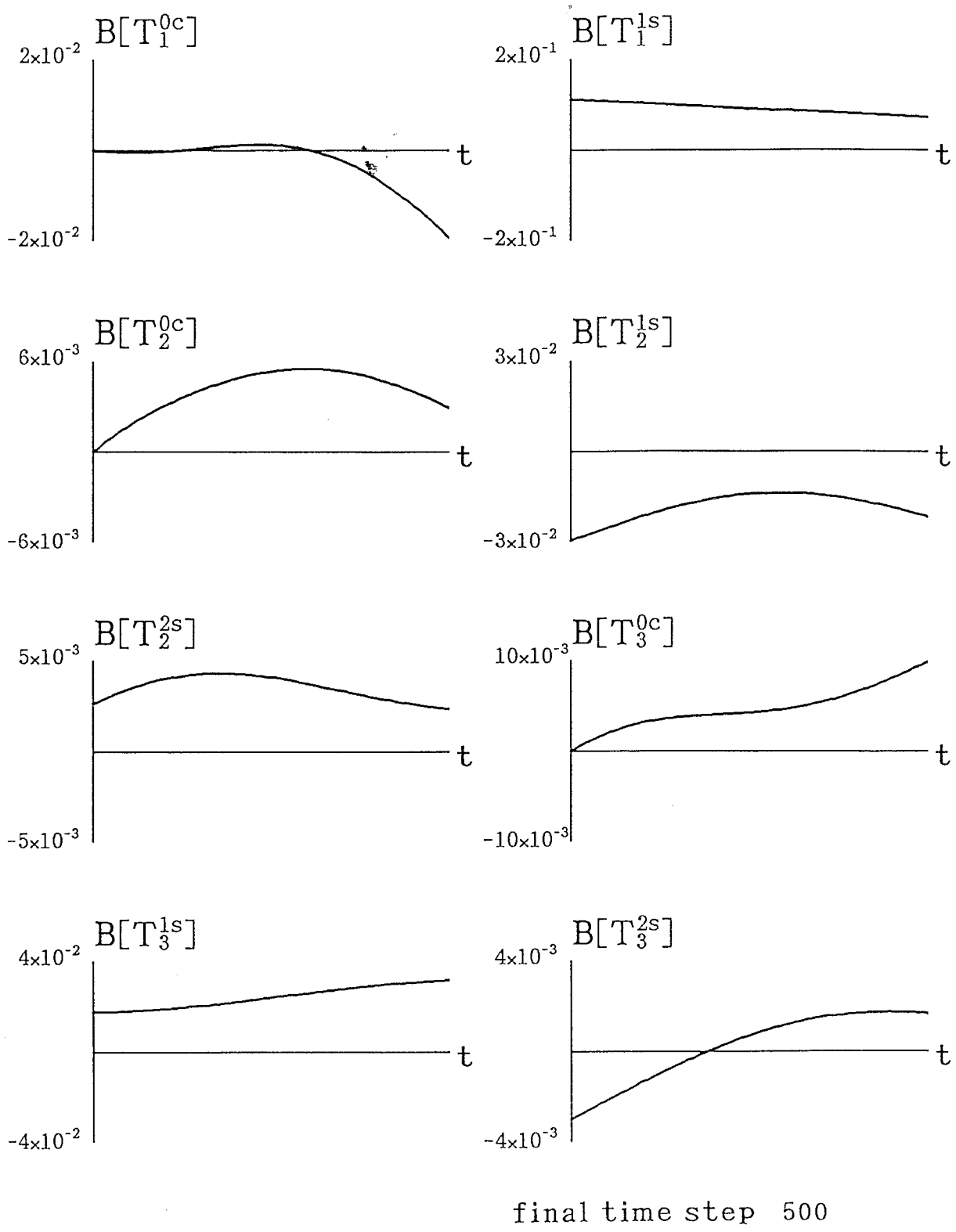

Fig. 4.9. Time-dependent behavior of toroidal magnetic fields for Case 6 up to $500\Delta t$ (the time step $\Delta t = 6.92\times10^{-6}$). The lines indicate non-dimensional values of radial functions at $x = 0.8$ ($r = 0.93r_{oc}$).

invariable even in this case. This is reasonable, since some interaction terms have been neglected in deriving fluid motion in the core. We have assumed in Case 6 that the main inducing fields are the axial dipole magnetic field and toroidal magnetic fields inside the core and also, steady magnetic fields are maintained. The other, neglected induction terms are primarily responsible for secular variations of the Earth's magnetic field.

One noticeable characteristic of time variations of the magnetic field shown in Figs. 4.8 and 4.9 is that zonal toroidal magnetic fields are enhanced considerably. Various induction terms may contribute to the generation of the zonal toroidal magnetic fields. One possibility is as follows. Zonal toroidal motions, which have been expected to generate strong zonal toroidal magnetic fields (the ω-effect), were derived on the assumption that the motions are in a steady state as a result of the equilibrium among the inertia, the Lorentz, the Coriolis and the viscous forces in the Navier-Stokes equation. Eventually angular velocity field seems to adjust itself to the magnetic lines of force for axisymmetric poloidal fields, for example as shown in Fig. 3.16 for Case 5. The zonal toroidal motions are invariable in the kinematic dynamo calculation, whereas the axisymmetric poloidal magnetic fields would undergo time variations. Consequently, the shear in zonal toroidal motions effectively generates zonal toroidal magnetic fields.

It is also worth noting that axisymmetric poloidal magnetic fields, for example $B[S_1^0]$, $B[S_2^0]$ and $B[S_3^0]$ as shown in Fig. 4.8, little vary, compared with sectorial poloidal magnetic fields $B[S_1^{1c}]$ and $B[S_2^{2c}]$, in spite of the fact that in the present study we have not taken into consideration the induction terms by which the axisymmetric poloidal magnetic fields are generated. The inductive contribution to the magnetic field should consist of two opposite factors; one is the generation and the other is the destruction of the magnetic field. If those effects are comparable to each other,

the above feature would be understandable. In a sense, we may claim that even the fluid motion as derived only from non-axisymmetric poloidal magnetic fields represents an actually possible type of fluid motion in the Earth's outer core. This suggests that the characteristics of non-axisymmetric magnetic fields observed at the Earth's surface, for example their distribution and strength, are important manifestations of dynamo processes.

We show time-dependent behavior of magnetic energy E_b in Fig. 4.10. The value of E_b at $t = 500\Delta t$ is only about 1.2 times the initial value. Therefore, if we express time-dependence of magnetic fields as $\exp[\lambda t]$, Re $\lambda_{\max}$ for Case 6 is positive but closest to zero among those for Cases 1 to 6.

The above result was obtained for the truncation level $N = 9$. Although we mentioned, in Section 3, that if we wish to discuss quantitative nature of the derived fluid motion in detail, we should set the truncation level for Chebyshev polynomials at least at $N = 13$, time-dependent behavior of the magnetic field for $N = 13$ is not different significantly from that for $N = 9$. The value of magnetic energy E_b for $N = 13$ at $t = 500\Delta t$ is about 1.3 times the initial value. Therefore, when we check the validity of solutions and examine the plausibility of the fluid motion derived for respective cases, the truncation level for Chebyshev polynomials, N, would have only a very little effect.

4.3.7. Case 7

Finally, we examine time-dependent behavior of the magnetic field, using the result derived for Case 7. The velocity field is shown in Fig. 3.25 for $U[S_2^0] = -3\times10^{-6}$. Taking the time step as $\Delta t = 6.92\times10^{-6}$, time integration is performed up to $500\Delta t$, corresponding to 500 years. Time-evolution of poloidal and toroidal magnetic fields is shown in Figs. 4.11 and 4.12, respectively, for some modes. There

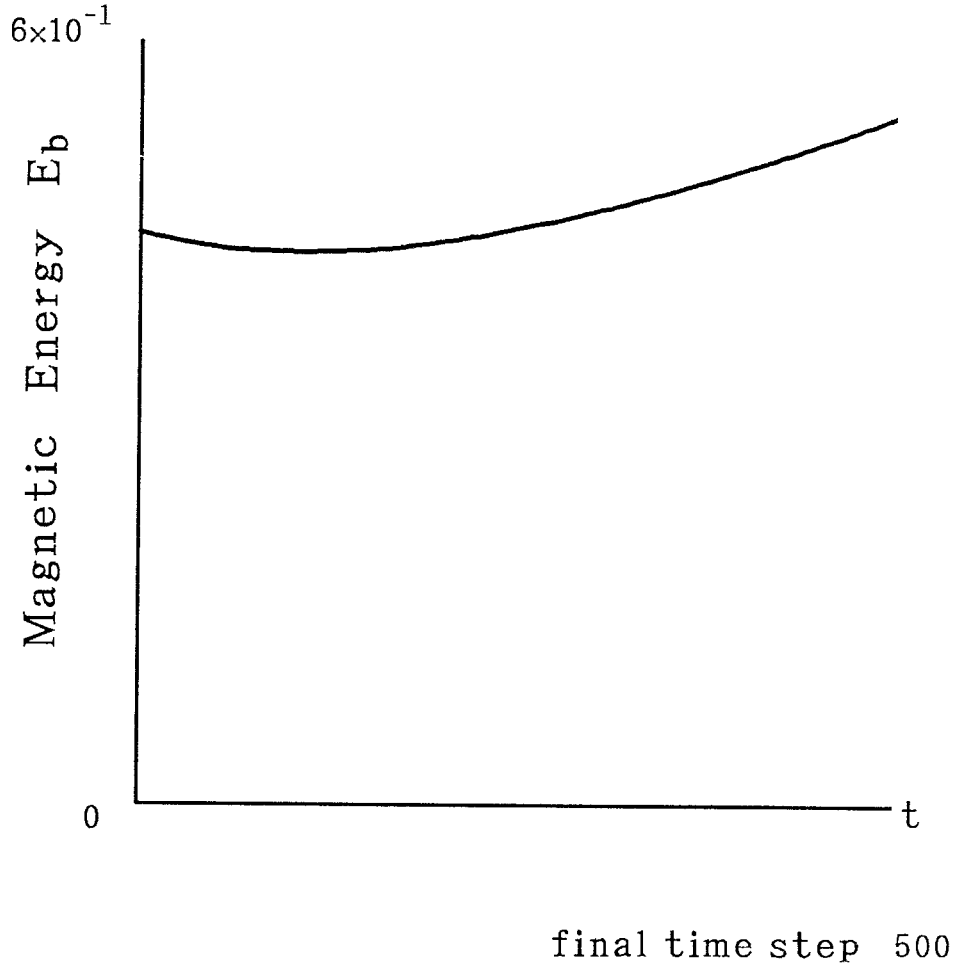

Fig. 4.10. Time-dependent behavior of magnetic energy E_b for Case 6.

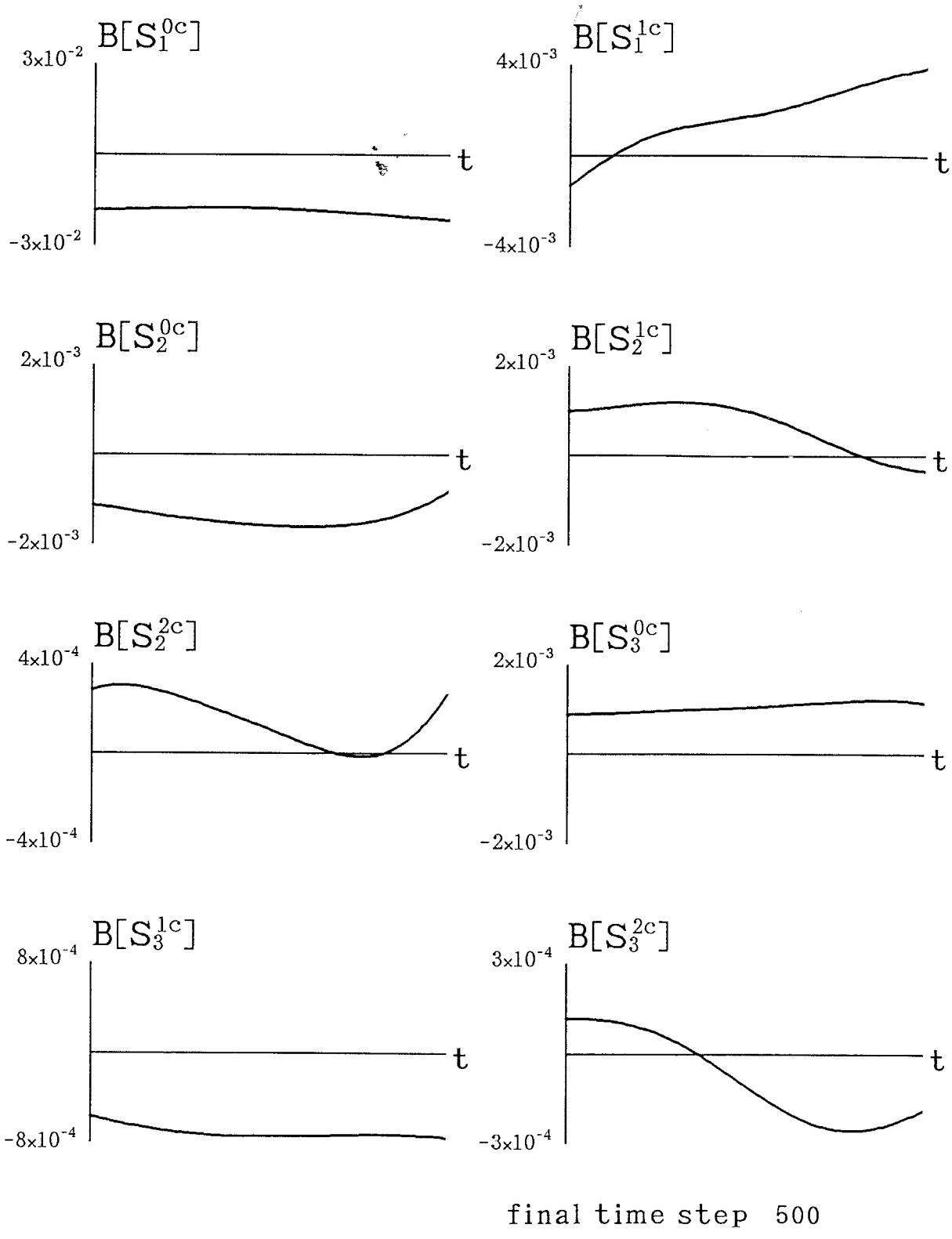

Fig. 4.11. Time-dependent behavior of poloidal magnetic fields for Case 7 up to $500\Delta t$ (the time step $\Delta t = 6.92\times10^{-6}$). The lines indicate non-dimensional values of radial functions at $x = 1$ ($r = r_{oc}$).

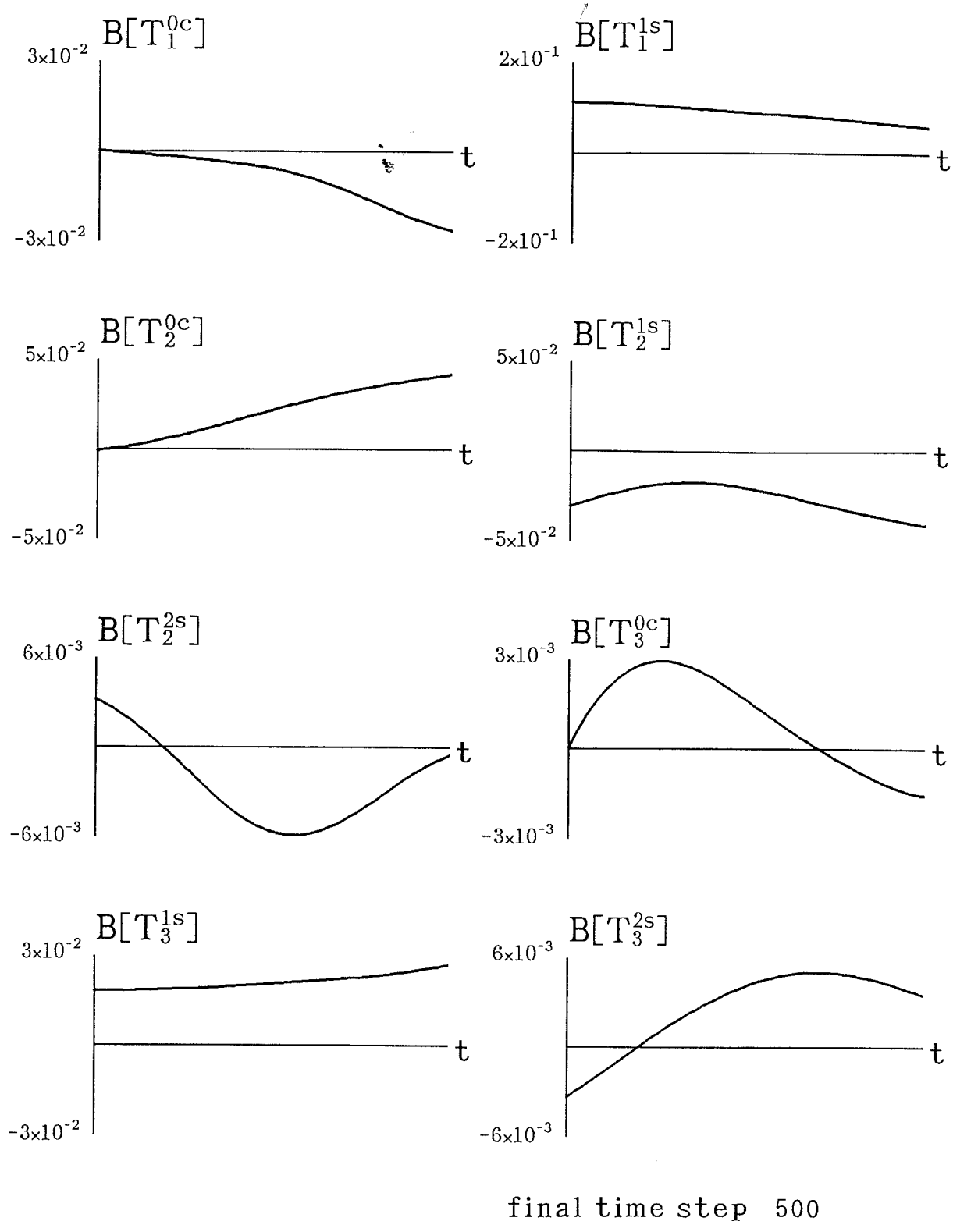

Fig. 4.12. Time-dependent behavior of toroidal magnetic fields for Case 7 up to $500\Delta t$ (the time step $\Delta t = 6.92\times10^{-6}$). The lines indicate non-dimensional values of radial functions at $x = 0.8$ ($r = 0.93r_{oc}$).

seems to be no significant difference between the results in Cases 6 and 7.

We show time-dependent behavior of magnetic energy E_b in Fig. 4.13. The value of E_b at $t = 500\Delta t$ is about 1.5 times the initial value. Re $\lambda_{\max}$ in this case would be larger that that in Case 6.

4.4. The effect of addition of meridional circulation

It is expected that additional meridional circulation introduced in Case 7 has some effects on a dynamo process as in some kinematic dynamo models (e.g. Roberts, 1972; Roberts and Stix, 1972). In fact, we derived a different result of time-dependent behavior of the magnetic field between Cases 4 and 5. As seen in Figs. 3.20 and 3.25, there is also a noticeable difference between the velocity fields derived in Cases 6 and 7; for instance, the westward flow in a zone near the equator. We may then expect that some significant differences appear during long time duration, if the mechanism explained above for the growth of zonal toroidal magnetic fields due to zonal toroidal motions for Case 6 is operative.

To examine this possibility, we examined time evolution of the magnetic field up to $5000\Delta t$ with the same time step $\Delta t = 6.92\times10^{-6}$; corresponding to 5000 years, ten times longer than in the previous calculation.

Time-dependent behavior of the magnetic field in Case 6 is shown in Figs. 4.14 and 4.15 for poloidal and toroidal constituents, respectively. Similarly, Figs. 4.16 and 4.17 show time-dependent behavior in Case 7. The most noticeable difference appears in time-dependent behavior of the axial dipole magnetic field $B[S_1^0]$. In Fig. 4.14 for Case 6, the absolute value of scalar function at $r = r_{oc}$ for the dipole magnetic field oscillates but gradually decreases with an eventual polarity change. In Fig. 4.16 for Case 7, the absolute value decreases as in Case 6 until around $3000\Delta t$, but it returns to the initial value, more or less. As for absolute values for the other

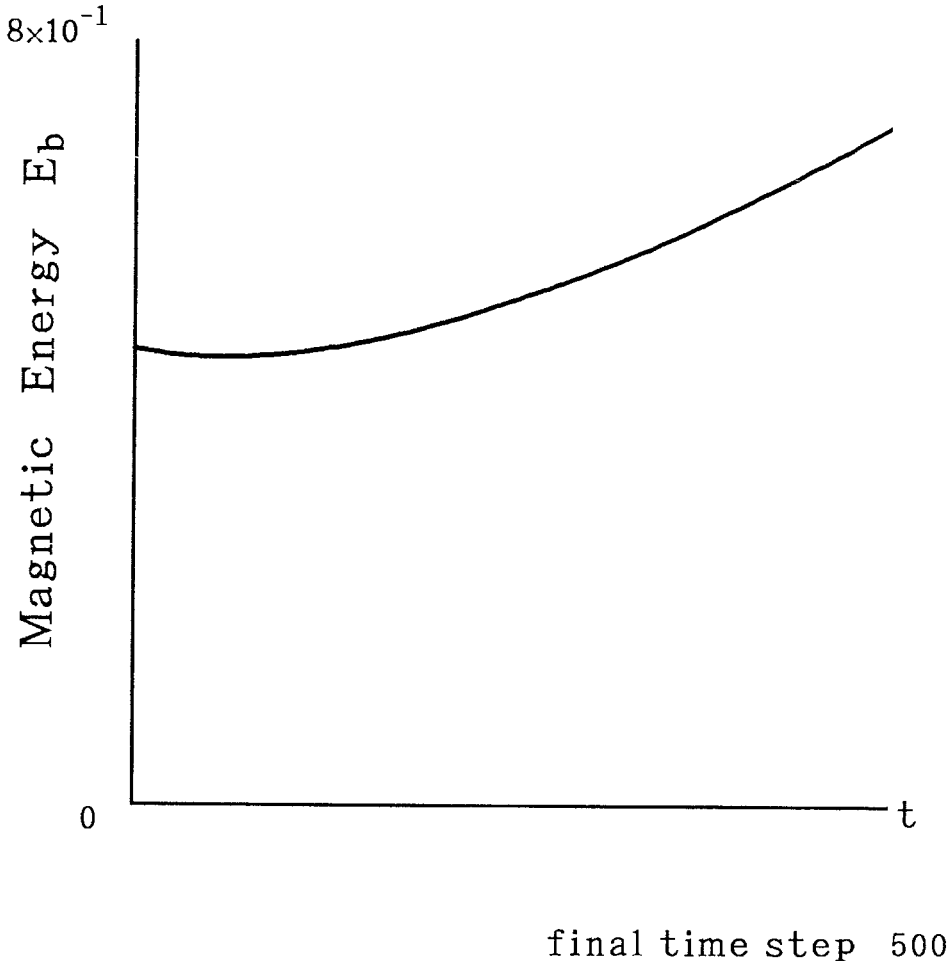

Fig. 4.13. Time-dependent behavior of magnetic energy E_b for Case 7.

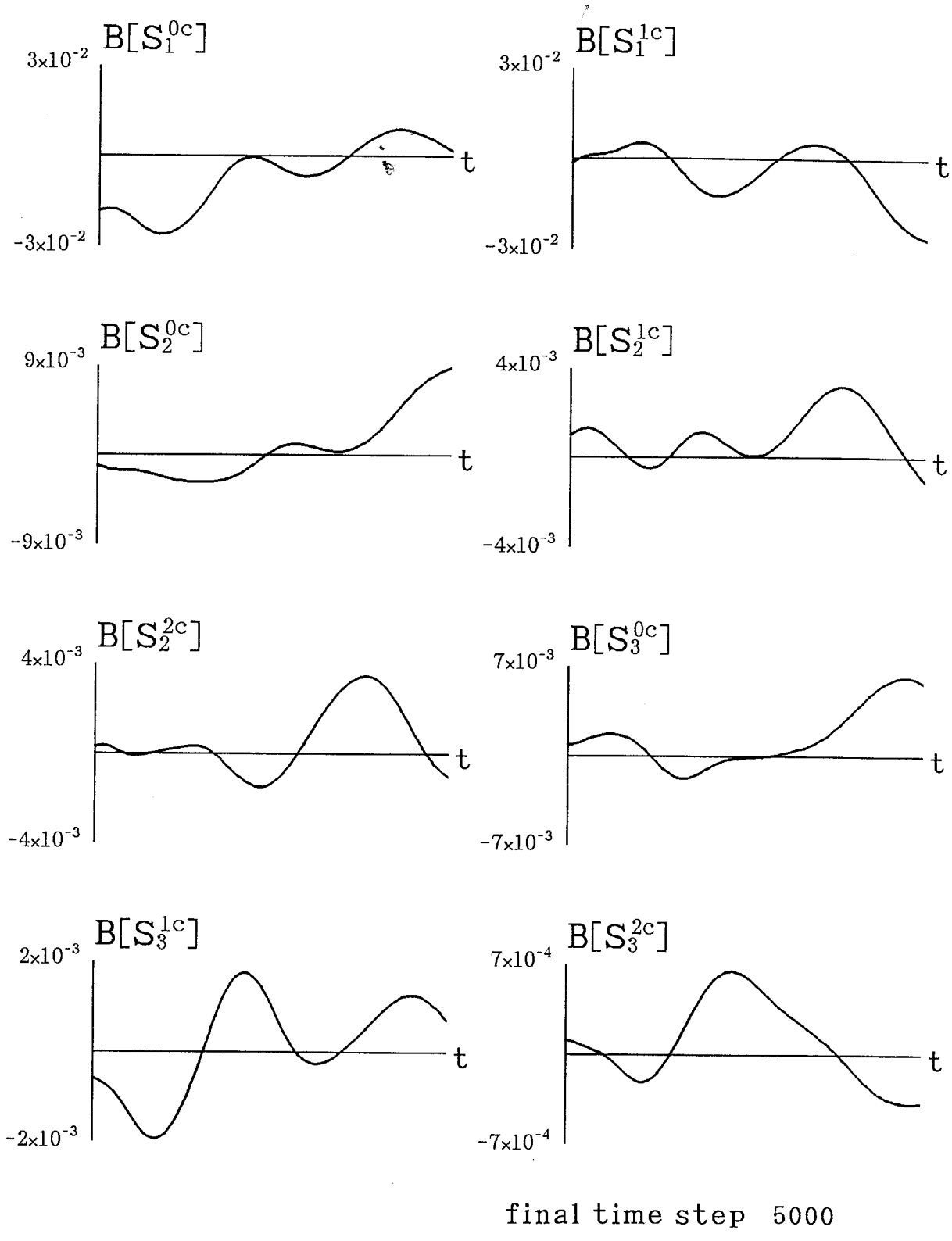

Fig. 4.14. Time-dependent behavior of poloidal magnetic fields for Case 6 up to $5000\Delta t$ (the time step $\Delta t = 6.92\times10^{-6}$). The lines indicate non-dimensional values of radial functions at $x = 1$ ($r = r_{oc}$).

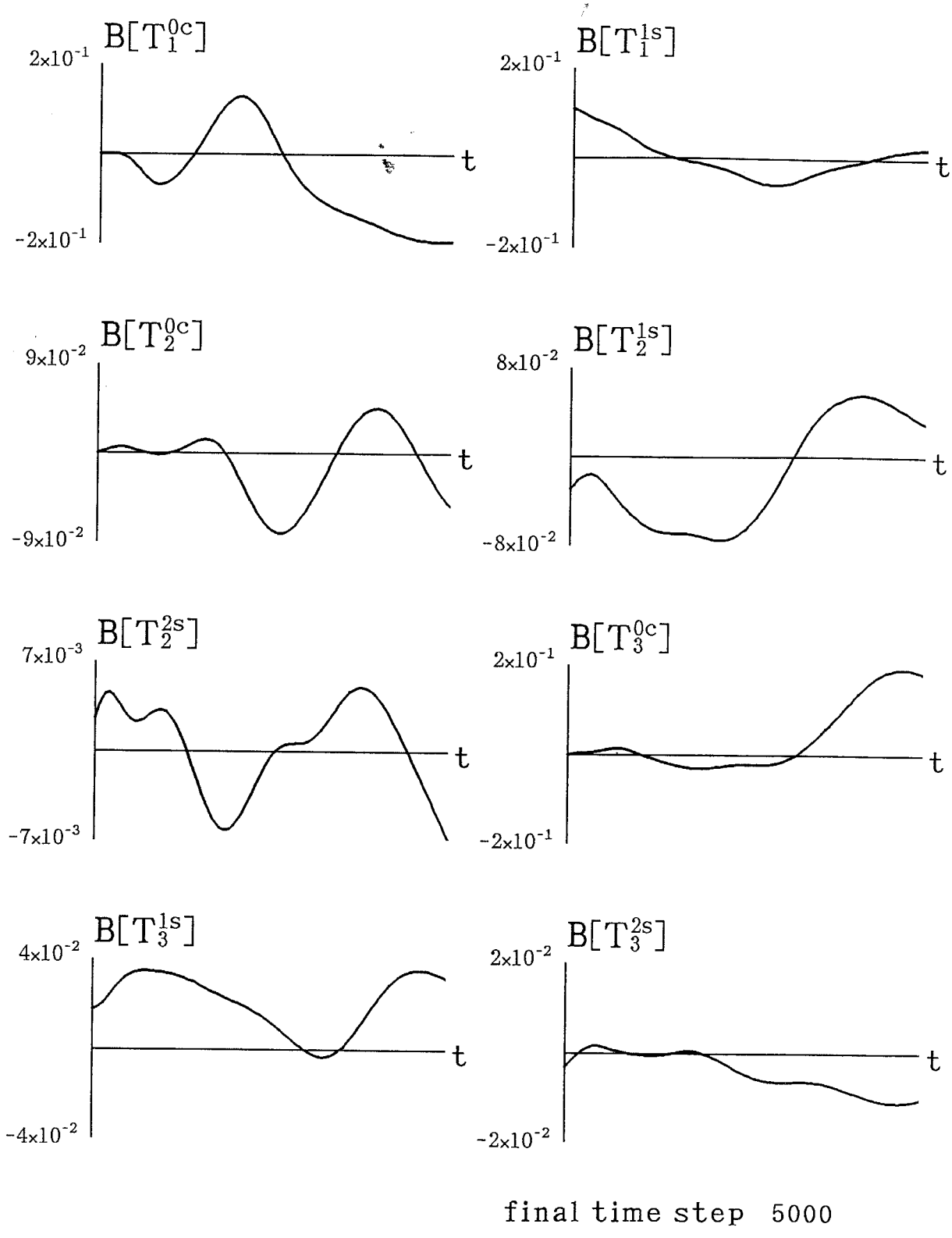

Fig. 4.15. Time-dependent behavior of toroidal magnetic fields for Case 6 up to $5000\Delta t$ (the time step $\Delta t = 6.92\times10^{-6}$). The lines indicate non-dimensional values of radial functions at $x = 0.8$ ($r = 0.93r_{oc}$).

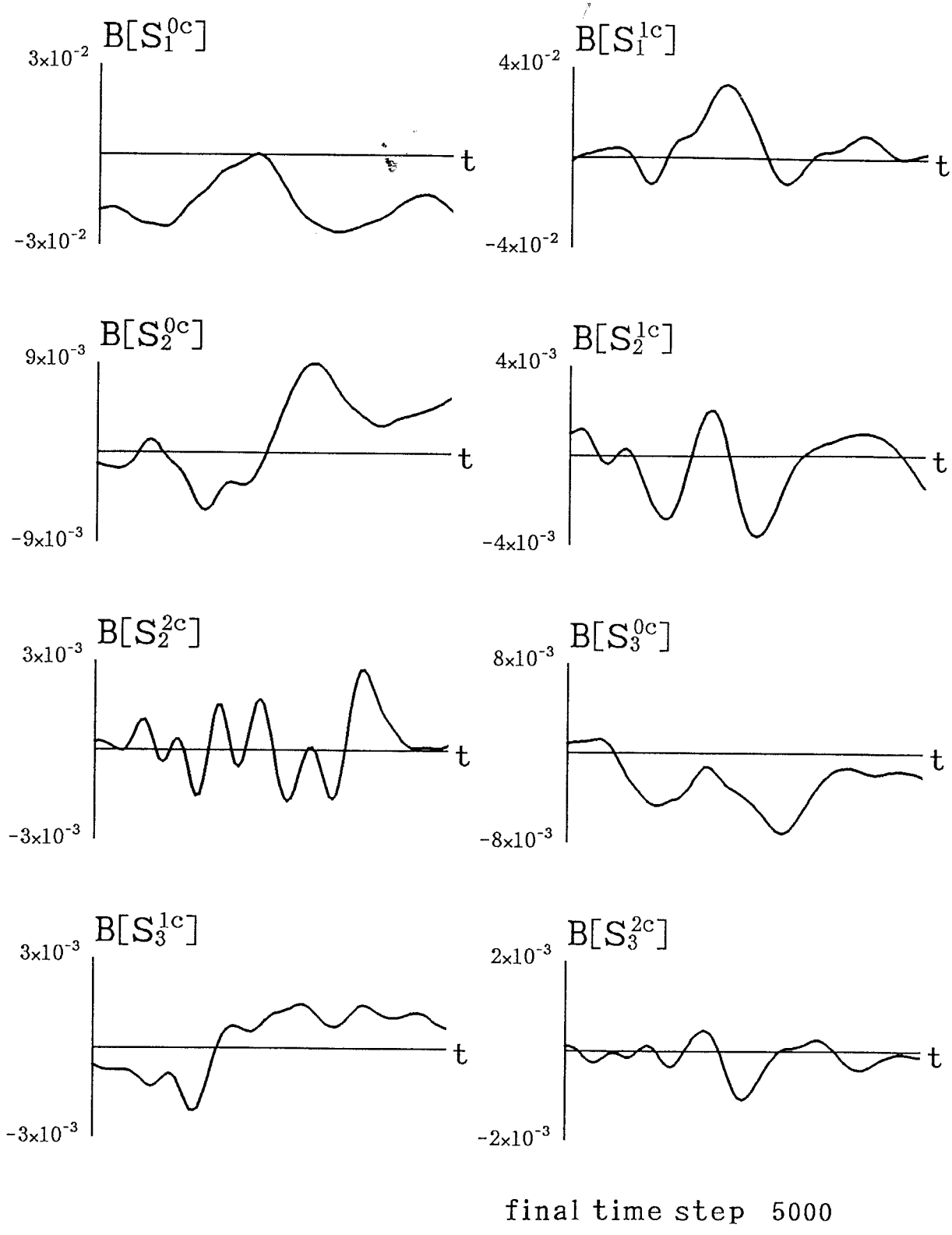

Fig. 4.16. Time-dependent behavior of poloidal magnetic fields for Case 7 up to $5000\Delta t$ (the time step $\Delta t = 6.92\times10^{-6}$). The lines indicate non-dimensional values of radial functions at $x = 1$ ($r = r_{oc}$).

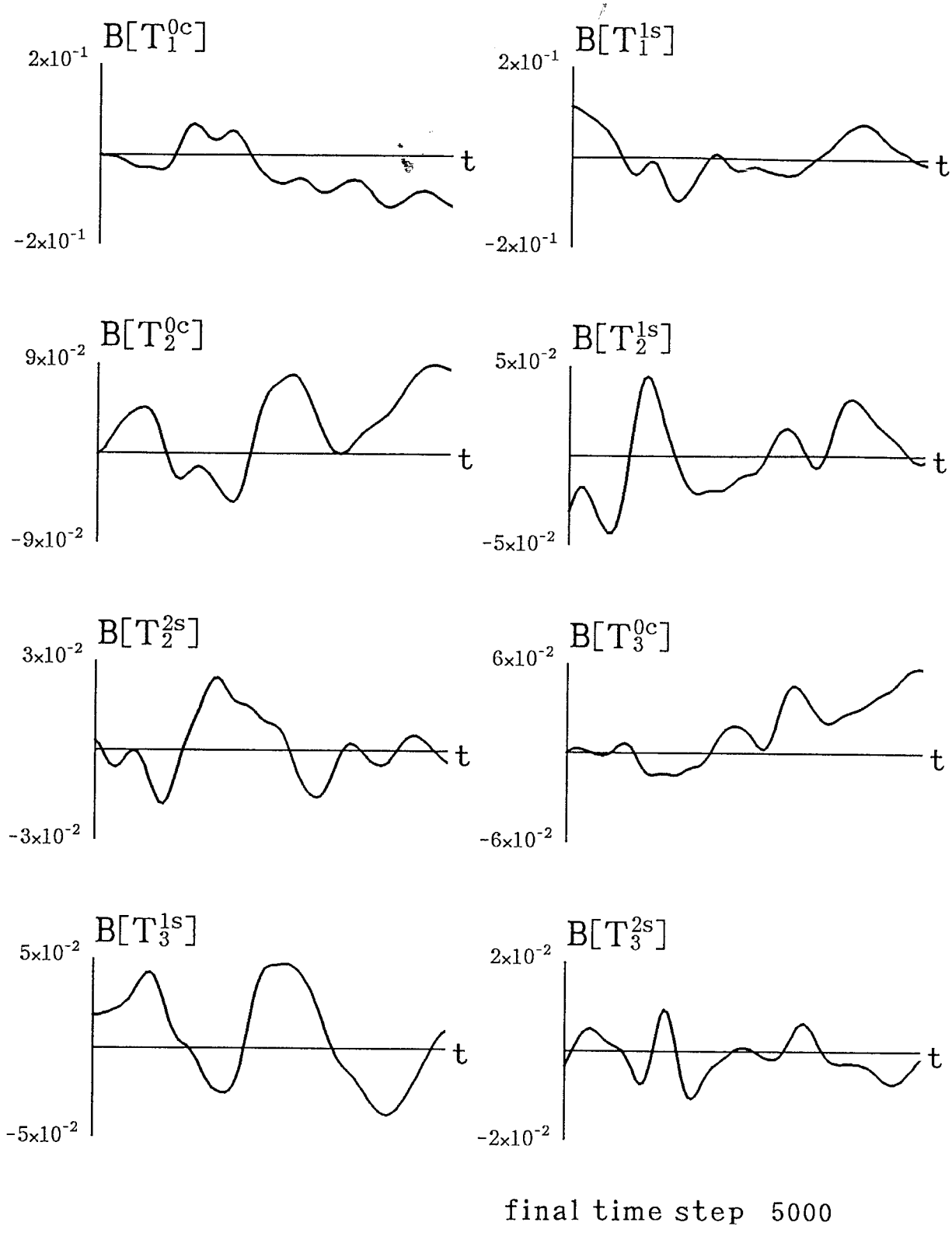

Fig. 4.17. Time-dependent behavior of toroidal magnetic fields for Case 7 up to $5000\Delta t$ (the time step $\Delta t = 6.92\times10^{-6}$). The lines indicate non-dimensional values of radial functions at $x = 0.8$ ($r = 0.93r_{oc}$).

modes, there is no significant difference between the two cases except the characteristic time of fluctuation which seems to be shorter in Case 7 than that in Case 6. This nature of fluctuation may be attributed to zonal toroidal motions caused by additional meridional circulation, since the velocity fields derived on the assumptions made in Cases 6 and 7 are similar to each other except for zonal toroidal motions. Comparing the rms velocity for the non-zonal toroidal constituent, we obtain $V_{\rm rms}[T]$ = 9.06×10^{-5} ms^{-1} for Case 6 and $V_{\rm rms}[T]$ = 9.33×10^{-5} ms^{-1} for Case 7. The rms toroidal velocity for all the modes in Case 7, however, amounts to 2.13×10^{-4} ms^{-1}.

Among the zonal toroidal motions, the rotation of spherical surfaces $V[T_1^0]$, which is caused by an axisymmetric poloidal motion $V[S_2^0]$ considered in the present study, can be responsible for the westward drift which is one of the well known features of the geomagnetic field. Madden and Le Mouël (1982), for example, regarded the westward drift as a manifestation of the zonal toroidal motion $V[T_1^0]$ near the CMB. On the other hand, Jault *et al.* (1988) derived zonal toroidal motions at the CMB from the apparent drift of the magnetic field observed at the Earth's surface based on the frozen-flux and the geostrophic approximations. They pointed out that the zonal toroidal motion is not expressed by a body rotation but by a latitude-dependent differential rotation which is symmetric with respect to the equator, and interpreted the result as indicating the rigid rotation of co-axial cylindrical annuli.

Zonal toroidal motions $V[T_1^0]$ and $V[T_3^0]$ are given rise to mainly by additional meridional circulation $V[S_2^0]$ introduced in the present study. Figure 4.18 shows the distributions of angular velocity in the core derived in Cases 6 and 7. The magnitude of rotation rate is entirely different; contour intervals in Figs. 4.18(a) and (b) are 10^{-13} s^{-1} and 2×10^{-11} s^{-1}, respectively. The overall feature, however, is similar to each other; westward flow near the equator and eastward flow near the rotation axis.

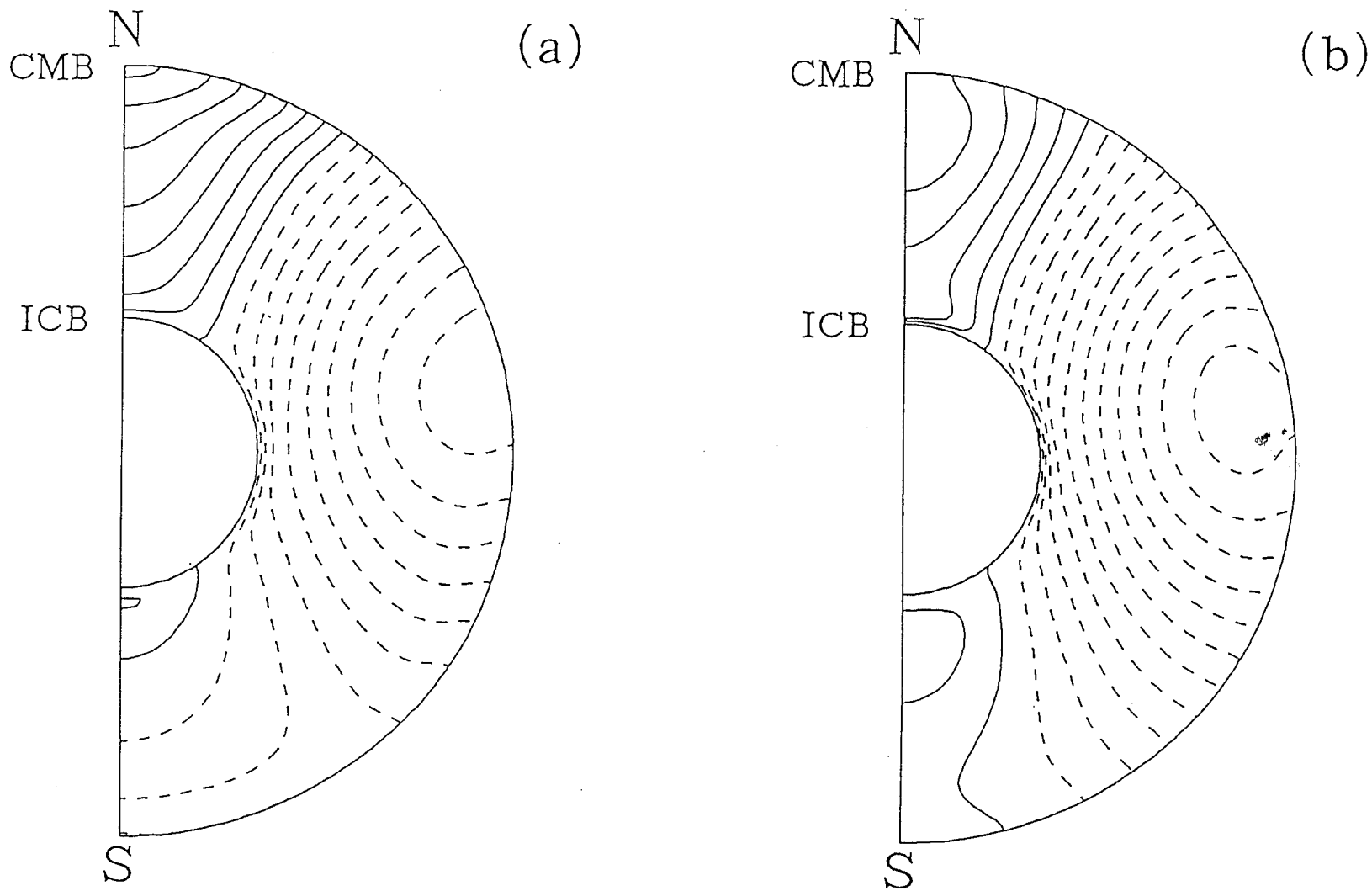

Fig. 4.18. Distribution of angular velocity in the outer core derived for (a) Case 6 and (b) Case 7. Solid contours indicate positive (eastward) values in units of (a) 1×10^{-13} rad·s^{-1} and (b) 2×10^{-11} rad·s^{-1}, and broken contours negative (westward) values.

The distribution of zonal toroidal motion near the CMB is similar to the result of Jault *et al.* (1988). Meridional-dependent zonal motions can also be responsible for the drift of the geomagnetic field as observed at the Earth's surface.

The feature of drifting magnetic field is well illustrated in $B[S_l^{mc}]-B[S_l^{ms}]$ plane, as pointed out by Yukutake (1985). In the $B[S_l^{mc}]-B[S_l^{ms}]$ diagram, the clockwise trajectory of ($B[S_l^{mc}]$, $B[S_l^{ms}]$) corresponds to westward drift. Figure 4.19 shows the $B[S_l^{mc}]-B[S_l^{ms}]$ diagrams for (l, m) = (1, 1), (2, 1), (2, 2) and (3, 3) taken from Fig. 4.16. In these figures, the westward drift is seen for (l, m) = (1, 1), (2, 2) and (3, 3), although it is not straightforward to interpret the trajectory for (l, m) = (2, 1). Thus the nature of fluctuation seen in Figs. 4.16 and 4.17 can be attributed to zonal toroidal motions, primarily $V[T_1^0]$ and $V[T_3^0]$. For the magnitude of zonal motion of 5×10^{-4} ms^{-1} at the equator, the characteristic drift time is about 1400 years. Time variation of the magnetic field is by no means purely periodic, but variations covering three periods for $B[S_1^{1c}]$ and six periods for $B[S_2^{2c}]$ are seen during 5000 years as shown in Fig. 4.16. Thus the period is indeed correlated to the characteristic drift time associated with the zonal toroidal motion.

In relation to the westward drift of the geomagnetic field, there are some arguments. As mentioned in Section 2, secular variations of the geomagnetic field have been investigated mostly in terms of time variations of Gauss coefficients. Yukutake and Tachinaka (1969) further examined the time variations and separated the non-axisymmetric magnetic fields into standing and drifting parts. Differences are not negligible, however, between the Gauss coefficients determined from the observed magnetic field data and those derived from the model of Yukutake and Tachinaka (1969). In order to improve the model, Yukutake (1985) introduced another drifting mode, that is an eastward drifting constituent. The non-axisymmetric magnetic field is then composed of standing, westward drifting and eastward drifting parts.

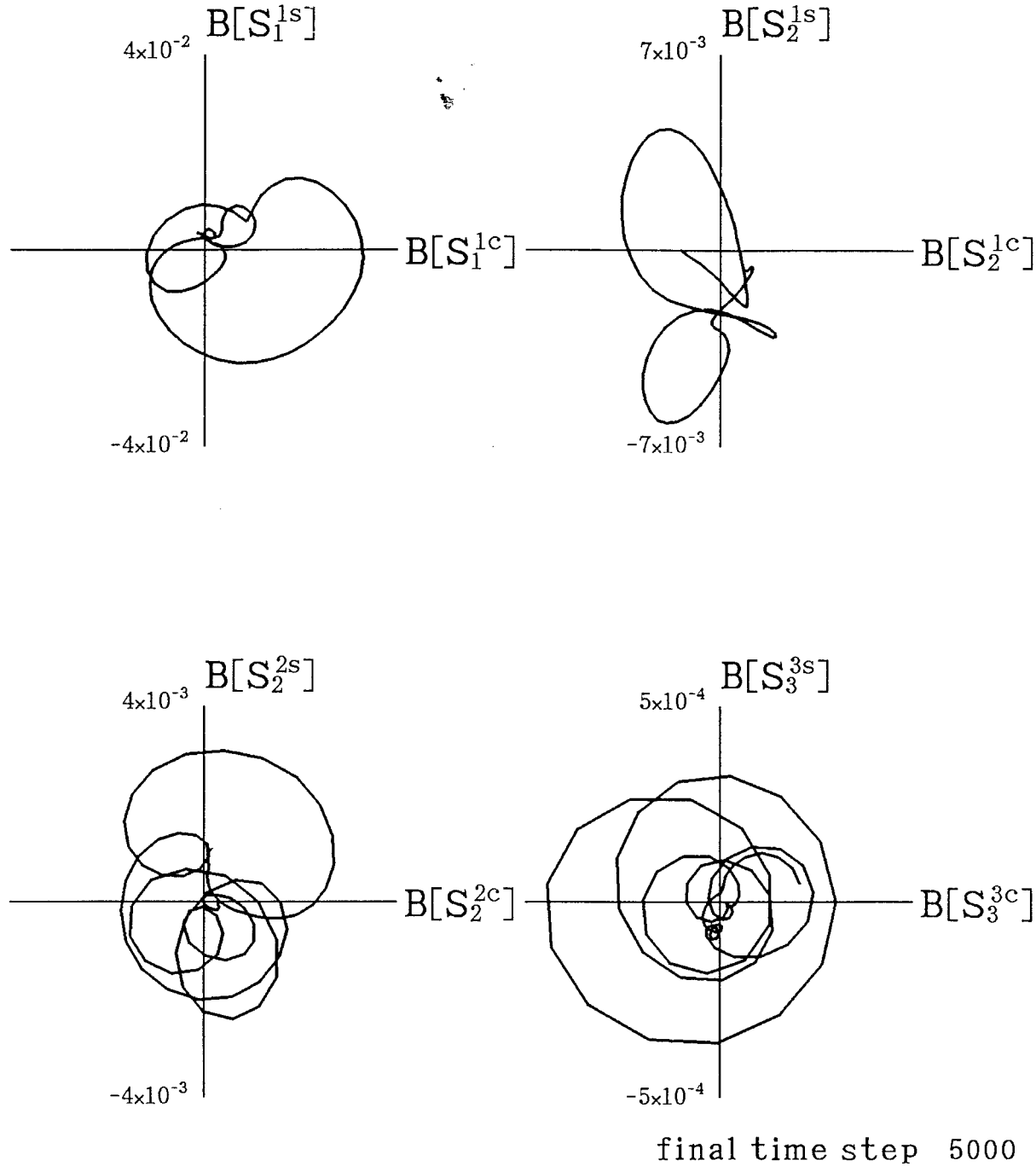

Fig. 4.19. Trajectories of $(B[S_l^{mc}], B[S_l^{ms}])$, corresponding to Fig. 4.16, on $B[S_l^{mc}]-B[S_l^{ms}]$ diagrams.

According to Yukutake (1985), one possibility of explaining coexistence of these modes is that the outer core consists of two layers as proposed by Yukutake (1981); it is the westward rotation of the surface layer that is responsible for the westward drifting mode. Meanwhile, Matsushima and Honkura (1988) introduced fluctuations in the amplitudes of the standing and the drifting parts, in view of a possible manifestation of non-linear nature inherent in the geodynamo. As a characteristic of the fluctuations, they pointed out that the relationship between the amplitude and the period of fluctuations for the standing part is different from that for the drifting part, and suggested that the fluctuation of the drifting part originates near the core surface.

On the other hand, Bloxham and Gubbins (1985) showed that the secular variations, including the westward drift, of the geomagnetic field at the CMB are confined mostly to the Atlantic hemisphere 90° E to 90° W, whereas only slight time variations are seen in the other hemisphere. This feature in the geomagnetic field is reflected in the pattern of fluid motion at the core surface derived on the frozen-flux approximation; that is, the westward flow in a zone near the equator is a common feature in many models of fluid flow.

It is not clear, however, whether the expression in terms of the standing and the drifting parts corresponds to the feature at the CMB as pointed out by Bloxham and Gubbins (1985), such as significant secular variations in the Atlantic hemisphere and rather static features in the Pacific hemisphere. It has also been unclear whether the westward drift is a persistent feature or a temporal one, since secular variations of the geomagnetic field are known only for recent hundreds of years. In this respect, studies of paleomagnetic secular variations are of great importance.

4.5. Short time-scale variations of the magnetic field

If non-zonal fluid flow is primarily responsible for secular variations, including the westward drift of the non-axisymmetric magnetic field, as in the core surface flows derived on the frozen-flux approximation, we may expect that the velocity field which contains less zonal motions as derived on the assumption in Case 6 gives rise to time variations of the geomagnetic field. In other words, the interaction terms which are not considered in deriving fluid motion in Case 6, but are considered in the frozen-flux approximation, are responsible for time variations of the magnetic field. In order to examine this possibility, we derive fluid motion in the core from geomagnetic field data, DGRF 1950 and DGRF 1965, shown in Table 2.3. Then we estimate time variations of the magnetic field for some tens of years. For the initial states corresponding to DGRF 1950 and DGRF 1965, the velocity fields derived from the respective DGRF's are used to perform time integration.

The results are shown in Fig. 4.20. In each figure, the ordinate is normalized with respect to the interval between maximum and minimum values under consideration. Larger circles denote the values of Gauss coefficients given by DGRF's; left for DGRF 1950, center for DGRF 1965, and right for DGRF 1980, while smaller circles on lines denote the Gauss coefficients into which the calculated magnetic field is transformed. In these figures, there are few modes in which the calculated magnetic field coincides with the observed one. In some modes, for instance (2, 1, s), (3, 2, s) and (3, 3, s), time variations are opposite. This indicates that the present approach to fluid motion in the core is by no means sufficient, mainly because we have assumed a quasi-steady state.

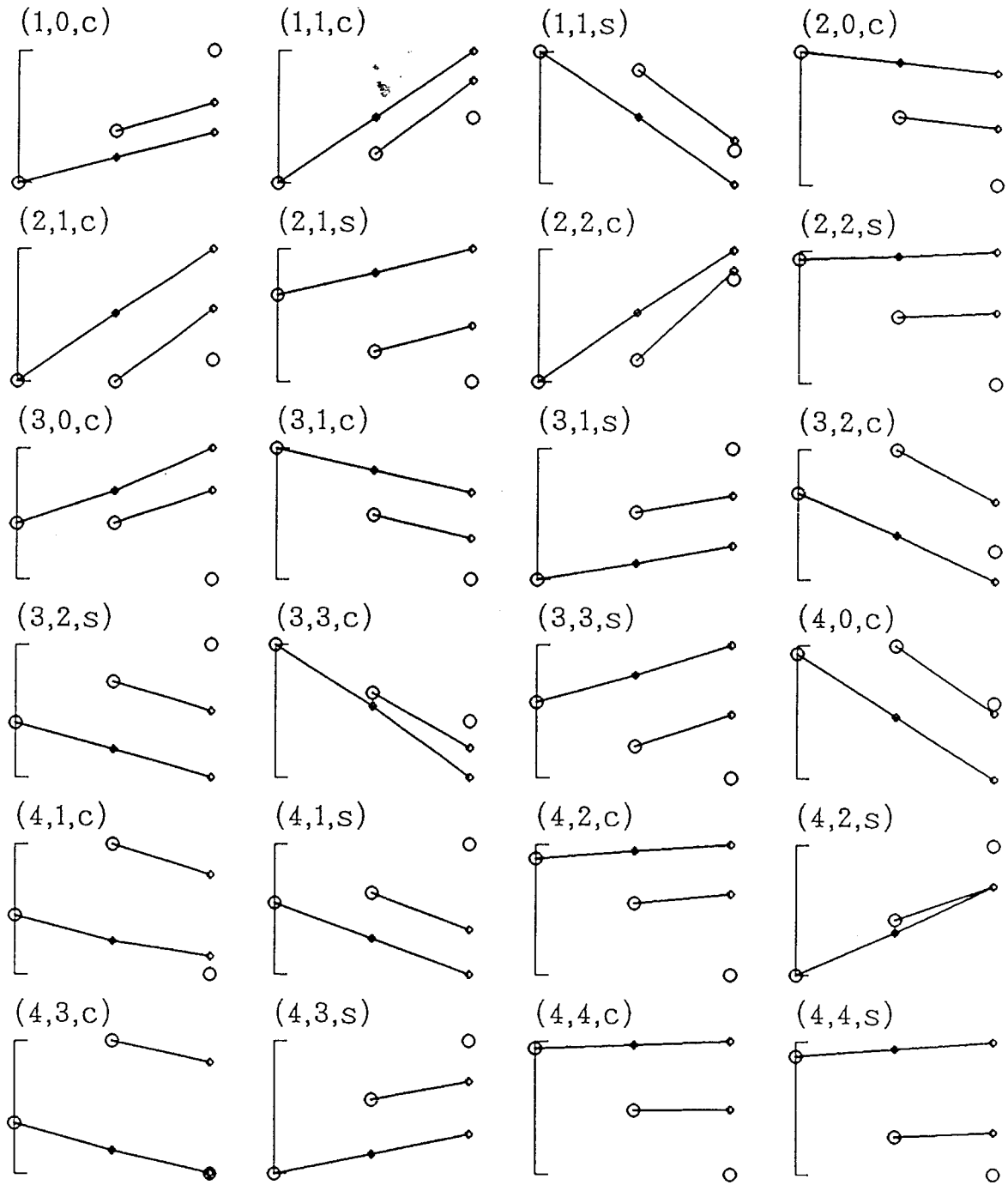

Fig. 4.20. Large circles denote secular variations of Gauss coefficients represented by DGRF 1950, DGRF 1965 and DGRF 1980. The ordinate is normalized with respect to the maximum and the minimum values. Solid lines were derived from numerical computations for a kinematic dynamo with the velocity field at 1950 and 1965 derived from the DGRF data at respective epochs.

5. Discussion

5.1. Cases 1 and 2

5.1.1 Case 1

Case 1 is aimed at reexamining Matsushima and Honkura (1989b) in which it is assumed that strong zonal toroidal magnetic fields are generated by the interaction between the axial dipole magnetic field and zonal toroidal motions (the ω-effect), and also that non-axisymmetric poloidal magnetic fields as observed at the Earth's surface are generated only by the interaction between the zonal toroidal magnetic fields and poloidal convective motions. The rms velocity, defined by (3.6), for the poloidal velocity field $V_{\rm rms}[S] = 3.95\times10^{-3}$ ms^{-1} is much larger than that for the toroidal velocity field $V_{\rm rms}[T] = 3.01\times10^{-5}$ ms^{-1}. Thus the poloidal velocity field derived on the assumption made in Case 1 is dominant, as also seen in Fig. 3.3.

Noticeable modes of poloidal velocity field are $(l, m) = (2, 1)$ and $(4, 3)$, which are antisymmetric with respect to the equator. According to the selection rules (Bullard and Gellman, 1954), the interaction between $\boldsymbol{V}[S_2^{1s}]$ and $\boldsymbol{B}[T_l^0]$, for instance, generates poloidal magnetic fields $\boldsymbol{B}[S_{l+1-2k}^{1c}]$ $(k = 0, 1, \cdots, [l/2])$, while the interaction between $\boldsymbol{V}[S_4^{3s}]$ and $\boldsymbol{B}[T_l^0]$ does $\boldsymbol{B}[S_{l+3-2k}^{3c}]$ $(k = 0, 1, \cdots, [l/2])$, where the expression used by Yokoyama and Yukutake (1989) for induced magnetic fields is here referred to. The strongest zonal toroidal magnetic field is $\boldsymbol{B}[T_4^0]$. The result discloses a simple relationship between the strength of the geomagnetic field and the magnitude of velocity fields derived for respective spherical harmonic modes. The induction term $(V[S_\alpha]B[T_\beta]S_\gamma)$ is written as (Bullard and Gellman, 1954)

$$(V[S_\alpha]B[T_\beta]S_\gamma) = -\frac{L_{\alpha\beta\gamma}}{N_\gamma}\alpha(\alpha+1)\,V[S_\alpha]B[T_\beta]. \tag{5.1}$$

Since inducing magnetic fields are assumed to be zonal toroidal magnetic fields, the

order m of spherical harmonics for induced magnetic fields is the same as that for the velocity fields. For example, the induction equations for $B[S_3^{3c}]$ and $B[S_4^{3c}]$ are written as

$$r^2\frac{d^2B[S_3^{3c}]}{dr^2} - 12B[S_3^{3c}] + R_m\Big[V[S_3^{3s}](3B[T_1^0] - 2B[T_3^0]) + V[S_4^{3s}]\left[\frac{35}{3}B[T_2^0] - \frac{350}{33}B[T_4^0]\right]\Big] = 0, \tag{5.2}$$

$$r^2\frac{d^2B[S_4^{3c}]}{dr^2} - 20B[S_4^{3c}] + R_m\left[V[S_3^{3s}]\left[\frac{27}{35}B[T_2^0] - \frac{54}{77}B[T_4^0]\right] + V[S_4^{3s}]\left[3B[T_1^0] + \frac{18}{11}B[T_3^0]\right]\right] = 0. \tag{5.3}$$

Although $B[T_4^0]$ is dominant, the radial dependence of $B[T_4^0](r)$ is complicated and in particular the polarity changes as clearly seen in Fig. 3.2(b). Induction terms are expressed by the summation of multiplication of scalar functions for velocity and magnetic fields. Therefore, determination of magnitudes $U[S_3^{3s}]$ and $U[S_4^{3s}]$ depends not only on the strength of inducing magnetic fields but also on their radial dependence. Hence the relationship between the strength of geomagnetic field and the magnitude of derived velocity fields is not so simple. Instead, $U[S_\alpha^{mc}]$ and $U[S_\alpha^{ms}]$ are simply related to $B[S_\beta^{ms}]$ and $B[S_\beta^{mc}]$, respectively, as long as inducing magnetic fields are assumed to be zonal toroidal magnetic fields.

It has been assumed that non-axisymmetric poloidal magnetic fields are generated only by the interaction between strong zonal toroidal magnetic fields and poloidal velocity fields. However, as shown in Fig. 3.2(b), the zonal toroidal magnetic fields are not so strong, amounting to 10^{-4} T at most. This means that the assumption does not hold. Because of weak zonal toroidal magnetic fields which are

supposed to be primary inducing magnetic fields, the magnitude of derived poloidal velocity field is too large. This result is reflected in time-dependent behavior of the magnetic field with the derived velocity field fixed. As shown in Fig. 4.2, the magnetic fields vary rapidly and tend to diverge. This means that the induction term $(V[S_\alpha]B[T^0_\beta]S_\gamma)$, which is assumed to be predominant in the generation of steady magnetic fields, is not dominant actually; that is, we should take into consideration other interaction terms as well. In view of the fact that weak zonal toroidal magnetic fields are due to a weak zonal toroidal motion, we introduced some terms which are effective in generating zonal toroidal velocity fields. In this way we attempted to improve the method of deriving fluid motion in the core.

5.1.2. Case 2

We first introduced meridional circulation as Case 2. The assumed induction processes are the same as those considered in Case 1. We have adopted an axisymmetric poloidal velocity field $\boldsymbol{V}[S^0_2]$ as meridional circulation. This possesses one convection cell in the Northern and the Southern Hemispheres, respectively; that is, for a negative value of $U[S^0_2]$, fluid in the core moves upward near the equator and downward near the poles. Meridional circulation affects zonal toroidal motion through the interaction $(V[S_\alpha]S^\Omega_1 S_\gamma)$ in (2.8); $\boldsymbol{V}[S^0_2]$ is related to $\boldsymbol{V}[T^0_1]$ and $\boldsymbol{V}[T^0_3]$. Zonal toroidal magnetic fields, which are assumed to be inducing magnetic fields, then become stronger than in Case 1.

In the present study, the magnitude $U[S^0_2]$ has been taken as a parameter. We should examine to what extent the assumed value is valid. In approaches to fluid motion near the CMB on the basis of the frozen-flux approximation, toroidal flow or geostrophic flow, for example, is assumed to remove the ambiguity of the solution. In the toroidal flow constraint, which would be expected in the case that light material

is concentrated near the CMB (Fearn and Loper, 1981) or sub-adiabatic temperature gradient at the top of the core is realized as in some models of the Earth's thermal history (Gubbins *et al.*, 1982), no poloidal motions are taken into consideration. In the geostrophic flow constraint, which is equivalent to the condition

$$\nabla_H \cdot (V \cos\theta) = 0, \tag{5.4}$$

where ∇_H is the horizontal divergence operator given as

$$\nabla_H = \left[0, \frac{1}{r}\frac{\partial}{\partial\theta}, \frac{1}{r\sin\theta}\frac{\partial}{\partial\phi}\right], \tag{5.5}$$

axisymmetric poloidal motions should vanish (Le Mouël *et al.*, 1985; Backus and Le Mouël, 1986). Thus it is expected that even if such meridional circulation exists, the magnitude would be very small.

Meanwhile, Yokoyama (1989) claimed that the magnitude of $V[S_2^0]$ should amount to 5.0×10^{-7} ms^{-1} in a model for a sixty year variation of the geomagnetic field. According to Yokoyama (1989), the sixty year variation is due to the magnetohydrodynamic (MHD) oscillation in a thin layer beneath the CMB. For example, the MHD oscillation among $B[S_1^0]$, $B[T_2^0]$, $V[S_2^0]$, and $V[T_1^0]$ occurs in the thin layer through the Lorentz force, the Coriolis force, and induction processes. For the sixty year variation of the axial dipole magnetic field, whose amplitude is 9.6×10^{-7} T, the magnitude of $V[S_2^0]$ amounts to 5.0×10^{-7} ms^{-1} and that of $V[T_1^0]$ to 3.5×10^{-4} ms^{-1} as long as the fluctuation is caused by the interaction between $V[S_2^0]$ and $B[S_1^0]$.

However, the magnitude of $V[T_1^0]$ amounting to 3.5×10^{-4} ms^{-1} corresponds to the value derived on the frozen-flux approximation (e.g. Madden and Le Mouël, 1982), that is, the westward drift rate of the non-dipole magnetic field (about 0.2° year^{-1}). Therefore, oscillation with such a large amplitude of $V[T_1^0]$ is unlikely. We may accept, however, the magnitude of $V[S_2^0]$ 5.0×10^{-7} ms^{-1} as the maximum,

while we consider the balance between the Lorentz force due to zonal toroidal magnetic fields and the Coriolis force due to $V[S_2^0]$. The order of magnitude of $V[S_2^0]$ 10^{-7} ms^{-1} corresponds to $U[S_2^0] \sim 10^{-3}$ if the radial dependence of poloidal velocity is given by (2.43). Then we can accept both the velocity fields, with different values of $U[S_2^0]$ shown in Figs. 3.5 and 3.7. As long as zonal toroidal magnetic fields are assumed to be inducing magnetic fields, the ambiguity of $U[S_2^0]$ remains. This is simply because the induction term ($V[S_\alpha^0]B[T_\beta^0]S_\gamma$) generates no poloidal magnetic field. There is no way to determine the magnitude $U[S_2^0]$.

If we consider fluid motion in a steady state and neglect the advection, the Lorentz force and the viscous terms, we obtain

$$2(\boldsymbol{\Omega}\cdot\nabla)\boldsymbol{V} = -g(r)\hat{\boldsymbol{r}} \times \nabla C, \tag{5.6}$$

taking the curl of (2.2). The horizontal components of (5.6) are written as

$$2\Omega\left(\frac{\partial V_\theta}{\partial z} - \frac{V_r \sin\theta}{r}\right) = \frac{g(r)}{r\sin\theta}\frac{\partial C}{\partial \phi}, \tag{5.7}$$

$$2\Omega\frac{\partial V_\phi}{\partial z} = -\frac{g(r)}{r}\frac{\partial C}{\partial \theta}, \tag{5.8}$$

which are known as the thermal-wind equations (e.g. Pedlosky, 1986). According to Olson (1989), even small lateral temperature differences, of the order of 10^{-3} Kkm^{-1}, can excite thermal winds, and hence zonal toroidal motions are excited. If the horizontal dependence of $C(r, \theta, \phi)$ is expressed in terms of $P_2(\cos\theta)$, zonal toroidal motions $V[T_1^0]$ and $V[T_3^0]$ are excited. Furthermore, it is expected from the Navier-Stokes equation (2.2) that $V[S_2^0]$ motion is excited by the horizontal dependence P_2 of $C(r, \theta, \phi)$. Although (5.6) restrains axisymmetric convection, other terms neglected in introducing (5.6) would actually contribute to the momentum equation. Then such axisymmetric convective motions would exist in the core. In view of this,

meridional circulation has been introduced.

For $U[S_2^0] = -10^{-5}$, the derived velocity field, shown in Fig. 3.5, is nearly the same as that in Case 1. For $U[S_2^0] = -10^{-3}$, however, the derived velocity field, shown in Fig. 3.7, is affected by the introduction of meridional circulation and the flow pattern becomes entirely different from the previous ones. This difference is quantitatively represented by the rms velocity; for $U[S_2^0] = -10^{-5}$, $V_{\rm rms}[S] = 3.43\times10^{-3}$ ms^{-1} and $V_{\rm rms}[T] = 3.13\times10^{-6}$ ms^{-1}, whereas for $U[S_2^0] = -10^{-3}$, $V_{\rm rms}[S] = 2.41\times10^{-3}$ ms^{-1} and $V_{\rm rms}[T] = 2.03\times10^{-5}$ ms^{-1}. The larger magnitude of zonal toroidal motions gives rise to stronger zonal toroidal magnetic fields. Indeed contour intervals in Fig. 3.6 are five times larger than those in Fig. 3.4. The rms velocity for the toroidal constituent for $U[S_2^0] = -10^{-3}$ is about 6.5 times larger than that for $U[S_2^0] = -10^{-5}$, whereas the rms velocity for the poloidal constituent is reduced to 70 % of that for $U[S_2^0] = -10^{-5}$.

The dominant mode of poloidal motion for $U[S_2^0] = -10^{-3}$ is $(l, m) = (2, 2)$, which is symmetric with respect to the equator and characterized by two upwellings and two downwellings at the equator. Dominant convective regions seem to be confined to a zone near the equator, bounded by colatitudes $\theta = 45°$ and $135°$. The difference between the poloidal velocity fields derived for $U[S_2^0] = -10^{-5}$ and $U[S_2^0] = -10^{-3}$ would result from the difference between the distributions of zonal toroidal magnetic fields in the core as shown in Figs. 3.4(b) and 3.6(b). For $U[S_2^0] = -10^{-5}$, magnetic energy E_b, defined in (4.7), for $B[T_2^0]$ and $B[T_4^0]$ are derived as $E_b[T_2^0] = 2.72\times10^{-13}$ and $E_b[T_4^0] = 8.96\times10^{-6}$, whereas for $U[S_2^0] = -10^{-3}$, $E_b[T_2^0] = 1.58\times10^{-4}$ and $E_b[T_4^0] = 2.55\times10^{-4}$. Thus the difference between zonal toroidal magnetic fields, in particular $B[T_2^0]$, is clear. It is likely, therefore, that the derived fluid motion as shown in Fig. 3.5 results from the introduction of meridional circulation $V[S_2^0]$.

For the steady and slow motion of an inviscid fluid, Taylor's condition (Taylor, 1963), given by (3.9), is known as a dynamical constraint. It is known that if there is no thermal wind, an $\alpha\omega$-dynamo which satisfies Taylor's condition will not work (Roberts and Gubbins, 1987). In this sense, the introduction of meridional circulation would be significant.

As shown in Fig. 3.4(b), however, the zonal toroidal magnetic fields are not strong enough, either, to be assumed as primary inducing magnetic fields. This indicates that the assumption made in Case 2 does not hold. As in Case 1, the magnitude of the velocity field derived for Case 2 is also too large. Then, as shown in Fig. 4.3, the magnetic field grows rapidly with the velocity field fixed. Therefore, we should improve the approach based on the presumption that strong zonal toroidal magnetic fields are generated by the ω-effect.

5.2. Cases 3, 4 and 5

5.2.1. Case 3

In Case 3, we have taken the axial dipole magnetic field as one of the inducing magnetic fields for the generation of non-axisymmetric poloidal magnetic fields, since zonal toroidal magnetic fields, which had been expected to be strong, turned out to be too weak to be significant primary inducing magnetic fields. For the velocity field shown in Fig. 3.9, $V_{\rm rms}[S] = 1.20\times10^{-2}$ ms^{-1} and $V_{\rm rms}[T] = 2.92\times10^{-5}$ ms^{-1}. On the other hand, for the velocity field shown in Fig. 3.12 as another solution, $V_{\rm rms}[S] = 3.03\times10^{-2}$ ms^{-1} and $V_{\rm rms}[T] = 2.83\times10^{-3}$ ms^{-1}. Since the rms velocity for the toroidal constituent is larger in the latter solution, it would be expected that the rms velocity for the poloidal constituent is smaller than in the former solution. Contrary to our expectation, however, this is not the case. This result arises probably from the competition between dominant inducing magnetic fields. Among the inducing

magnetic fields, the strength of the axial dipole magnetic field is fixed, whereas for the zonal toroidal magnetic fields, the magnetic energy amounts to 2.89×10^{-8} and 2.74×10^{-4} in the former and latter cases, respectively.

For simplicity, we consider inducing magnetic fields $B[S_1^0]$ and $B[T_4^0]$, and induced magnetic fields $B[S_3^{2c}]$ and $B[S_3^{2s}]$. The induction equations for $B[S_3^{2c}]$ and $B[S_3^{2s}]$ in the steady state are written as

$$r^2\frac{d^2B[S_3^{2c}]}{dr^2} - 12B[S_3^{2c}] + R_m\left[-\frac{2}{5}V[S_2^{2c}]\frac{dB[S_1^0]}{dr} + \frac{4}{15}\frac{dV[S_2^{2c}]}{dr}B[S_1^0]\right.$$
$$+ \frac{10}{3}V[S_4^{2c}]\frac{dB[S_1^0]}{dr} + \frac{5}{3}\frac{dV[S_4^{2c}]}{dr}B[S_1^0] \qquad (5.9)$$
$$\left. - \frac{1}{3}V[S_2^{2s}]B[T_4^0] + \frac{50}{11}V[S_4^{2s}]B[T_4^0]\right] = 0,$$

$$r^2\frac{d^2B[S_3^{2s}]}{dr^2} - 12B[S_3^{2s}] + R_m\left[-\frac{2}{5}V[S_2^{2s}]\frac{dB[S_1^0]}{dr} + \frac{4}{15}\frac{dV[S_2^{2s}]}{dr}B[S_1^0]\right.$$
$$+ \frac{10}{3}V[S_4^{2s}]\frac{dB[S_1^0]}{dr} + \frac{5}{3}\frac{dV[S_4^{2s}]}{dr}B[S_1^0] \qquad (5.10)$$
$$\left. + \frac{1}{3}V[S_2^{2c}]B[T_4^0] - \frac{50}{11}V[S_4^{2c}]B[T_4^0]\right] = 0.$$

Since inducing magnetic fields are assumed to be axisymmetric fields alone, the order m of spherical harmonics for induced magnetic fields is the same as that for the velocity field by which those are generated. If the dipole magnetic field $B[S_1^0]$ is a dominant inducing magnetic field, fluid motion would be determined as shown in Fig. 3.9. For larger $B[T_4^0]$, however, the derived fluid motion depends on the strength and the sign of $B[T_4^0]$. Since stronger zonal toroidal magnetic fields are generated by a larger

zonal motion, which would also arise from the advection terms, the result would eventually be controlled by non-linear nature of the problem.

In order to check the validity of the solution, we have examined time-dependent behavior of the magnetic field with the derived velocity field fixed. As shown in Fig. 4.4, the magnetic fields tend to diverge only in two years. This indicates that the magnitude of the velocity field derived on the assumption made in Case 3 is too large; that is, the velocity field is not a plausible one.

5.2.2. Case 4

The same interpretation is applicable to the velocity field derived on the assumption made in Case 4, in which axisymmetric non-dipole magnetic fields are further taken into consideration as inducing magnetic fields. In other words, the result of time evolution of the magnetic field with the velocity field fixed indicates that this velocity field is not a plausible one, either.

5.2.3. Case 5

The results for Case 5 were derived by introducing meridional circulation $V[S_2^0]$ into Case 4. For $U[S_2^0] = 10^{-5}$, the rms velocity for the toroidal and poloidal constituents are $V_{\rm rms}[T] = 6.40\times10^{-4}$ ms^{-1} and $V_{\rm rms}[S] = 1.22\times10^{-4}$ ms^{-1}, respectively; that is, the zonal toroidal motion is dominant as shown in Fig. 3.17. Although the growth rate of magnetic field is much smaller than those in Cases 3 and 4, as seen in Fig. 4.6, the value of magnetic energy E_b, defined in (4.7), becomes nearly nineteen times larger after 500 years.

5.3. Cases 6 and 7

5.3.1. Case 6

The results for Case 6 were obtained by taking non-zonal toroidal magnetic and non-zonal toroidal velocity fields into consideration. The main feature of the derived velocity field shown in Fig. 3.20 is two pairs of vortices; one, seen at around 90° W, is symmetric with respect to the equator, whereas the other at around 30° E is antisymmetric. The westward flow is restricted mainly in a zone near the equator from around 150° W to 0° in longitude. In addition, two columnar convective motions are seen in Fig. 3.22. The derived fluid motion at the CMB as shown in Fig. 3.20 does not necessarily coincide with those derived on the basis of the frozen-flux approximation.

5.3.2. Case 7

The results for Case 7 were obtained by introducing additional meridional circulation into Case 6. The velocity field shown in Fig. 3.25 is characterized by a marked westward flow in a zone near the equator, due to the additional $\boldsymbol{V}[S_2^0]$. However, the features in non-zonal toroidal motion are similar to those in the velocity field derived for Case 6. It is likely, therefore, that non-zonal toroidal magnetic fields, which are assumed to be generated mainly by non-zonal toroidal motions, are more marked than zonal toroidal magnetic fields. This may imply that non-zonal toroidal motions are essential in a rotating convective system.

In this sense, velocity fields derived in Cases 6 and 7 are plausible ones. This is also reflected in time-dependent behavior of the magnetic field. For Case 6, the value of magnetic energy E_b becomes only 1.2 times larger after 500 years, while 1.5 times larger for Case 7. Although this difference may not be significant, it should be noted that the axisymmetric poloidal velocity field $\boldsymbol{V}[S_2^0]$ has been added arbitrarily in the

present study. Estimation of meridional circulation is required, as a future problem, in order to further improve the approach.

5.4. Comparison with other models

As mentioned above, the fluid motion in the core derived in the present study does not necessarily coincide with those derived on the frozen-flux approximation. However, there are some similar features as discussed in the following.

In the frozen-flux approximation, the magnetic diffusion term in the induction equation is totally neglected for the time scale much shorter than the magnetic diffusion time which is controlled by the electrical conductivity of the core. The core conductivity is so high that the core is treated as a perfect conductor and the magnetic lines of force move along with the fluid at the core surface. In this case, the induction equation is written, with the diffusion term neglected, as

$$\frac{\partial \boldsymbol{B}}{\partial t} = \nabla \times (\boldsymbol{V} \times \boldsymbol{B}). \tag{5.11}$$

Since the radial velocity is zero at the core surface, the radial component of (5.11) at $r = r_{oc}$ gives

$$\frac{\partial B_r}{\partial t} + \nabla_H \cdot (\boldsymbol{V} B_r) = 0, \tag{5.12}$$

where B_r denotes the radial component of the magnetic field at the CMB and ∇_H is given in (5.5). Fluid motion at the core surface is then derived so as to yield the observed secular variation of geomagnetic field, using the poloidal magnetic field and its time derivative at the CMB. Furthermore, according to Barraclough *et al.* (1989), the horizontal components of the magnetic field can also be used in determining fluid motion at the core surface. Lloyd and Gubbins (1990) derived toroidal motion at the core surface from the three components of the induction equation. In any case, the

induction process at the CMB is supposed to be primarily responsible for the secular variation of geomagnetic field in the frozen-flux approximation.

In the present approach, on the other hand, fluid motion in the core is derived on the assumption that non-axisymmetric poloidal magnetic fields are maintained so as to be in a steady state by the induction processes inside the outer core. The main interaction term responsible for the observed non-axisymmetric poloidal magnetic field is expressed in terms of $(V[S_\alpha]B[T_\beta]S_\gamma)$, in contrast to $(V[S_\alpha]B[S_\beta]S_\gamma)$ and $(V[T_\alpha]B[S_\beta]S_\gamma)$ in the frozen-flux approximation. Hence it is not surprising that the velocity field derived in Case 6 is different from those derived on the frozen-flux approximation.

Nevertheless, some partial similarities can be recognized between the velocity field shown in Fig. 3.20 and many results derived on the frozen-flux hypothesis. One similarity is a counterclockwise flow at around 30° E in the Southern Hemisphere. The vortex consists of currents from the South Pole toward the equator at around 90° E, westward currents near the equator, and return currents from the equator to the South Pole at around 0° longitude, as shown in Fig. 3.20.

For example, based on the geostrophic approximation, Le Mouël *et al.* (1985) derived the westward flow concentrating near the equator from 90° E to 90° W and the poloidal flow consisting of one upwelling and one downwelling at the equator. This poloidal flow is expressed by $V[S_1^1]$. The westward flow is deflected toward the poles at around 90° W, turning into the return flow from the poles toward the equator at around 90° E. Their result includes three dominant modes; $V[T_1^0]$, $V[S_1^1]$ and $V[T_2^1]$.

Based on the assumption of steady motion, Voorhies (1986) also derived the vortex beneath the southwest Indian Ocean. Besides, vortex pairs beneath the north and the south central Pacific Ocean, and the northern Atlantic Ocean and the south

tip of South America were also derived. Voorhies (1986) claimed that the result suggests a geostrophic flow, since these two vortex pairs seem to represent the tops of Taylor columns and there is no strong meridional flow at the equator. Some of the features in the model obtained by Voorhies (1986) are very similar to those of the velocity field shown in Fig. 3.20; for example, vortices beneath the southwest Indian Ocean and the south central Pacific Ocean. The noticeable difference is the direction of fluid flow in a zone near the equator from 0° to 90° W; the flow is westward in the model of Voorhies (1986), whereas eastward in Fig. 3.20.

Whaler and Clarke (1988) and Whaler (1990) derived the westward flow in a zone near the equator and the counterclockwise circulation beneath the southern Indian Ocean. They also pointed out that meridional flow is not significant at the equator, which suggests a largely geostrophic flow, although ageostrophic flows are notable beneath South America and Indonesia.

Bloxham (1989) assumed that the fluid flow at the core surface is steady over a finite time interval and derived the flow on the frozen-flux approximation. Furthermore, the condition that the flow is toroidal was imposed as a constraint, since it leads to better fit than the geostrophic flow (Bloxham, 1988b). The derived flow is characterized by a simple pattern which is symmetric with respect to the equator; currents from the poles toward the equator at around 90° E, westward motion in a zone near the equator from 90° E to 90° W, and return currents from the equator toward the poles at around 90° W.

Lloyd and Gubbins (1990) derived the toroidal fluid motion at the core surface. The flow is characterized by two vortices in the Atlantic hemisphere which are symmetric with respect to the equator, characterized by strong westward flow near the equator and eastward return flow in high-latitudes.

Based on the tangentially geostrophic approximation, Gire and Le Mouël (1990)

derived fluid motion at the core surface. The overall feature of the velocity field is similar to those obtained by Le Mouël *et al.* (1985). For the poloidal velocity field, one upwelling beneath the Indian Ocean at the equator and one downwelling area west of Peru are notable. For the toroidal velocity field, one main feature is a strong westward flow in the equatorial zone from 90° E to 90° W. The flow is deflected toward the poles at around 100° W. In the total geostrophic flow, shown in Fig. 12 of Gire and Le Mouël (1990), we notice some features similar to those of the velocity field derived in the present study, as shown in Fig. 3.20; besides the counterclockwise vortex beneath the southwest Indian Ocean, a clockwise vortex beneath the south of Australia and a counterclockwise vortex beneath the North America are clearly seen.

Hulot *et al.* (1990) also derived the tangentially geostrophic flow at the core surface, which is also symmetric with respect to the equator. They suggested that the non-axisymmetric component of the derived flow would be the surface expression of the core flow organized in columnar convective motions parallel to the rotation axis, as proposed by Busse (1975), and two cylinders symmetric with respect to the meridional plane passing through $\phi = 90° - 270°$ were also pointed out.

Despite variously imposed additional constraints in the frozen-flux approximation, some common features of velocity fields at the core surface have been noted. In particular, the counterclockwise vortex beneath the southwest Indian Ocean is in harmony with the velocity field derived in the present study, as shown in Fig. 3.20, in spite of entirely different approaches. The westward flow is concentrated in a zone near the equator as seen in the models based on the frozen-flux approximation, although the locations where the westward flow prevails are different from those in the velocity field shown in Fig. 3.20. These seem to be essential features in fluid motion at the core surface.

Another entirely different approach was attempted by Kohler and Stevenson

(1990) to estimate fluid motion at the core surface without geomagnetic field data. They rely upon the thermal wind equations, in which the Coriolis force, pressure gradients and horizontal density gradients are balanced. Assuming that the Lorentz force is small near the CMB and the thermal wind is confined to a thin layer, compared with the core radius, they obtained

$$V_\theta = -\frac{g\alpha\varepsilon}{2\Omega \sin\theta \cos\theta}\frac{\partial\Theta}{\partial\phi}, \quad V_\phi = \frac{g\alpha\varepsilon}{2\Omega\cos\theta}\frac{\partial\Theta}{\partial\theta}, \tag{5.14}$$

where ε is the ratio of the layer thickness to the core radius. The lateral temperature variations are assumed to be due to the CMB topography variations. The differences are taken as 10^{-3} Kkm^{-1}, as suggested by Olson (1989) who claimed that zonal toroidal motion in the core is accounted for partly by thermal wind flow.

Velocity fields were calculated for two models of CMB topography, since the results highly depend on topography models. One of the common features between the two results is a counterclockwise vortex beneath the Indian Ocean due to the CMB topography high there. It is surprising that this also agrees with the result in the present study, although the vortex location is not exactly the same as that given by Kohler and Stevenson (1990). Except for the above feature, little correlation can be seen between the CMB topography and fluid flows at the core surface derived in the present study and on the frozen-flux approximation. However, it would be worthy of considering the effect of the CMB topography.

Although Kohler and Stevenson (1990) considered lateral temperature variations due to the CMB topography, it is also possible that such temperature variations originate in the lower mantle itself. The thermal interaction between the core and the lower mantle is often introduced in order to explain some features in the geomagnetic field. Bloxham and Gubbins (1985) showed static features in the Earth's magnetic field at the CMB and suggested that fluid motion in the core may be coupled to the

mantle through thermal, electromagnetic and topographic interactions. Bloxham and Gubbins (1987) also proposed a thermal interaction between the core and the lower mantle; stationary features in the magnetic field are ascribed to magnetic flux concentration due to downwellings beneath cold regions of the lower mantle, while upwellings beneath hot regions expel magnetic flux from the core. Gubbins (1988) suggested thermal core-mantle interactions from paleomagnetic field data. Using a simple two-dimensional convection model, King and Hager (1989) pointed out that the thermal boundary conditions strongly affect the fluid flow of convective system and supported the claim of Bloxham and Gubbins (1987) on the relationship between hot (cold) regions of the lower mantle and upwellings (downwellings).

5.5. Relation between the velocity and the magnetic fields

5.5.1. Velocity field

If there exist temperature anomalies, or lateral heat flux variations, at the CMB, fluid flow in the core would be controlled, at least partly, by them. Such mantle temperature anomalies are considered to be stationary for the core, since the viscosity of the mantle is much greater than that of the core, and the velocity of mantle convection is much smaller than that of core convection. Provided that static features in the geomagnetic field are to be reflected in the velocity field derived in the present study, the convective motion in the core which are responsible for steady magnetic fields should also remain almost stationary. In this respect, we attempted to derive fluid motion in the core from geomagnetic field data during the last several hundred years, in particular from a secular variation model, model C of Matsushima and Honkura (1988).

Figures 5.1(a), (b), (c) and (d) show the horizontal velocity field at the core surface for the epochs of 1600, 1700, 1800 and 1900 AD, respectively. It is clearly seen

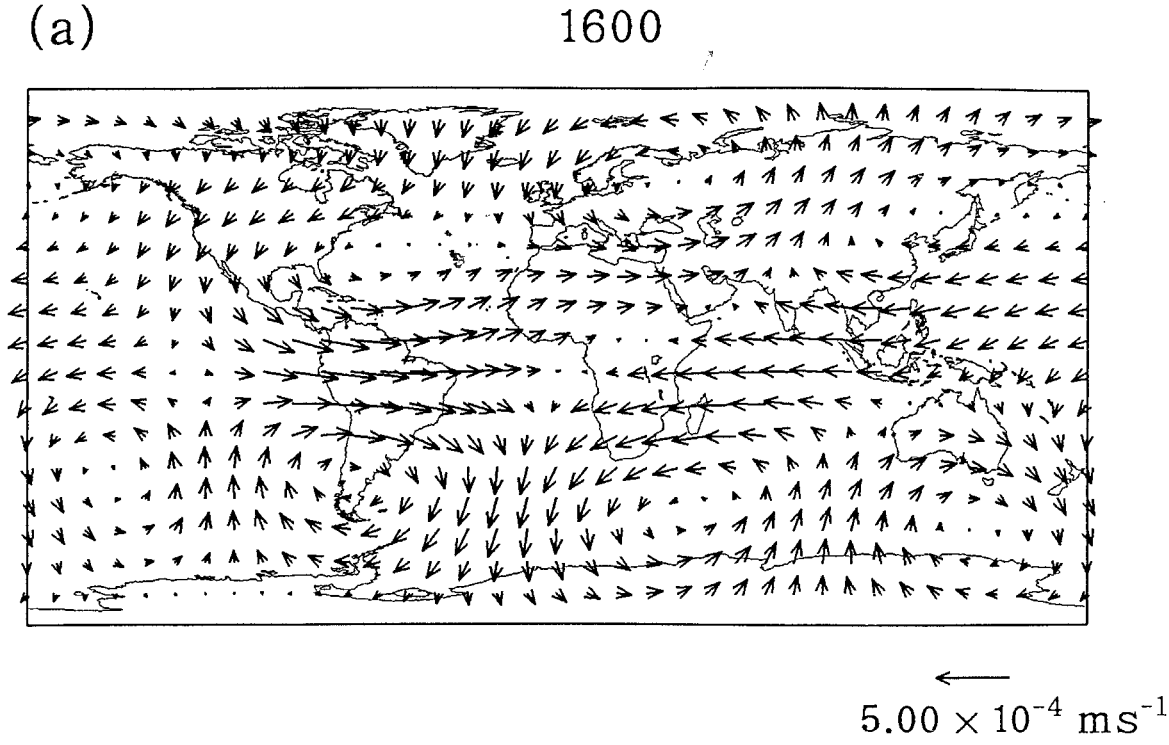

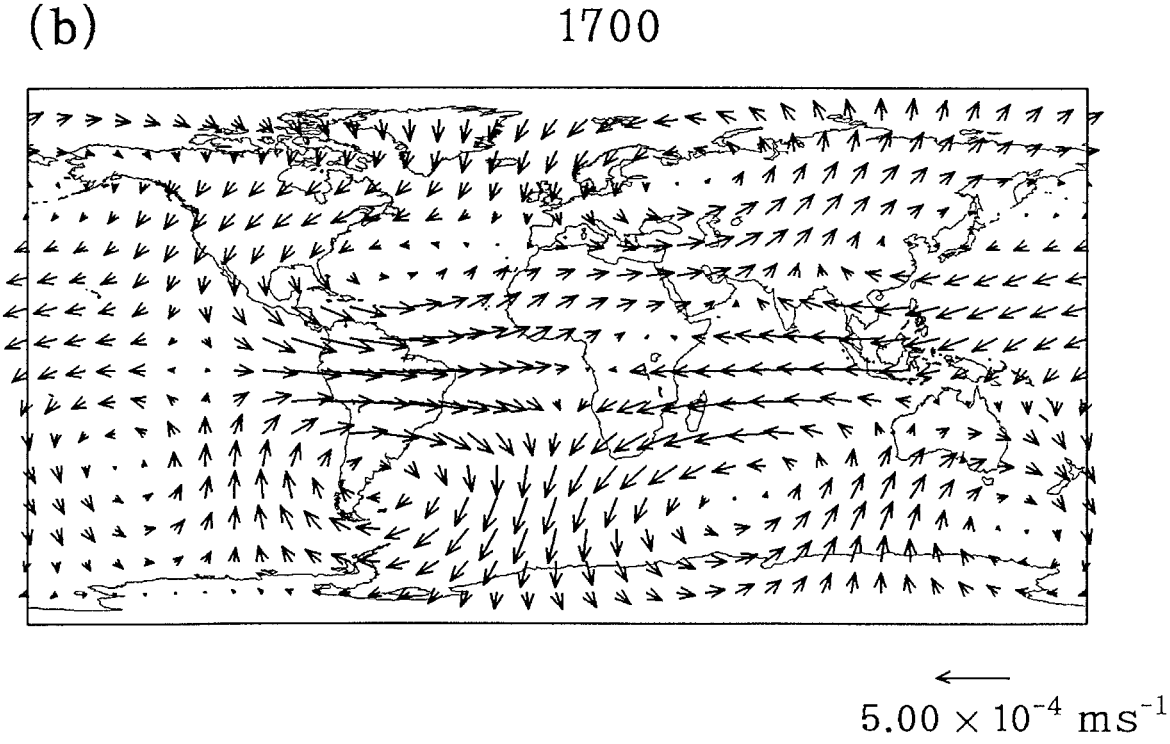

Fig. 5.1. Horizontal velocity fields at the core surface for the epochs of (a) 1600, (b) 1700, (c) 1800 and (d) 1900 AD. The arrow for scale length corresponds to 5×10^{-4} ms^{-1}.

(c) 1800

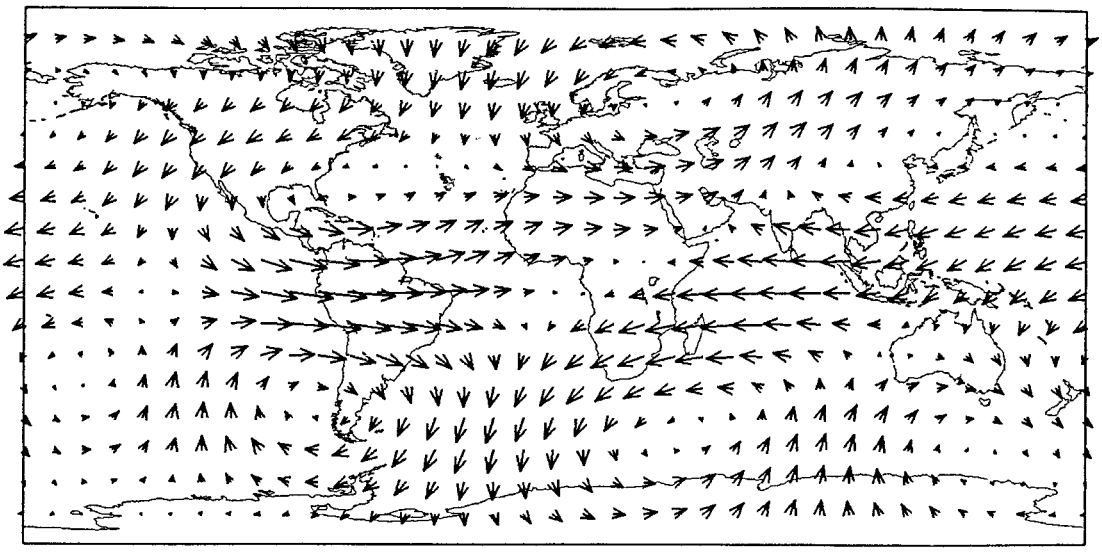

5.00×10^{-4} ms^{-1}

(d) 1900

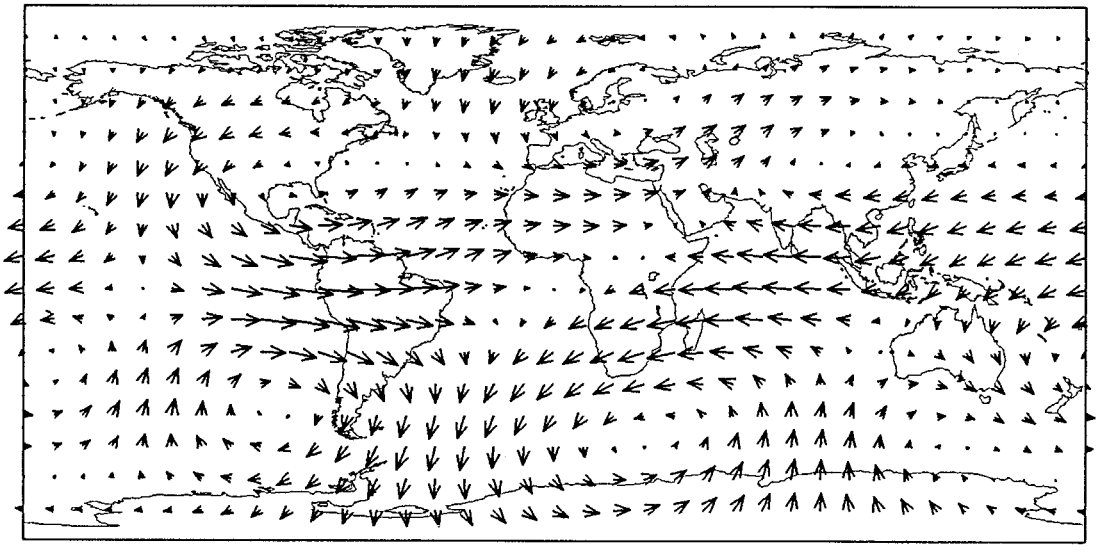

5.00×10^{-4} ms^{-1}

Fig. 5.1. (continued).

in Fig. 5.1 that the overall pattern of fluid motion at the core surface changes little, although the magnitude of velocity field is different from one epoch to another. In other words, throughout the epochs, the fluid motion is characterized by a pair of vortices located along 90° W longitude, counterclockwise vortices beneath the southwest Indian Ocean and Scandinavian Peninsula, respectively, and westward flow in a zone near the equator from 150° W to 0° in longitude. Two columnar convective motions, one along 90° W and the other along (60° S, 30° E)–(60° N, 90° E) line, also seem to be stationary.

Table 5.1. The rms velocities for the epochs of 1600, 1700, 1800 and 1900 AD.

AD	$V_{\rm rms}$ ($\rm ms^{-1}$)
1600	8.45×10^{-5}
1700	1.03×10^{-4}
1800	7.18×10^{-5}
1900	6.57×10^{-5}

The rms velocities for respective epochs are shown in Table 5.1. The differences are noted in the magnitude of velocity vectors drawn in the figures. It seems, however, that the magnitudes for the counterclockwise vortex flow beneath the southwest Indian Ocean and a pair of vortices along 90° W in longitude do not change much, whereas the magnitude for the counterclockwise vortex flow beneath Scandinavian Peninsula changes considerably. Time variations of the rms velocity seem to be controlled by these vortex flows.

5.5.2. Magnetic field

Since the fluid motion in the outer core was derived from the geomagnetic field data on some assumptions, the derived velocity field should reflect characteristic

features of the geomagnetic field. In the present study, it is the magnitude of poloidal velocity field that was constrained by the geomagnetic field data. It should be noted, however, that we have not considered the mechanism by which axisymmetric poloidal magnetic fields are generated; that is, as the magnetic field data by which the velocity field is constrained, only non-axisymmetric poloidal magnetic fields have been considered. We show the distributions of the radial component of non-axisymmetric poloidal magnetic field, synthesized from spherical harmonics of up to degree four, at the CMB for the epochs of 1600, 1700, 1800 and 1900 AD in Figs. 5.2(a), (b), (c) and (d), respectively. Here we used model C of Matsushima and Honkura (1988).

Solid contours represent magnetic flux into the core and broken contours magnetic flux out of the core, in units of 50 μT. Time variations of non-axisymmetric poloidal magnetic field at the CMB are largely characterized as follows. Static patches of magnetic flux into the core are observed beneath Canada, Siberia, southern Africa, and central Pacific Ocean, while those of magnetic flux out of the core beneath northern Atlantic Ocean and southern Australia. A magnetic flux patch beneath Japan at 1600 AD slightly moved eastward. On the other hand, a negative focus beneath South America observed at 1600 AD disappeared at 1900 AD. A patch of magnetic flux out of the core observed beneath vicinity of Indonesia at 1600 AD moved westward. Some of the above features were also pointed out by Bloxham and Gubbins (1985). For example, static flux bundles beneath Canada and Siberia are also observed in their models.

The feature of null flux can be easily recognized if we superpose the radial component of the axisymmetric poloidal magnetic field on the maps shown in Fig. 5.2. The resulting distributions of the radial component of the magnetic field, up to degree four in spherical harmonics, at the CMB for the epochs of 1600, 1700, 1800

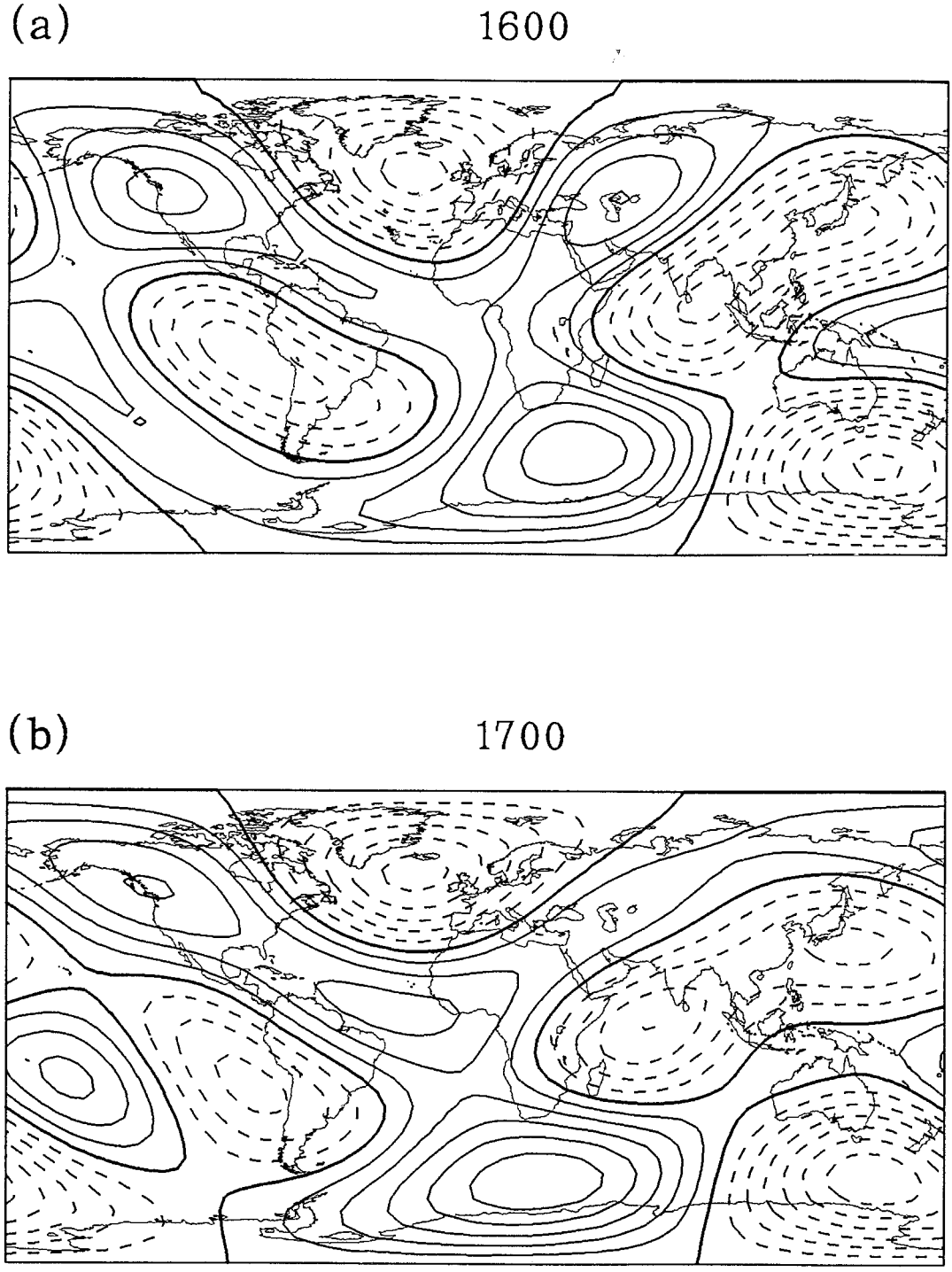

Fig. 5.2. Distributions of the radial component of the non-axisymmetric magnetic field, synthesized from spherical harmonics of degree up to four, at the CMB for the epochs of (a) 1600, (b) 1700, (c) 1800 and (d) 1900 AD. Model C of Matsushima and Honkura (1988) was used as the magnetic field data. Contour intervals are 50 μT. Solid contours represent magnetic flux into the core and broken contours magnetic flux out of the core. Bold contours represent null radial field lines.

(c) 1800

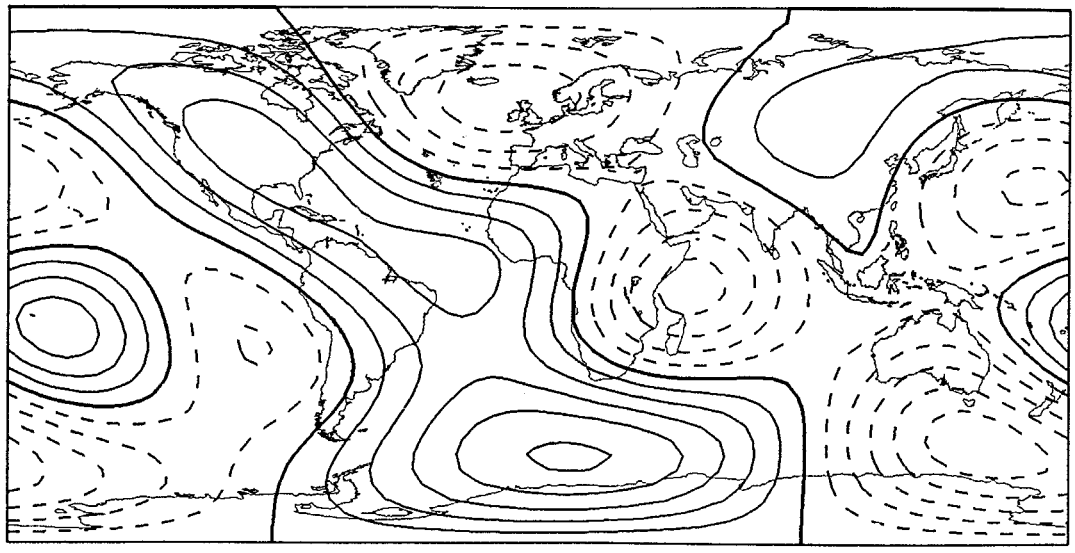

(d) 1900

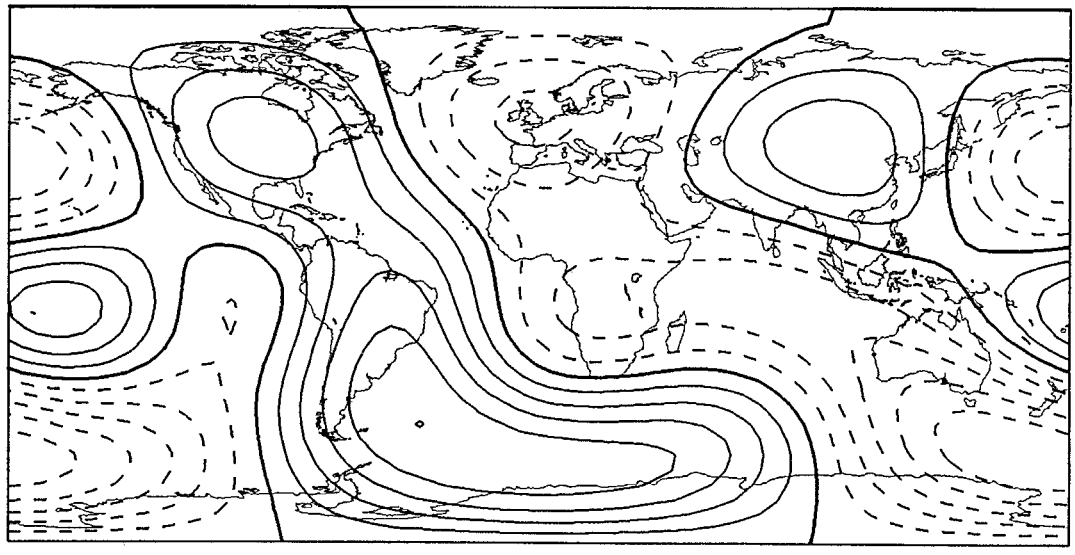

Fig. 5.2. (continued).

and 1900 AD are shown in Figs. 5.3(a), (b), (c) and (d), respectively. Contour intervals are 100 μT. Foci beneath Canada and Siberia, respectively, are notable. There is a region where flux intensity is weak near the North Pole, which would correspond to the null flux patch pointed out by Bloxham and Gubbins (1985).

We further show, rather in detail, the distributions of the radial component of the magnetic field at the CMB for the epoch of 1980 AD. Figures 5.4(a) and (b) show the distributions for the non-axisymmetric poloidal magnetic field up to degree four and six, respectively, while Figs. 5.5(a) and (b) show the distributions for the total radial component up to degree four and six, respectively. Contour intervals are 50 μT in Fig. 5.4 and 100 μT in Fig. 5.5. In Fig. 5.5(b), we see a 'core spot' beneath southern Africa, which Bloxham and Gubbins (1987) first pointed out and interpreted as indicating the expulsion of toroidal magnetic field from the core into the mantle. In Fig. 5.5(a), however, such a feature is not so clear. This means that the fluid motion derived in the present study reflects only large-scale features in the geomagnetic field and small-scale features such as core spots cannot be brought to light. We should recall that the truncation level L in spherical harmonics is four in the present study.

5.5.3. The truncation level L

Bloxham (1988a) claimed that the strong flow beneath the Pacific Ocean shown in the model of Voorhies (1986) would be an apparent one arising from the low truncation level (L = 8). In the present case, we have considered only a large-scale fluid motion and a large-scale magnetic field from the presumption that a large-scale magnetic field, such as the dipole magnetic field, would primarily be generated by a large-scale fluid motion in the core. For this reason we set the truncation level at L = 4. If we consider a higher truncation level, for example, L = 5 and N = 9 in Case

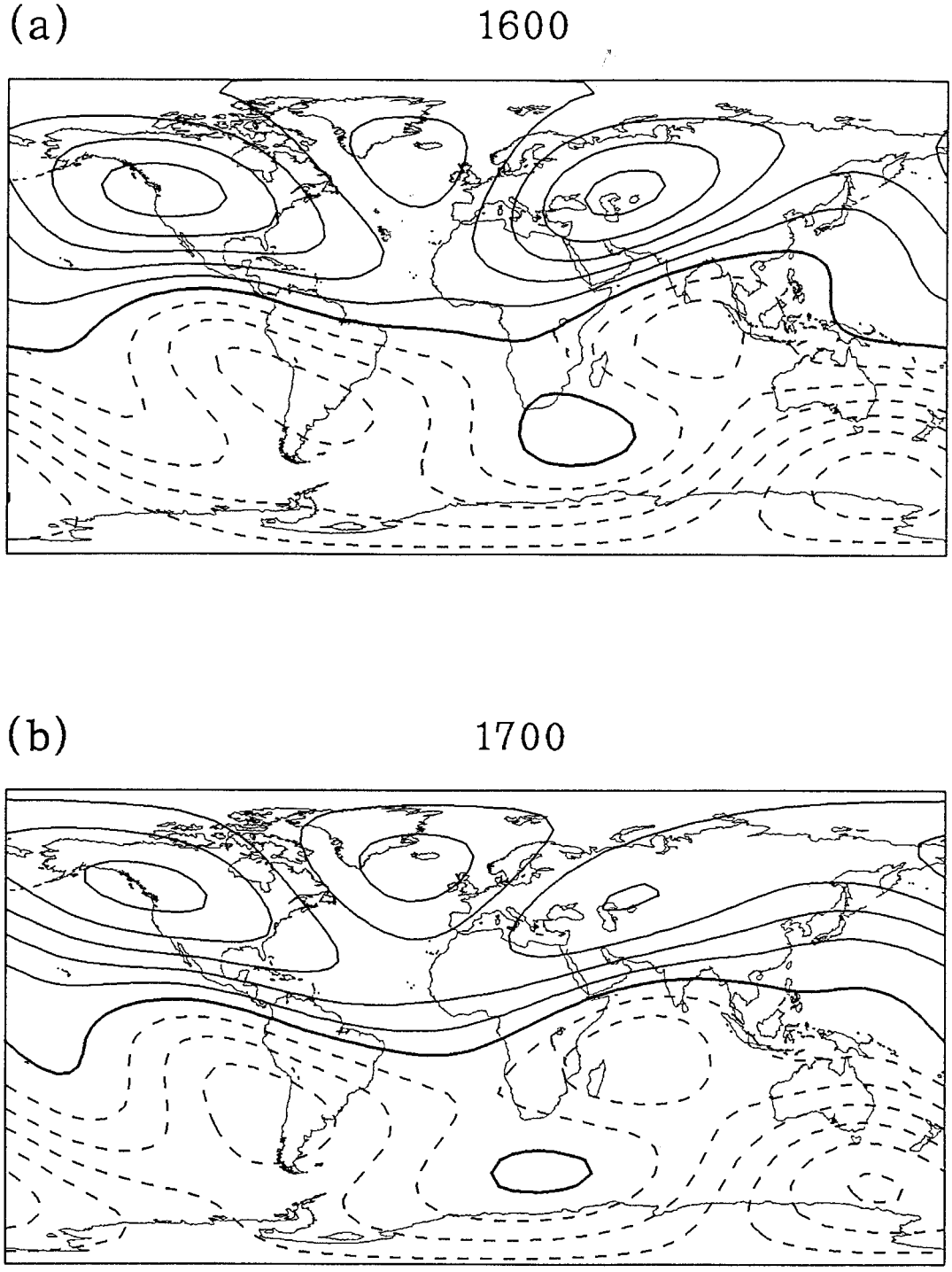

Fig. 5.3. Distributions of the radial component of the magnetic field, synthesized from spherical harmonics of degree up to four, at the CMB for the epochs of (a) 1600, (b) 1700, (c) 1800 and (d) 1900 AD. Model C of Matsushima and Honkura (1988) was used as magnetic field data. Contour intervals are 100 μT. Solid contours represent magnetic flux into the core and broken contours magnetic flux out of the core. Bold contours represent null radial field lines.

(c) 1800

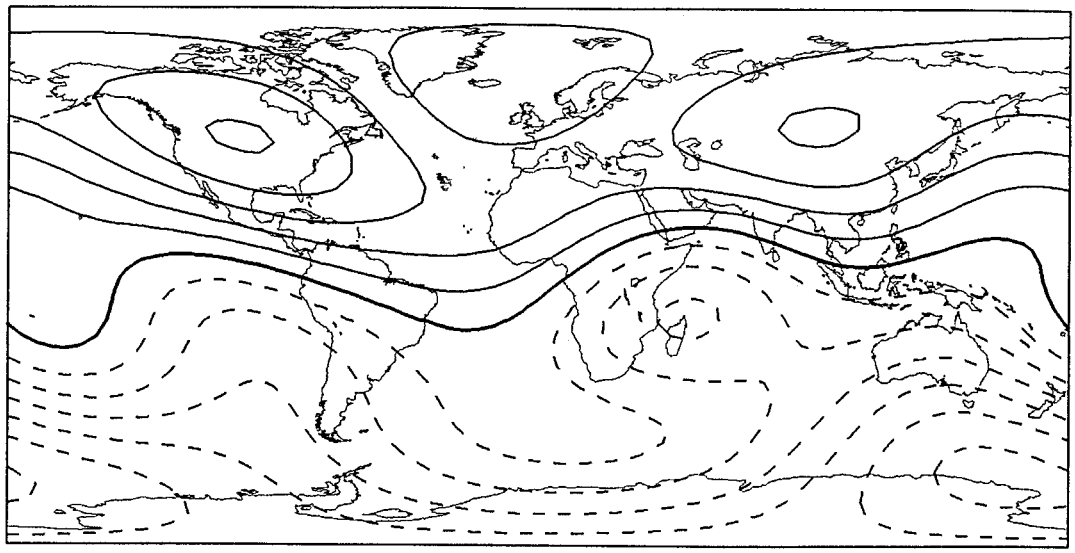

(d) 1900

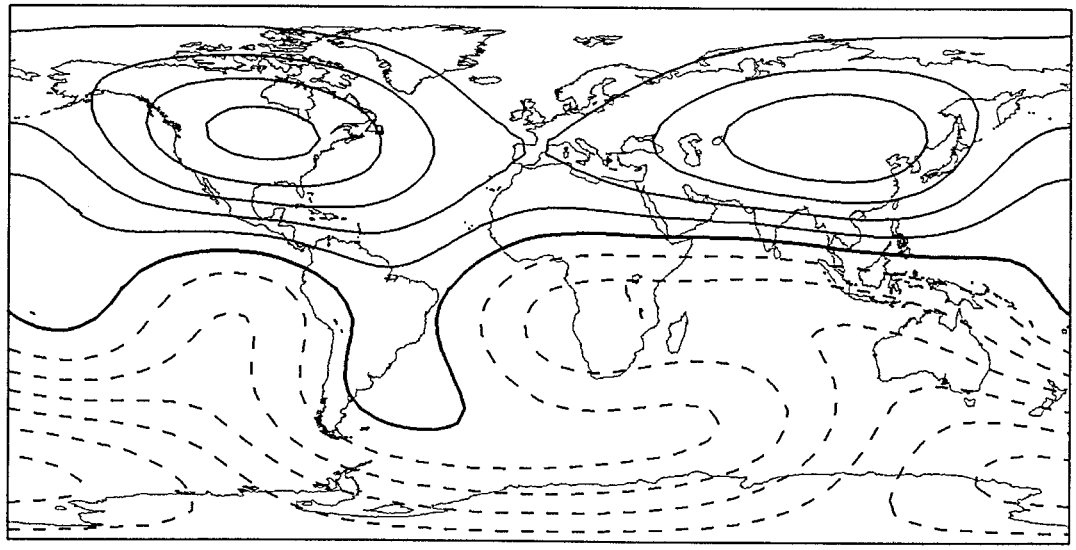

Fig. 5.3. (continued).

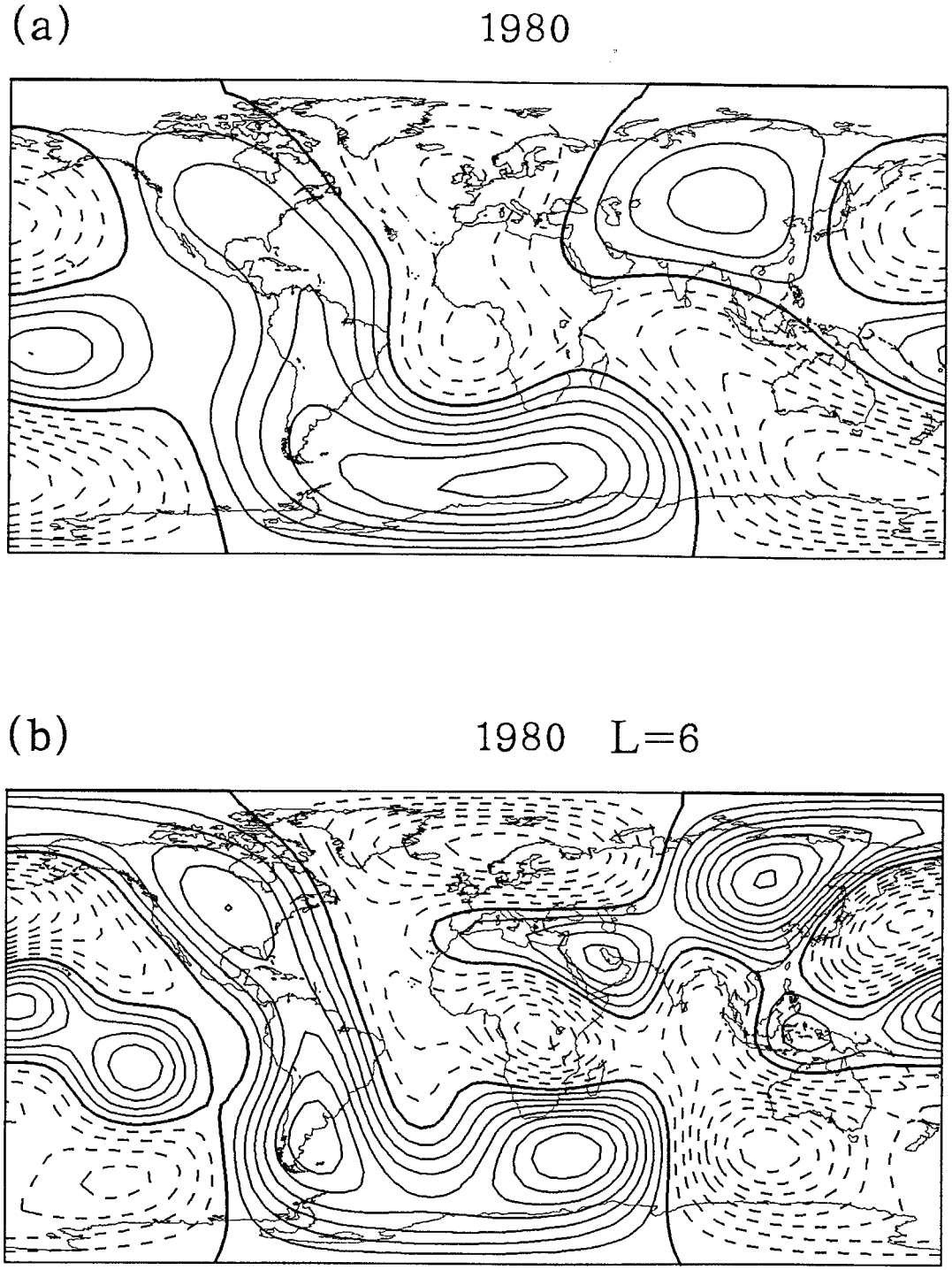

Fig. 5.4. Distributions of the radial component of the non-axisymmetric magnetic field at the CMB for the epoch of 1980 AD: (a) up to degree four and (b) up to degree six. Model C of Matsushima and Honkura (1988) was used as the magnetic field data. Contour intervals are 50 μT. Solid contours represent magnetic flux into the core and broken contours magnetic flux out of the core. Bold contours represent null radial field lines.

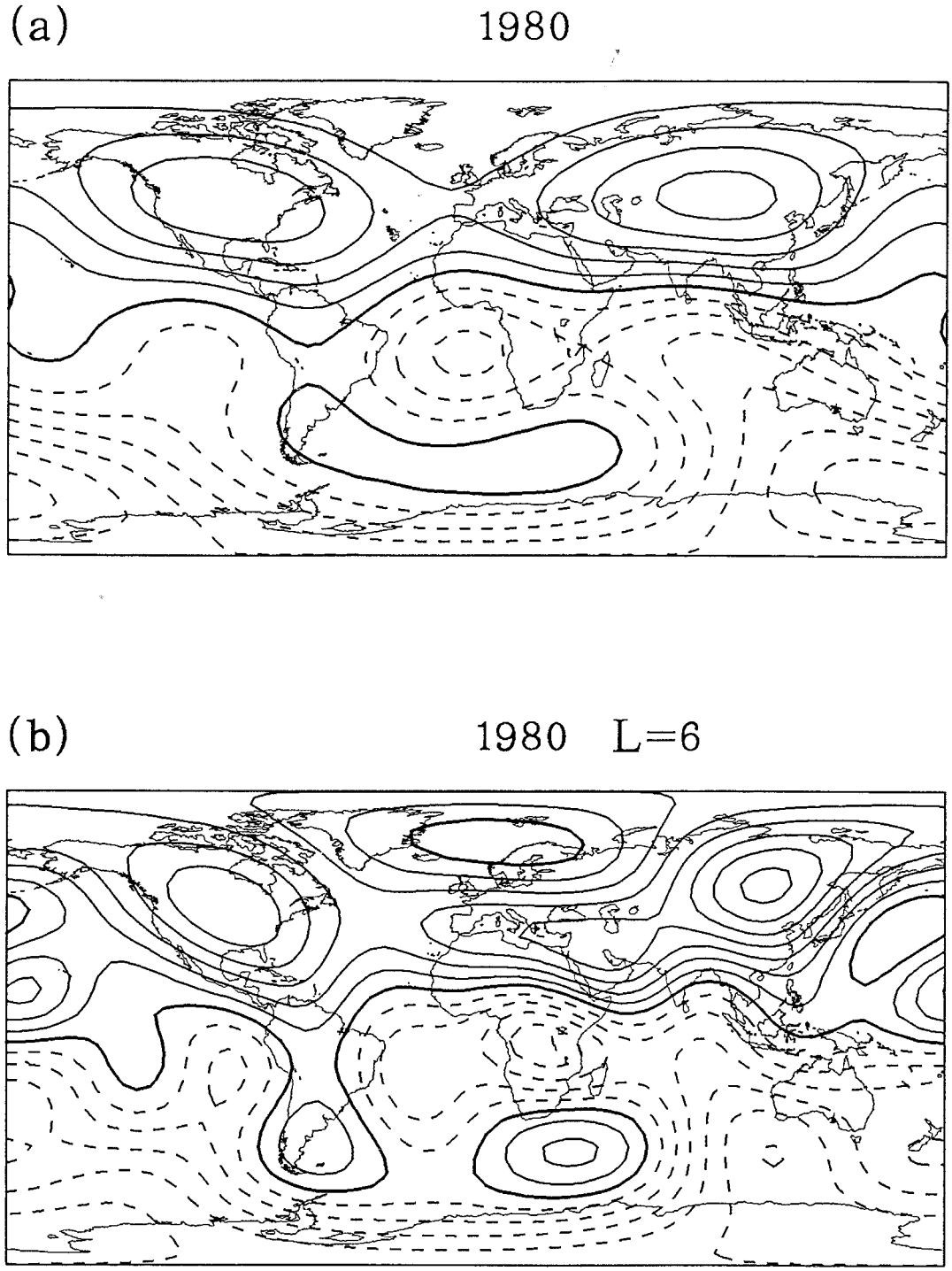

Fig. 5.5. Distributions of the radial component of the magnetic field at the CMB for the epoch of 1980 AD: (a) up to degree four and (b) up to degree six. Model C of Matsushima and Honkura (1988) was used as the magnetic field data. Contour intervals are 100 μT. Solid contours represent magnetic flux into the core and broken contours magnetic flux out of the core. Bold contours represent null radial field lines.

6, the total number of unknowns is 1030; for $L = 6$ and $N = 9$ it is 1422. The difference between the distributions of the radial magnetic field at the CMB shown in Figs. 5.5(a) and (b) clearly indicates that the fluid motion in the core depends on the truncation level. Since small-scale features in the magnetic field seem to be correlated to high secular variations, time variations of the geomagnetic field must be fully taken into consideration if we are to study small-scale fluid motion in the core.

5.5.4. Relation between the velocity and the magnetic fields

Columnar convective motions found along 90°W longitude and (60°S, 30°E)–(60°N, 90°E) line seem to be correlated with the regions of magnetic flux concentration beneath Canada and Siberia, respectively. In this respect, Gubbins and Bloxham (1987) suggested that four magnetic flux concentrations, which are antisymmetric with respect to the equator, seen in their magnetic field model are the manifestation of two convection rolls parallel to the rotation axis and tangential to the inner core. Such a geodynamo model in terms of convection rolls has been proposed by Busse (1975). Although the size of rolls in Busse's model is much smaller, it depends critically on the Taylor number. Figure 5.6 shows the fluid motion at the core surface already shown in Fig. 3.20 but seen from the North Pole and the South Pole, respectively. The inner circle in each figure denotes the size of the inner core. Although vortices corresponding to the convective rolls are indistinct in the Northern Hemisphere, the convection rolls seem to be tangential to the inner core (see also Fig. 3.22). One is parallel to the rotation axis, whereas the other is inclined.

These features would also be reflected in the toroidal magnetic fields which are regarded as primary inducing magnetic fields. We show magnetic lines of force for the toroidal constituent on spherical surfaces in Fig. 5.7; (a) at $r = 0.9r_{oc}$, (b) at $r = 0.8r_{oc}$, (c) at $r = 0.7r_{oc}$, and (d) at $r = 0.6r_{oc}$. The magnetic field is stronger where

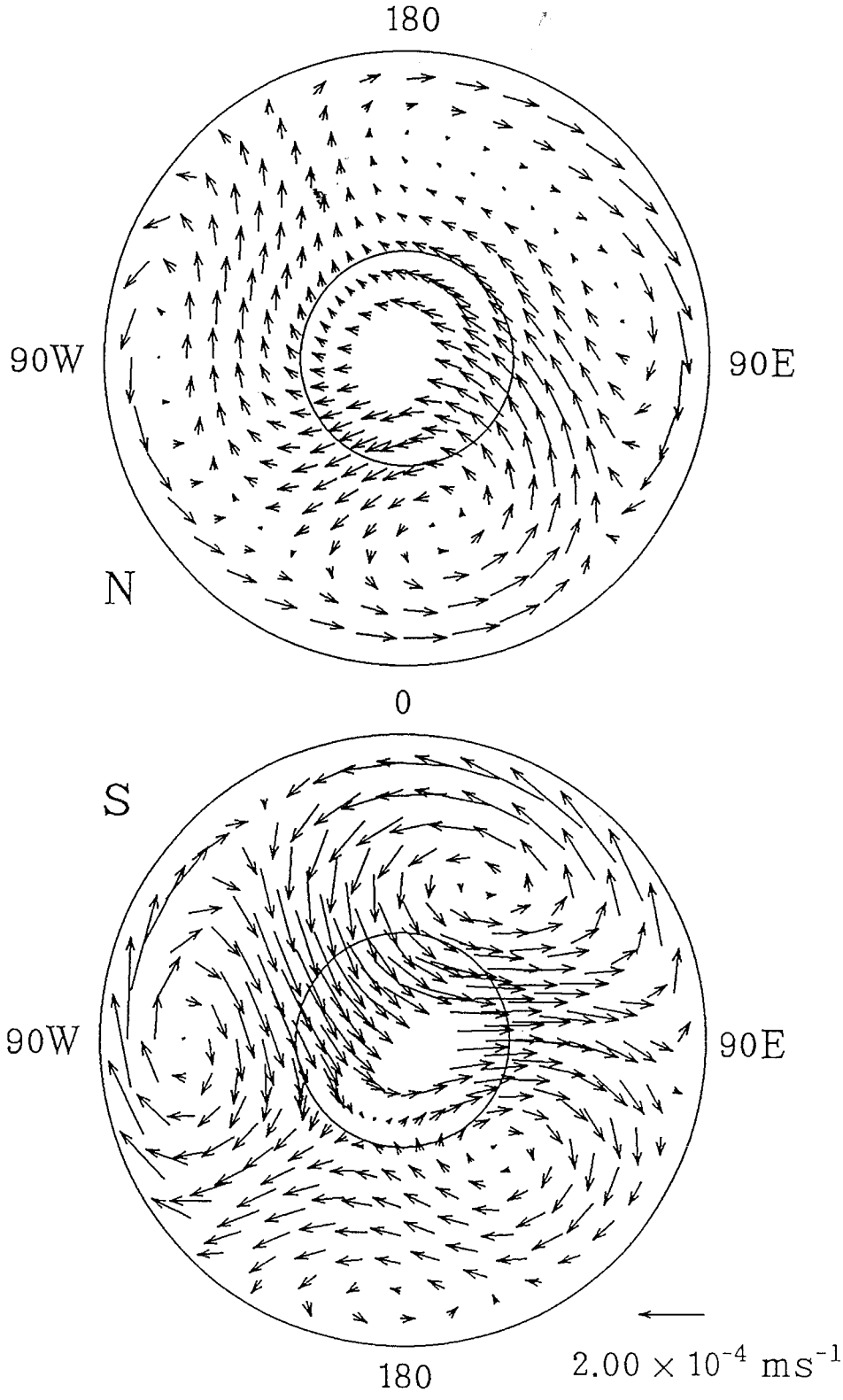

Fig. 5.6. The horizontal velocity fields at the core surface (shown in Fig. 3.20) as seen from North Pole and the South Pole. The arrow for scale length corresponds to 2×10^{-4} ms^{-1}.

(a)

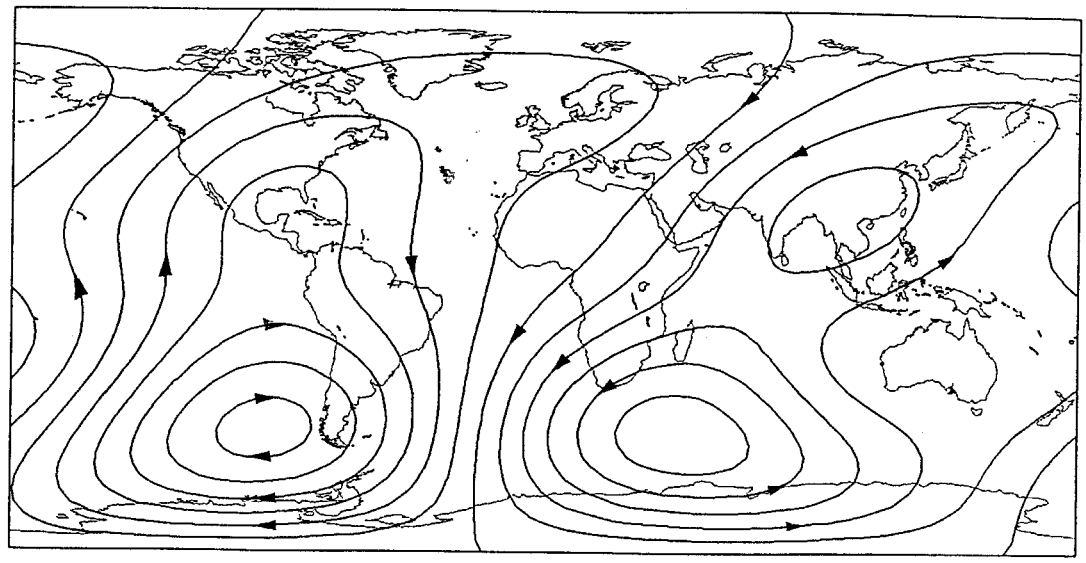

(b)

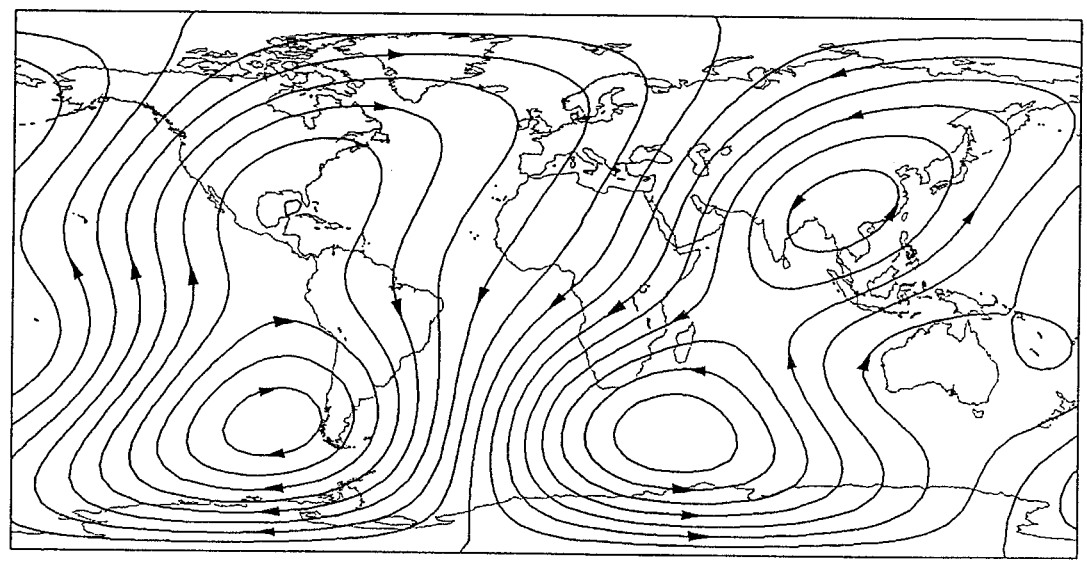

Fig. 5.7. Magnetic lines of force for the toroidal constituent on spherical surfaces (a) at $r = 0.9r_{oc}$, (b) at $r = 0.8r_{oc}$, (c) at $r = 0.7r_{oc}$, and (d) at $r = 0.6r_{oc}$ for the epoch of 1980 AD.

(c)

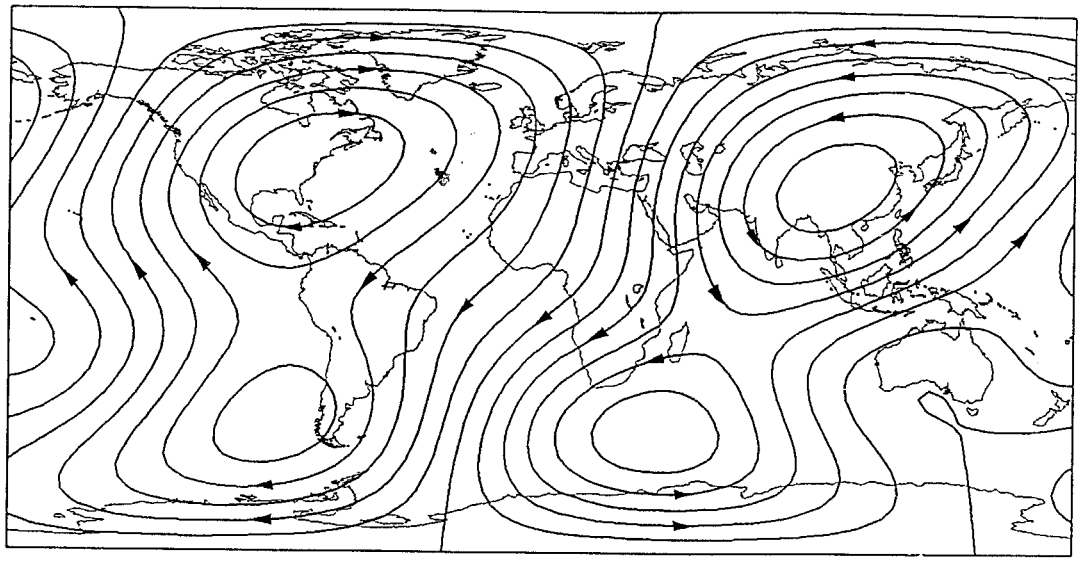

(d)

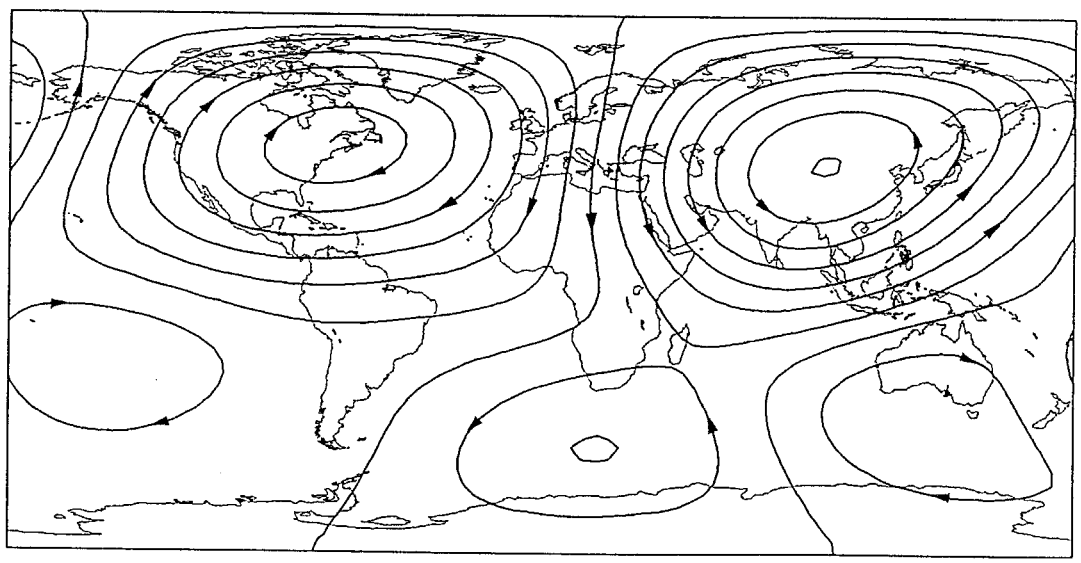

Fig. 5.7. (continued).

magnetic lines of force are dense. Maximum strength is about 8×10^{-3} T in Fig. 5.7(a), about 10^{-2} T in Fig. 5.7(b), and about 7×10^{-3} T in Figs. 5.7(c) and (d). Magnetic energy E_b for the toroidal constituent is $E_b[T] = 4.11\times10^{-2}$, while for the poloidal constituent, $E_b[S] = 1.87\times10^{-2}$. Strong toroidal magnetic field regions are located near the CMB. The features in fluid motion in the core, which are persistent from 1600 to 1980 AD, should be reflected in the toroidal magnetic field as well. We show magnetic lines of force for the toroidal constituent at $r = 0.9r_{oc}$ for the epochs of 1600, 1700, 1800 and 1900 AD in Figs. 5.8(a), (b), (c) and (d), respectively. As we expected, the pattern of magnetic lines of force is largely persistent during the period.

5.6. Implications for the geodynamo

From all these results, we speculate some dynamical properties in the core and a possible geodynamo as follows. The regions where magnetic flux extends from the mantle into the core are located mainly beneath Canada and Siberia. Some magnetic flux entering the core beneath Canada shifts toward the northern Atlantic, resulting in a null flux patch near the North Pole, some sifts southward, and the rest moves southward directly. Magnetic flux entering the core beneath Siberia moves southwestward. In the southern Atlantic, where the toroidal magnetic field is very strong, some flux comes out of the core and returns back into the core, as pointed out by Bloxham and Gubbins (1985) and Bloxham (1986). In addition, the magnetic flux moves toward the southern Pacific, and some flux comes out of the core and the rest moves northward beneath the Pacific, where the toroidal magnetic field is weak. This may be related to the cause of low secular variations observed in the Pacific hemisphere.

The fluid motion in the outer core derived in the present study is characterized by two convection rolls; one is along 90° W and the other along (60° S,

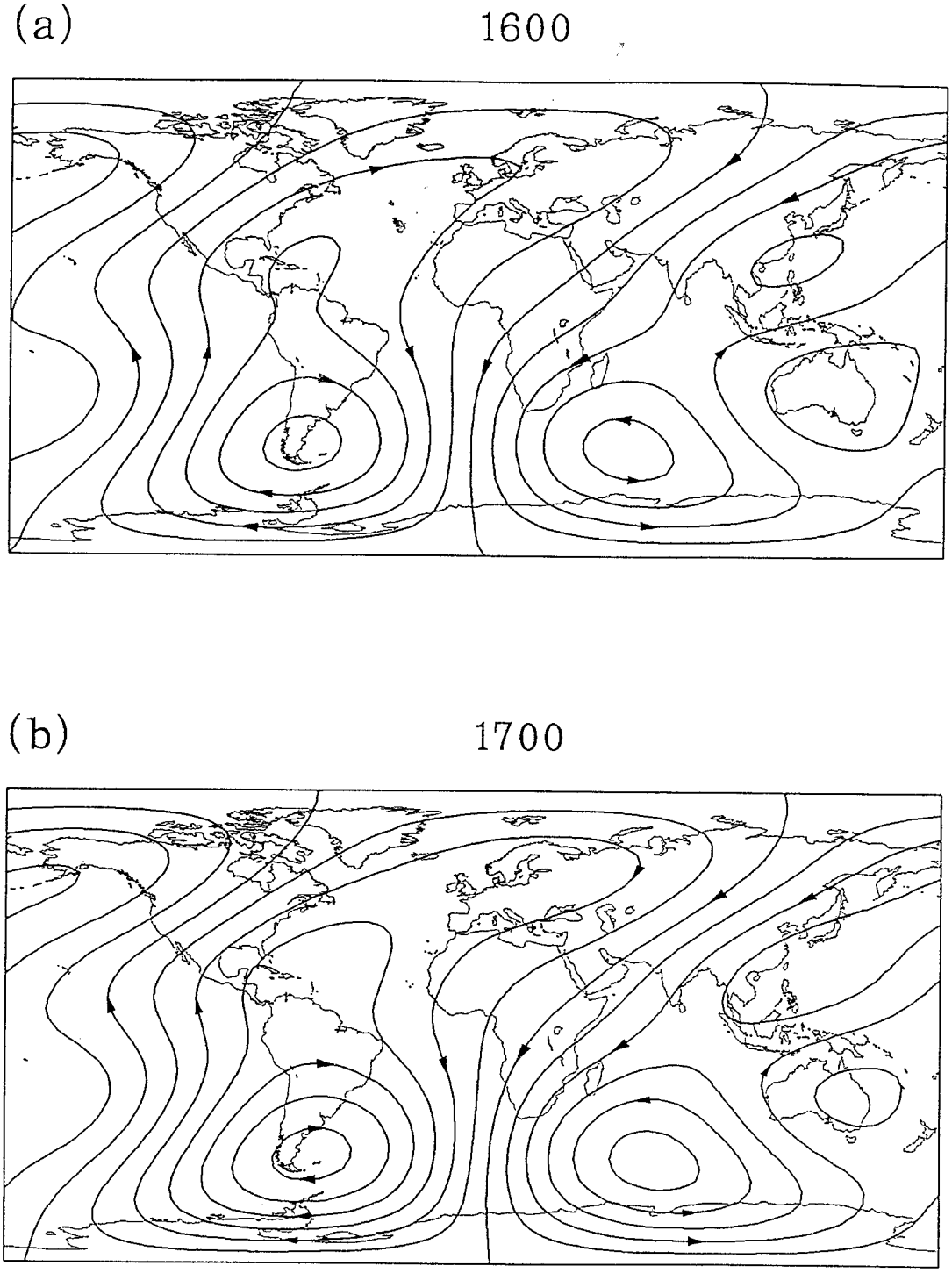

Fig. 5.8. Magnetic lines of force for the toroidal constituent on a spherical surface at $r = 0.9r_{oc}$ for the epochs of (a) 1600, (b) 1700, (c) 1800, and (d) 1900 AD.

(c) 1800

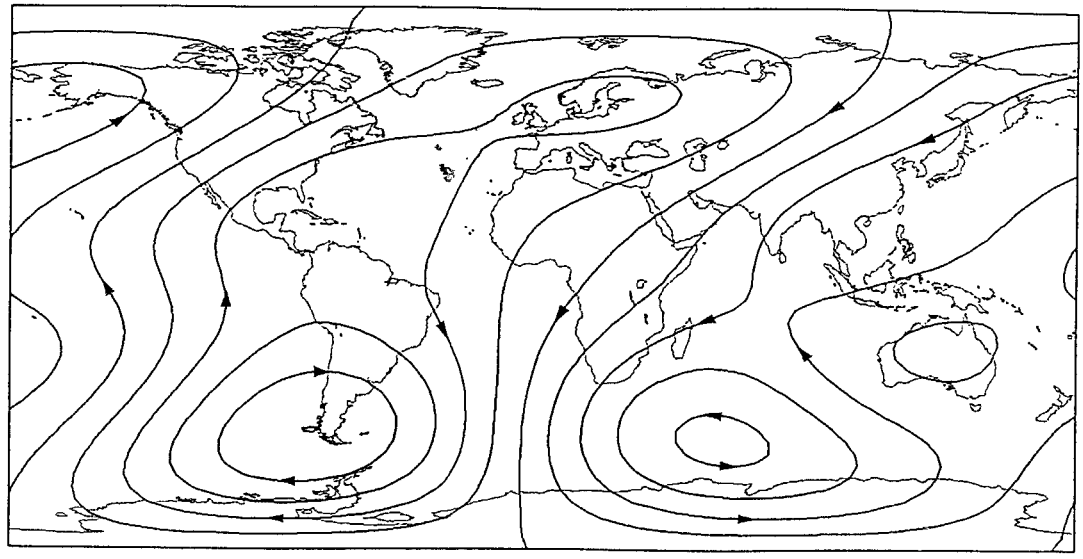

(d) 1900

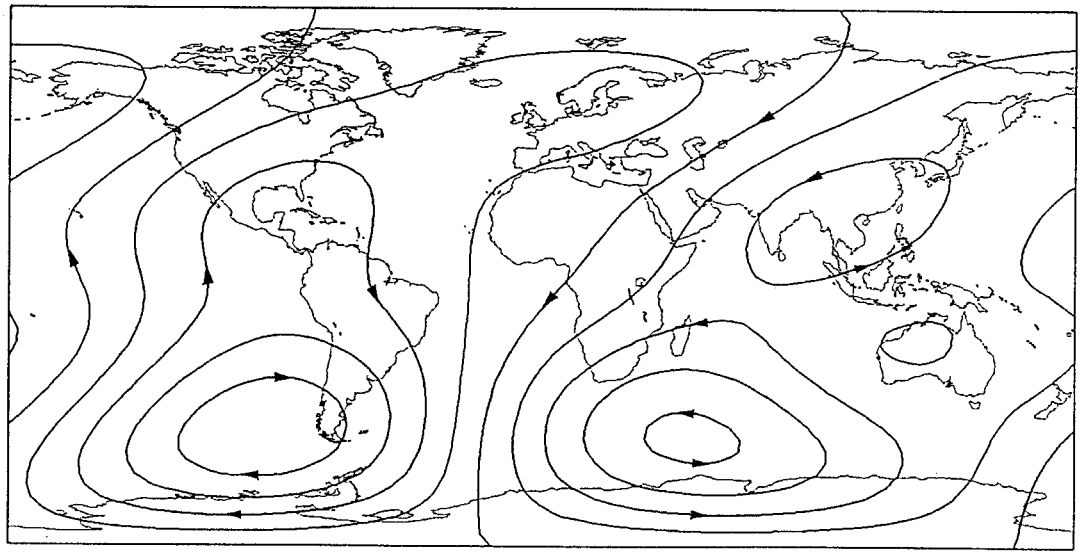

Fig. 5.8. (continued).

30°E)–(60°N, 90°E) line. The edges of the convection rolls in the Northern Hemisphere correspond to magnetic flux concentration at the CMB. The directions of convection rolls seem to be related to magnetic lines of force for the toroidal constituent.

It is well known that the onset of convection in a rotating system is hampered by the Coriolis force, which tend to rearrange fluid flow into a two-dimensional one; known as the Taylor-Proudman theorem (Chandrasekhar, 1961). The magnetic field also hampers, in general, the onset of convection. When both the rotation and the magnetic field act together, the magnetic field tends to break the Coriolis constraint. As a simple example, we consider thermal instability in a horizontal fluid layer with the gravitational force acting in the vertical direction. If the rotation vector is vertical, the vertical fluid motion is hampered by the Taylor-Proudman theorem. If the rotation vector is horizontal, however, convection can occur, without violating the Taylor-Proudman theorem, in a roll form with the axis parallel to the rotation vector. If the magnetic field is horizontal, similar convection can occur. When the horizontal model is generalized to spherical geometry, the existence of convection rolls as derived in the present study is likely. Such convection rolls effectively generate magnetic fields, as in Busse's dynamo model (1975). No strong zonal toroidal motion and no strong zonal toroidal magnetic field are required. In this sense, the derived fluid motion implies that the geodynamo is of α^2-type rather than of $\alpha\omega$-type.

The scale of two convection rolls derived in the present study is larger than that of Busse's model. In this respect, Busse (1975) pointed out that the typical wavenumber of motion is quantitatively influenced by the magnetic field, since in his model the Lorentz force is assumed to be small compared with the Coriolis force. If we take into consideration the effect of the Lorentz force in the core, the present two convection rolls are reasonable. The locations of convection rolls are related to the magnetic flux concentration beneath Canada and Siberia and also the toroidal

magnetic field in the core. Since the main features of the derived fluid motion are persistent at least for the last several hundred years, it is further speculated that the locations are controlled by thermal interactions between the core and mantle, as proposed by Bloxham and Gubbins (1987). As regards the thermal interaction, Jones (1977) suggested that the frequency of magnetic polarity reversals may be controlled by fluctuations in the temperature at the CMB due to intermittent convection in the mantle, for example, such as plumes arising from a boundary layer above the CMB. In order to further clarify the dynamical nature as implied in the present study in relation to the geodynamo, intensive multidisciplinary researches on the Earth's core are strongly required.

5.7. Future problems

So far we have tentatively taken into consideration the induction terms as assumed in Subsection 3.4, and obtained the results as described in Sections 3, 4 and 5, for Case 6. We here examine the effect of the other induction terms; that is, we examine the contribution of respective interaction terms from the velocity and the magnetic fields derived for Case 6.

Comparing the induction terms, given in (2.6) and (2.7), with each other, it turned out that the magnitude of various interaction terms is comparable to each other. This indicates that we should not rely on any approximations for dominant induction terms, but take all the interaction terms into consideration. The problem then becomes extremely difficult.

If we proceed further with the present basic strategy kept unchanged, that is, by taking into consideration the induction processes inside the core and solving the induction and the Navier-Stokes equations, we should loosen the restriction of the steady state in view of the non-linear nature of the problem. The approach, however,

is beyond the present study. Even though we can treat the non-steady state, it is extremely difficult to derive a realistic fluid motion in the sense that the observed secular variations of the geomagnetic field are accounted for.

In another aspect, the result that various interaction terms equally contribute the induction process suggests that the geodynamo would not be of $\alpha\omega$-type but rather of α^2-type. In order to understand a realistic geodynamo mechanism, for instance, based on the Earth's magnetic field, we should aim at studying the geodynamo always with the result as obtained in the present study in mind.

6. Conclusions

We attempted to derive fluid motion in the Earth's outer core from geomagnetic field data by solving the induction and the Navier-Stokes equations for various cases. The present approach can be regarded as an inbetween problem, compared with kinematic dynamo and magnetohydrodynamic dynamo problems, because the magnitude of poloidal velocity field is constrained by the observed data but its radial dependence is assumed, and the toroidal velocity field is derived by solving the Navier-Stokes equation. We also assumed that the velocity and magnetic fields are in a quasi-steady state for specified epochs. In order to check the validity of the derived solutions and examine whether the derived velocity field can maintain the magnetic field, we examined time-dependent behavior of the magnetic field with the velocity field fixed for respective cases. The conclusions are summarized as follows.

(1) In Cases 1 and 2, we assumed that zonal toroidal magnetic fields are primary inducing magnetic fields with (Case 2) and without (Case 1) meridional circulation. The derived fluid motions, however, turned out to be geophysically implausible.

(2) In Cases 3, 4 and 5, we included axisymmetric poloidal magnetic fields in primary inducing magnetic fields, with (Case 5) and without (Cases 3 and 4) meridional circulation. The derived fluid motions are again geophysically implausible.

(3) In Cases 6 and 7, we took into consideration non-zonal toroidal velocity and non-zonal toroidal magnetic fields. The velocity field derived for Case 6 is the most plausible one in the sense that the condition of quasi-steady state is not violated; the magnetic energy increases only by 20 % during 500 years in kinematic dynamo calculation. Some of the features in the velocity field are in common

with the core surface motion derived on the frozen-flux approximation.

(4) The fluid motion in the core derived for Case 6 is characterized by two convection rolls; one is along 90°W in longitude and the other along (60°S, 30°E)–(60°N, 90°E) line. The edges of convection rolls correspond to two pairs of vortices at the CMB. One of them is located beneath the southwest Indian Ocean and is consistent with the fluid motion derived on the frozen-flux approximation. A westward flow exists in a zone near the equator from around 150°W to 0° in longitude.

(5) The edges of convection rolls in the Northern Hemisphere are located beneath Canada and Siberia, where magnetic flux concentrations are also observed at the CMB. Convection rolls parallel to the Earth's rotation axis have been proposed by Busse (1975) as a dynamo model, and their relation to the flux concentrations has been suggested by Gubbins and Bloxham (1987). In the derived fluid motion, one convection roll is indeed parallel to the rotation axis, but the other is inclined. This feature seems to be related to the toroidal magnetic field in the core. The locations of these convection rolls are rather persistent and hence may be controlled by the thermal interactions between the core and the mantle, as proposed by Bloxham and Gubbins (1987).

(6) All these results suggest that the geodynamo is of α^2-type rather than of $\alpha\omega$-type.

We set the truncation level at $L = 4$ for the degree of spherical harmonics, since we considered a large-scale convective motion which in turn generates a large-scale magnetic field. If we are requested to increase the truncation level, improvement of the present approach is required so that time variations of the geomagnetic field can be included in models, since small-scale features in the geomagnetic field seem to be subject to rather rapid secular variations.

References

Akaike, H., A new look at the statistical model identification, *IEEE Trans. Autom. Contr.*, **AC-19**, 716–723, 1974.

Babcock, H. W., The topology of the Sun's magnetic field and the 22-year cycle, *Astrophys. J.*, **133**, 572–587, 1961.

Backus, G. E., Kinematics of the geomagnetic secular variation in a prefectly conducting core, *Phil. Trans. Roy. Soc. Lond. A*, **263**, 239–266, 1968.

Backus, G., Poloidal and toroidal fields in geomagnetic field modeling, *Rev. Geophys.*, **24**, 75–109, 1986.

Backus, G. E. and J.-L. Le Mouël, The region on the core-mantle boundary where a geostrophic velocity can be determined from frozen-flux magnetic data, *Geophys. J. Roy. Astr. Soc.*, **85**, 617–628, 1986.

Barraclough, D., D. Gubbins, and D. Kerridge, On the use of horizontal components of magnetic field in determining core motions, *Geophys. J. Int.*, **98**, 293–299, 1989.

Bloxham, J., The expulsion of magnetic flux from the Earth's core, *Geophys. J. Roy. Astr. Soc.*, **87**, 669–678, 1986.

Bloxham, J., The determination of fluid flow at the core surface from geomagnetic observations, in *Mathematical Geophysics, A Survey of Recent Development in Seismology and Geodynamics,* edited by N. J. Vlaar, G. Nolet, M. J. R. Wortel, and S. A. P. L. Cloetingh, pp. 189–208, D. Reidel, Dordrecht, 1988a.

Bloxham, J., The dynamical regime of fluid flow at the core surface, *Geophys. Res. Lett.*, **15**, 585–588, 1988b.

Bloxham, J., Simple models of fluid flow at the core surface derived from geomagnetic field models, *Geophys. J. Int.*, **99**, 173–182, 1989.

Bloxham, J. and D. Gubbins, The secular variation of Earth's magnetic field, *Nature,* **317**, 777–781, 1985.

Bloxham, J. and D. Gubbins, Geomagnetic field analysis–IV. Testing the frozen-flux hypothesis, *Geophys. J. Roy. Astr. Soc.,* **84**, 139–152, 1986.

Bloxham, J. and D. Gubbins, Thermal core-mantle interactions, *Nature,* **325**, 511–513, 1987.

Bullard, E. C., The magnetic field within the earth, *Proc. Roy. Soc. Lond. A,* **197**, 433–453, 1949.

Bullard, E. C., The stability of a homopolar dynamo, *Proc. Camb. Phil. Soc.,* **51**, 744–760, 1955.

Bullard, E. C. and H. Gellman, Homogeneous dynamos and terrestrial magnetism, *Phil. Trans. Roy. Soc. Lond. A,* **247**, 213–278, 1954.

Busse, F. H., Differential rotation in stellar convection zones, *Astrophys. J.,* **159**, 629–639, 1970.

Busse, F. H., A model of geodynamo, *Geophys. J. Roy. Astr. Soc.,* **42**, 437–459, 1975.

Chandrasekhar, S., *Hydrodynamic and Hydromagnetic Stability,* 652 pp., Oxford Univ. Press, New York, 1961.

Cox, A., Length of geomagnetic polarity intervals, *J. Geophys. Res.,* **73**, 3247–3260, 1968.

Cox, A., Geomagnetic reversals, *Science,* **163**, 237–245, 1969.

Elsasser, W. M., Induction effects in terrestrial magnetism, 1: Theory, *Phys. Rev.,* **69**, 106–116, 1946.

Fearn, D. R. and D. E. Loper, Compositional convection and stratification of the Earth's liquid core, *Nature,* **289**, 393–394, 1981.

Frazer, M. C., Spherical harmonic analysis of the Navier-Stokes equation in

magnetofluid dynamics, *Phys. Earth Planet. Inter.*, **8**, 75–82, 1974.

Gans, R. F., Viscosity of the Earth's core, *J. Geophys. Res.*, **77**, 360–366, 1972.

Gardiner, R. B. and F. D. Stacey, Electrical resistivity of the core, *Phys. Earth Planet. Inter.*, **4**, 406–410, 1971.

Gire, C. and J.-L. Le Mouël, Tangentially geostrophic flow at the core-mantle boundary compatible with the observed geomagnetic secular variation: the large-scale component of the flow, *Phys. Earth Planet. Inter.*, **59**, 259–287, 1990.

Glatzmaier, G. A., Numerical simulations of stellar convective dynamos, 1. The model and method, *J. Comp. Phys.*, **55**, 461–484, 1984.

Gubbins, D., Finding core motions from magnetic observations, *Phil. Trans. Roy. Soc. Lond. A*, **306**, 247–254, 1982.

Gubbins, D., Thermal core-mantle interactions and time-averaged paleomagnetic field, *J. Geophys. Res.*, **93**, 3413–3420, 1988.

Gubbins, D. and J. Bloxham, Morphology of the geomagnetic field and implications for the geodynamo, *Nature*, **325**, 509–511, 1987.

Gubbins, D. and P. H. Roberts, Magnetohydrodynamics of the Earth's core, in *Geomagnetism*, Vol. 2, edited by J. A. Jacobs, pp. 1–183, Academic Press, Orland, 1987.

Gubbins, D., C. J. Thomson, and K. A. Whaler, Stable regions in the Earth's liquid core, *Geophys. J. Roy. Astr. Soc.*, **68**, 241–251, 1982.

Honkura, Y. and M. Matsushima, Lower bound for the electrical conductivity of the Earth's outer core, *Geophys. Res. Lett.*, **15**, 689–692, 1988a.

Honkura, Y. and M. Matsushima, Fluctuation of the nondipole magnetic field and its implication for the process of geomagnetic polarity reversal in the Cox model, *J. Geophys. Res.*, **93**, 11,631–11,642, 1988b.

Honkura, Y. and M. Matsushima, Time-dependent pattern of core motion inferred

from fluctuations of standing and drifting non-dipole fields, *J. Geomag. Geoelectr.*, **40**, 1511–1522, 1988c.

Honkura, Y. and T. Rikitake, Core motion as inferred from drifting and standing non-dipole fields, *J. Geomag. Geoelectr.*, **24**, 223–230, 1972.

Hulot, G., J.-L. Le Mouël, and D. Jault, The flow at the core-mantle boundary: symmetry properties, *J. Geomag. Geoelectr.*, **42**, 857–874, 1990.

IAGA Division I Working Group 1, International Geomagnetic Reference Field Revision 1987, *Geophys. J.*, **93**, 187–189, 1988.

Jain, A. and R. Evans, Calculation of the electrical conductivity of liquid iron in the Earth's core, *Nature Phys. Sci.*, **235**, 165–167, 1972.

Jault, D., C. Gire, and J.-L. Le Mouël, Westward drift, core motions and exchanges of angular momentum between core and mantle, *Nature*, **333**, 353–356, 1988.

Johnston, M. J. S. and R. G. J. Strens, Electrical conductivity of molten Fe-Ni-S-C core mix, *Phys. Earth Planet. Inter.*, **7**, 217–128, 1973.

Jones, G. M., Thermal interaction of the core and the mantle and long-term behavior of the geomagnetic field, *J. Geophys. Res.*, **82**, 1703–1709, 1977.

Kimura, R., Cell formation in the convective mixed layer, *Fluid Dyn. Res.*, **3**, 395–399, 1988.

King, S. D. and B. H. Hager, Coupling of mantle temperature anomalies and the flow pattern in the core: interpretation based on simple convection calculation, *Phys. Earth Planet. Inter.*, **58**, 118–125, 1989.

Knitlle, E., R. Jeanloz, A. C. Mitchell, and W. J. Nellis, Metallization of $Fe_{0.94}O$ at elevated pressures and temperatures observed by shock-wave resistivity measurements, *Solid State Commun.*, **59**, 513–515, 1986.

Kohler, M. D. and D. J. Stevenson, Modeling core fluid motions and the drift of magnetic field patterns at the CMB by use of topography obtained by seismic

inversion, *Geophys. Res. Lett.*, **17**, 1473–1476, 1990.

Kono, M., Computer algebra for automatically solving kinematic dynamo problems, *J. Geomag. Geoelectr.*, **42**, 35–55, 1990.

Le Mouël, J.-L., C. Gire, and T. Madden, Motions at core surface in the geostrophic approximation, *Phys. Earth Planet. Inter.*, **39**, 270–287, 1985.

Lilley, F. E. M., On kinematic dynamos, *Proc. Roy. Soc. Lond. A*, **316**, 153–167, 1970.

Lloyd, D. and D. Gubbins, Toroidal motion at the top of the Earth's core, *Geophys. J. Int.*, **100**, 455–467, 1990.

Madden, T. and J.-L. Le Mouël, The recent secular variation and the motions at the core surface, *Phil. Trans. Roy. Soc. Lond. A*, **306**, 271–280, 1982.

Matsushima, M. and Y. Honkura, Fluctuation of the standing and the drifting parts of the Earth's magnetic field, *Geophys. J.*, **94**, 35–50, 1988.

Matsushima, M. and Y. Honkura, Large-scale fluid motion in the Earth's outer core estimated from non-dipole magnetic field data, *J. Geomag. Geoelectr.*, **41**, 963–1000, 1989a.

Matsushima, M. and Y. Honkura, Fluid motion in the Earth's core based on strong toroidal magnetic fields, Abstracts, 86th SGEPSS Fall Meeting, 1989b (in Japanese with English abstract).

Moffatt, H. K., *Magnetic Field Generation in Electrically Conducting Fluids,* 343 pp., Cambridge Univ. Press, London, 1978.

Olson, P., Toroidal flow in the outer core and the thermal regime below the core-mantle boundary, *Geophys. Res. Lett.*, **16**, 613–616, 1989.

Orszag, S. A., Spectral methods for problems in complex geometries, *J. Comp. Phys.*, **37**, 70–92, 1980.

Pedlosky, J., *Geophysical Fluid Dynamics,* 2nd ed., 710 pp., Springer-Verlag, New

York, 1987.

Rikitake, T., Non-dipole field and fluid motion in the earth's core, *J. Geomag. Geoelectr.*, **19**, 129–142, 1967.

Rikitake, T. and Y. Hagiwara, Non-steady Bullard-Gellman dynamo model (1), *J. Geomag. Geoelectr.*, **20**, 57–65, 1968.

Rikitake, T. and Y. Honkura, *Solid Earth Geomagnetism,* 384 pp., D. Reidel/Terra Sci., 1985.

Roberts, P. H., Kinematic dynamo models, *Phil. Trans. Roy. Soc. Lond. A,* **272**, 663–698, 1972.

Roberts, P. H. and D. Gubbins, Origin of the main field: kinematics, in *Geomagnetism,* Vol. 2, edited by J. A. Jacobs, pp. 185–249, Academic Press, Orland, 1987.

Roberts, P. H. and S. Scott, On analysis of the secular variation, 1. A hydromagnetic constraint: theory, *J. Geomag. Geoelectr.*, **17**, 137–151, 1965.

Roberts, P. H. and M. Stix, α-effect dynamos, by Bullard-Gellman formalism, *Astron. Astrophys.*, **18**, 453–466, 1972.

Shimizu, M. and Y. Honkura, Statistical nature of polarity reversals of the magnetic field in coupled-disk dynamo models, *J. Geomag. Geoelectr.*, **37**, 455–497, 1985.

Shimizu, M. and Y. Honkura, Fluctuations of magnetic fields in coupled-disk dynamo models and their implications for geomagnetic secular variations, *J. Geomag. Geoelectr.*, **38**, 611–632, 1986.

Stacey, F. D., Physical properties of the Earth's core, *Geophys. Surveys,* **1**, 99–119, 1972.

Suzuki, Y. and R. Sato, Viscosity determination in the Earth's outer core from ScS and SKS phases, *J. Phys. Earth,* **18**, 157–170, 1970.

Taylor, J. B., The magneto-hydrodynamics of a rotating fluid and the earth's

dynamo problem, *Proc. Roy. Soc. A*, **274**, 274–283, 1963.

Uno, S., Non-steady state of a Bullard-Gellman-Lilley dynamo model, *J. Geomag. Geoelectr.*, **24**, 203–222, 1972.

Voorhies, C. V., Steady flows at the top of earth's core derived from geomagnetic field models, *J. Geophys. Res.*, **91**, 12,444–12,466, 1986.

Wang, T.-W. and G.-Z. Qi, The model of the geomagnetic non-dipole field, *J. Geomag. Geoelectr.*, **35**, 255–280, 1983.

Watanabe, H. and T. Yukutake, Electromagnetic core-mantle coupling associated with changes in the geomagnetic dipole field, *J. Geomag. Geoelectr.*, **26**, 153–173, 1975.

Whaler, K. A., Does the whole of the Earth's core convect?, *Nature*, **287**, 528–530, 1980.

Whaler, K. A., A steady velocity field at the top of the Earth's core in the frozen-flux approximation—errata and further comments, *Geophys. J. Int*, **102**, 507–509, 1990.

Whaler, K. A. and S. O. Clarke, A steady velocity field at the top of the Earth's core in the frozen-flux approximation, *Geophys. J.*, **94**, 143–155, 1988.

Yokoyama, Y., Study of geomagnetic 60 year variation, Ph. D. thesis, 197 pp., Univ. of Tokyo, 1989.

Yokoyama, Y. and T. Yukutake, Calculation of induced modes of magnetic field in the geodynamo problem, *J. Geomag. Geoelectr.*, **41**, 421–442, 1989.

Yokoyama, Y. and T. Yukutake, Three processes of inducing the steady poloidal field in the Earth's core, *J. Geomag. Geoelectr.*, **42**, 93–108, 1990.

Yukutake, T., A stratified core motion inferred from geomagnetic secular variations, *Phys. Earth Planet. Inter.*, **24**, 253–258, 1981.

Yukutake, T., A preliminary study on variations in the Gauss coefficients of the

geomagnetic potential over several hundred years, *Phys. Earth Planet. Inter.*, **39**, 217–227, 1985.

Yukutake, T. and H. Tachinaka, Separation of the earth's magnetic field into the drifting and the standing parts, *Bull. Earthq. Res. Inst. Univ. Tokyo,* **47**, 65–97, 1969.